Black Holes with Topological Defects: The C-metric in Three and Four Dimensions

ANDREW DAVID SCOINS

Black Holes with Topological Defects

The C-metric in Three and Four Dimensions

Andrew D. Scoins

A thesis presented for the degree of
Doctor of Philosophy

Centre for Particle Theory
Department of Mathematical Sciences
Durham University
United Kingdom

February 2022

Black Holes with Topological Defects

The C-metric in Three and Four Dimensions

Andrew D. Scoins

Submitted for the degree of Doctor of Philosophy
February 2022

Abstract: We examine the effects of accelerating both isolated and coupled black holes in a variety of contexts.

A detailed investigation of the thermodynamic phase space of a charged, rotating, and accelerating black hole placed in a background of negative cosmological constant is performed, and novel effects due to acceleration are identified. A modified Christodoulou-Ruffini formula for the solution is shown to hold, providing compelling evidence that the mass used, identified using holographic techniques, is the correct one.

Motivated by the holographic results, we then identify the mass of an array of black holes connected by conical deficits and without cosmological constant, of which the C-metric is a special case. This mass is shown to obey a first law of thermodynamics, with the string tensions acting as a thermodynamic charge. The black holes are coupled in such a way that a variation applied to one affects all of the others. A similar Christodoulou-Ruffini formula is shown to hold in this context.

We then examine a family of three-dimensional solutions analogous to the four-dimensional C-metric. We identify three classes of geometry. From these, we construct stationary, accelerating conical deficits; novel one-parameter extensions of the static BTZ family which resemble the C-metric; and braneworld solutions. We comment on the extent to which our solutions may be considered "accelerating black holes".

Declaration

The work in this thesis is based on research carried out in the Department of Mathematical Sciences at Durham University. No part of this thesis has been submitted elsewhere for any degree or qualification.

The material appearing in chapter 4 majoritarily comprises work completed in collaboration with Ruth Gregory, previously appearing as

[1] R. Gregory, A. Scoins, *Accelerating black hole chemistry*, Physics Letters B, **796** (2019) 191-195.

It it also contains material produced in collaboration with Wasif Ahmed, Hong Zhe Chen, Elliott Gesteau, and Ruth Gregory, previously appearing as

[2] W. Ahmed et al., *Conical holographic heat engines*, Class. Quantum Grav., **36** (2019) 214001.

Chapter 5 comprises work completed in collaboration with Ruth Gregory and Zheng Liang Lim, previously published as

[3] R. Gregory, Z. Lim-Liang, A. Scoins, *Thermodynamics of many black holes*, Frontiers in Physics, **9** (2021) 187.

Chapter 6 contains work conducted in collaboration with Ruth Gregory, Gabriel Arenas-Henriquez, and Pavel Krtouš.

G. Arenas-Henriquez et al., *The Three-dimensional C-metric*, In preparation.

Acknowledgements

There are many people to thank for this completed thesis. These people are far more responsible for the existence of this document than I am.

Principally, I extend my profound gratitude to my supervisor for the majority of my degree, Ruth Gregory, who has been not only an academic mentor but also a friend throughout. Ruth has gone above and beyond in her support for me throughout my time at Durham, and I will be forever grateful for the opportunities studying under her has afforded me.

I also owe my thanks to my parents, to whom this thesis is dedicated, who have afforded me every conceivable advantage in the twenty-six year journey to this finished document. Not only did they provide my life with some wonderful initial conditions, they have always been there to give my evolution a nudge in the right direction when my global truncation error has gotten a little too large. I am truly grateful.

I extend my deepest thanks to Lauren, who has been at my side for the duration of this PhD as an invaluable source of support and reassurance. I also wish to thank Beverley and Mick for their hospitality and generosity.

I wish to thank Simon Ross for his guidance and comments on drafts of this thesis. My thanks also go out to my collaborators, Wasif Ahmed, Gabriel Arenas-Henriquez, Hong Zhe Chen, Lim Zheng Liang, Elliott Gesteau, Betti Hartmann, Pavel Krotouš, and Héctor Olivares, from each of whom I have learned a lot.

My dear friend Ashley Wilkins also deserves credit, as without the opportunity to discuss physics with him throughout our time as undergraduates, I would not be the physicist I am today.

My thanks go out to the Perimeter Institute for Theoretical Physics for accommodating me three times during my studies. I thank also The University of Oxford, The University of Southampton, and Newcastle University for similar reasons.

This work was supported by the Science and Technology Facilities Council. I am grateful to them—and by extension every taxpayer in the UK—for the privilege of engaging in blue skies research for four years of my life.

This thesis is dedicated,
with my deepest
gratitude,
to

Brian and Jennifer Scoins

The more the problem was analysed the sillier the solutions became.

— B. P. Block & J. Hostettler

Contents

List of figures

List of tables

Conventions

Throughout this thesis we will employ Planck units for which the speed of light, gravitational constant, reduced Planck constant and Boltzmann constant are set to unity:

$$c = G = \hbar = k_{\mathrm{B}} = 1\,.$$

We work with the mostly-minus signature $(+---\ldots)$ for Lorentzian geometries, with the Einstein summation convention implicit. Component indices may of course be raised and lowered by contraction with the relevant metric tensor. The action of general relativity is

$$S = \frac{1}{16\pi}\int d^D x\sqrt{|\det g|}\left(\mathrm{Tr}[g^{-1}\mathcal{R}(g)] - 2\Lambda\right) + \int d^D x\sqrt{|\det g|}\mathcal{L}_{\mathrm{matter}}\,,$$

where $\mathcal{R}(g)$ is the Ricci curvature of the metric g and where D is the dimension of the manifold. This gives the equations of motion

$$\mathcal{R}(g) - \frac{1}{2}g\,\mathrm{Tr}[g^{-1}\mathcal{R}(g)] + \Lambda g = 8\pi T\,,$$

with T the stress-energy tensor of the matter Lagrangian-density $\mathcal{L}$. The components of T are given by

$$T_{\mu\nu} = \frac{2}{\sqrt{|\det g|}}\frac{\delta\sqrt{|\det g|\,\mathcal{L}_{\mathrm{matter}}}}{\delta g^{\mu\nu}}\,.$$

When working with an anti-de Sitter (AdS) spacetime, for which $\Lambda \neq 0$, we will typically use the curvature length-scale ℓ in place of the cosmological constant Λ. The two are related by

$$\Lambda = -\frac{(D-1)(D-2)}{2\ell^2}\,.$$

Given a p-form A, a q-form B, and a coordinate basis $\{x^i\}$, we employ the following definitions of components and operators:

$$\begin{aligned}
A &= \frac{1}{p!} A_{\mu_1 \ldots \mu_p} dx^{\mu_1} \wedge \ldots \wedge dx^{\mu_p} \,, \\
A \wedge B &= \frac{1}{(p+q)!} \left(\frac{(p+q)!}{p!q!} A_{[\mu_1 \cdots \mu_p} B_{\mu_{p+1} \cdots \mu_{p+q}]} \right) dx^{\mu_1} \wedge \ldots \wedge dx^{\mu_{p+q}} \,, \\
dA &= \frac{1}{(p+1)!} \left((p+1)\, \partial_{[\mu_1} A_{\mu_2 \cdots \mu_{p+1}]} \right) dx^{\mu_1} \wedge \ldots \wedge dx^{\mu_{p+1}} \,, \\
\epsilon &= \sqrt{|\det g|}\; dx^0 \wedge \ldots \wedge dx^D \,, \\
\star A &= \frac{1}{(D-p)!} \left(\frac{1}{p!} A^{\mu_1 \cdots \mu_p} \epsilon_{\mu_1 \cdots \mu_p \nu_1 \cdots \nu_{D-p}} \right) dx^{\nu_1} \wedge \ldots \wedge dx^{\nu_{D-p}} \,.
\end{aligned}$$

Parenthesis and square brackets around indices denote totally symmetric or anti-symmetric combinations of tensor indices, respectively:

$$\begin{aligned}
A_{(\mu_1 \mu_2) \mu_3 \cdots \mu_p} &= \frac{1}{2} \left(A_{\mu_1 \mu_2 \mu_3 \cdots \mu_p} + A_{\mu_2 \mu_1 \mu_3 \cdots \mu_p} \right) \,, \\
A_{[\mu_1 \mu_2] \mu_3 \cdots \mu_p} &= \frac{1}{2} \left(A_{\mu_1 \mu_2 \mu_3 \cdots \mu_p} - A_{\mu_2 \mu_1 \mu_3 \cdots \mu_p} \right) \,.
\end{aligned}$$

We will occasionally denote contraction of tensor indices by $\cdot$, which for a pair of forms is

$$A \cdot B = \frac{1}{(p-1)!\,(q-1)!} A_{\mu_1 \cdots \mu_{p-1} \sigma} B^{\sigma}{}_{\mu_p \cdots \mu_{p+q-2}} dx^{\mu_1} \wedge \ldots \wedge dx^{\mu_{p+q-2}} \,.$$

Throughout the text, where the meaning is unambiguous from context, we will often denote the metric determinant $\det g$ simply as g.

Chapter 1

Introduction

General relativity [4, 5] is arguably one of the most successful theories in the history of the physical sciences. From its conception in 1916, the predictions of relativity have remained unfalsified to the present day. Its early successes reproducing the perihelion precession of Mercury and predicting the deflection of light on both solar system [6] and galactic [7] scales have paved the way for increasingly accurate tests of the validity of the theory. Even in the present day, experimental precision is not yet sufficient to observe significant incongruities [8].

One of the most striking predictions of the theory is the existence of black holes: regions of spacetime possessing such a strong gravitational field that not even photons may escape.

Though difficult to observe directly, there exists a substantial body of evidence for the existence of black holes. In particular, it is widely believed that at the centre of Earth's own galaxy lies a black hole, Sagittarius A*, possessing a mass around four million times that of the Sun [9–11]. This hypothesis has proven fruitful in explaining the orbits of stars [12]. Further, as recently as 2015 the first observations of gravitational waves were performed and accurately explained as a consquence of binary black hole merger [13]. Even more recently, in 2019 direct observations of the gravitational lensing of light around an extragalactic object proposed to be a black hole, Messier 87*, were performed [14–18]. The results are consistent with modeling the object using the Kerr metric [19], an appropriate description of the late-time behaviour of a rotating black hole [20, 21]. Additionally, a number of analogue systems exist [22–26] wherein the dynamics of the theory may be tested in a laboratory setting. Such analogue systems have been used to experimentally test a number of relativistic predictions about black holes, including the spontaneous emission of thermal radiation [27, 28], superradient scattering [29–

31], and cosmological effects[1] arising due to inflation [33].

In some sense, black holes are simple objects. The "no-hair theorems" limit the number of charges the black hole can carry. Axisymmetric stationary black holes with matter satisfying reasonable assumptions at infinity are uniquely characterised by their mass, electric charge(s), and spin(s)[2]. This simplicity is deceptive, however; black holes exhibit a variety of complex behaviours. In particular, classically they obey the *laws of black hole mechanics*, closely analogous to the laws of thermodynamics [36]. When one considers quantum effects, these laws are promoted to true thermodynamic relations. It was discovered by Hawking that stationary black holes emit black-body radiation [37–39] at a temperature T inversely-proportional to their mass M:

$$T = \frac{\hbar c^3}{8\pi G k_{\mathrm{B}} M} = 6 \times 10^{-8} \left(\frac{M_\odot}{M} \right) . \tag{1.0.1}$$

This discovery paved the way for an entirely new understanding of black objects as true thermodynamic objects with entropy.

In this thesis we analyse the thermodynamic effect of accelerating a black hole, and attempt to construct novel models of accelerating objects within general relativity. In chapter 2, we briefly review the thermodynamic laws which black holes obey. We then introduce the prototypical model of an accelerating black hole, the C-metric, in chapter 3. We outline its basic properties and review the formulation of the first law of thermodynamics and Smarr relation. In chapter 4, an investigation of the thermodynamic phase space of a charged, rotating, and accelerating black hole placed in a background of negative cosmological constant is undertaken. We analytically identify novel critical-points in phase space resulting from acceleration. We also use the model to add to the body of evidence that black hole mass should be interpreted as the enthalpy of spacetime. A modified Christodoulou-Ruffini formula — expressing the enthalpy as a function of other thermodynamic quantities — is shown to hold, indicating that the solution enthalpy decreases as acceleration is increased and providing evidence for the mass written in the literature. In chapter 5, we turn our attention to black holes in the absence of cosmological constant. We consider a static array of collinear black holes, of which the C-metric is a particular case. A first law of thermodynamics for the system is formulated, and the black holes are shown to be coupled; a variation of one black hole impacts all the others. A similar Christodoulou-Ruffini formula for the C-metric is shown in this case. Finally, in chapter 6, we attempt to identify novel solutions of gravity describing acceleration

[1] We refer the interested reader to [32] for a review of experimental tests of general relativity on cosmological scales.

[2] These theorems are now understood to be somewhat limited [34, 35], although the essential point is that a typical black hole is characterised by a small number of degrees of freedom.

so that one may better understand its effects. To this end, we examine a family of three-dimensional solutions analogous to the four-dimensional C-metric. We find three classes of geometry. From these, we construct stationary, accelerating conical deficits; novel one-parameter extensions of the static BTZ family of black holes, which resemble the C-metric; and braneworld-like solutions. We call into question the extent to which the black hole solutions may be considered "accelerating black holes", as has been suggested in the literature [40].

Chapter 2

Black hole thermodynamics

2.1 Early indications of black hole thermodynamics

The earliest indication that black holes might be thermodynamic objects was the discovery that, classically, black holes in general relativity obey a set of laws analogous to the four laws of thermodynamics [36].

Zeroth law: The surface gravity κ remains constant over an event horizon. If the matter content of the theory satisfies the Null Energy Condition, $T_{\mu\nu}v^\mu v^\nu \geq 0$ for all null vectors v, this can be proven when the black hole is either static [41], or stationary with a $(t, \varphi) \to (-t, -\varphi)$ reflection symmetry [42, 43]. A more general proof exists for all stationary solutions if the vector v is instead timelike [41].

First law: For two parametrically close, stationary, asymptotically flat black holes in four dimensions, the difference in horizon area is determined by the differences in mass M, spin J, and electric charge Q [36]:

$$\delta M = \frac{\kappa}{8\pi}\delta A + \Omega\delta J + \Phi\delta Q\,, \tag{2.1.1}$$

where Ω and Φ are potentials associated with the angular and electric charges. This law also holds for matter falling dynamically across the horizon, if the black hole returns to a stationary state [44].

Second law: In any classical process, the area of the event horizon cannot decrease [45, 46]:

$$\delta A \geq 0\,. \tag{2.1.2}$$

Third law: One cannot reduce the surface gravity of a horizon to zero in a finite number of steps [47].

Although the two sets of laws look similar, classically these laws are simply a formal analogy to the laws of thermodynamics. Since classically a black hole can only absorb matter and radiation, heat can never flow away from the horizon and it must have zero temperature. However, Bekenstein considered what would happen if an object was dropped across the horizon. The dropped object has entropy. On the other hand, both before and after the absorption of the object the black hole is completely determined by its mass, charge, and angular momentum. This suggests that the classical black hole has zero entropy and that the second law of thermodynamics has been violated during the absorption. One should therefore conclude that a purely classical viewpoint is naïve; the black hole does indeed possess an entropy. Bekenstein argued [48] that this entropy should be proportional to the area of the event horizon, a surprise given that entropy is extensive.

This hypothesis was vindicated a year later when Hawking [38] showed that horizons radiate a black-body spectrum at a temperature proportional to their surface gravity

$$T = \frac{\kappa}{2\pi} \,. \tag{2.1.3}$$

For a free field propagating on a classical black hole geometry, Hawking computed the expected number of particles in each mode at infinity at late times, discovering that it corresponds to a black body of finite size. Later it was shown [49] that all properties of the final state are congruent with black-body radiation. The result is quite general to theories of gravity, relying only on the the analysis of quantum fields exterior to the horizon; it does not rely on the gravitational field equations. The key insight in the calculation is that the null energy condition may be violated by the quantum fluctuations of the field, allowing the classical theorems we have discussed to be circumvented, allowing the black hole to radiate and decrease in size.

Given that quantum effects grant black holes a true physical temperature and one should expect a black hole to carry entropy, it is clear that the first law of black hole mechanics should indicate a true thermodynamic law. Insertion of the Hawking temperature (2.1.3) into the first law (2.1.1) indicates that one should identify the constant of proportionality between horizon area and entropy as one quarter:

$$S = \frac{A}{4} \,. \tag{2.1.4}$$

2.2 Black hole thermodynamics via the path integral

A thermal partition function associated with a given Lorentzian gravitational solution may be attained through a Wick rotation [50].

The partition function for a Euclidean gravitational solution with classical action $I[g, \psi_i]$ is given by

$$Z(\beta) = \int \mathcal{D}[g]\, \mathcal{D}[\psi_i]\, e^{-I[g,\psi_i]}\,. \tag{2.2.1}$$

The sum is taken over all (smooth) geometries g (and matter fields ψ_i) with an isometry along a compact direction with proper length β at infinity. The matter fields must also satisfy suitable fall-off conditions at infinity. For Lorentzian solutions with a Killing horizon, a possible conical singularity in the Euclidean section can appear at what was the horizon's location. The proper size of the compact direction shrinks to zero here. To attain a smooth solution, the singularity must be removed by a particular periodic identification. This required period β may be interpreted as an inverse temperature [50]. Working in a saddle-point approximation, we consider the classical contribution which possesses an extremised action.

$$-\log Z(\beta) \approx I[g, \psi_i]\,. \tag{2.2.2}$$

This approximation should give a reliable result for weakly curved spacetimes. Interpreting $Z(\beta)$ as the partition function for the canonical ensemble, we can equate the classical action with the product of the periodicity and Helmholtz[1] free energy $\mathcal{F}(T) = E(S) - TS$ of the system, since

$$\log Z(\beta) = -\beta\mathcal{F}\,. \tag{2.2.3}$$

The energy E and entropy S of the solution may then be calculated via the standard formulae

$$E = -\frac{\partial \log Z(\beta)}{\partial\beta}\,, \tag{2.2.4}$$

$$S = -\left(\beta\frac{\partial}{\partial\beta} - 1\right)\log Z(\beta)\,. \tag{2.2.5}$$

In order to evaluate the Euclidean action of the gravitational solution one requires some method of renormalisation, as the quantity is divergent. Early attempts at this, particularly when working with asymptotically flat space, came in the form

[1] As we will see later in this chapter, it is technically more correct to say that we are working in the Gibbs ensemble and that the free energy is the Gibbs free energy; in the absence of pressure and volume considerations, the two free energies coincide.

of background subraction [51], where one subtracts from the desired action that of a reference spacetime, typically flat space, with matching asymptotics. A more reliable approach—available for asymptotically anti-de Sitter spacetimes—has its footing in the holographic correspondence [52–54]: it has been shown that the intrinsic boundary geometry may be used to construct counterterms for the action which regulate its divergences [55].

This partition function-based approach also neatly illustrates the connection between horizon area and statistical entropy. Considering only the contribution to the action from an area of spacetime close to the horizon, we can choose coordinates (τ, r, ϕ_i) such that τ parametrises the time-circle, dr is normal to the horizon which lies at $r = r_+$, and a set of coordinates ϕ_i parametrise the other dimensions. We may integrate over a small disk $\mathcal{D}$, centred at the horizon point. The relevant contribution to the action is the Gibbons-Hawking-York boundary term for the edge of the disk, necessary to ensure that the action vanishes under arbitrary variations of the metric,

$$I_{\text{disc}} = \frac{1}{8\pi} \int_{\partial\mathcal{D}} d^{D-1}x \sqrt{\det h} \mathcal{K} \,, \tag{2.2.6}$$

where h is the induced metric on $\mathcal{D}$, and $\mathcal{K}$ is the trace of the extrinsic curvature over the boundary. Near the horizon, the metric is approximately $ds^2 \approx r^2\kappa^2 d\tau^2 + dr^2 + r_+^2 d\Omega^2$, where $d\Omega^2$ gives the metric on the unit S^{D-2} ball parametrised by the ϕ_i coordinates. Calculating the surface term,

$$I_{\text{disc}} = -\frac{1}{8\pi}\frac{\partial}{\partial\epsilon} \int_{r=r_++\epsilon} d^{D-1}x \sqrt{\det h} = -\frac{1}{8\pi}\frac{\partial}{\partial\epsilon} (2\pi\epsilon A) \tag{2.2.7}$$

By (2.2.5), the Euclidean calculation then gives an entropy which explicitly matches the numerical factor expected from combining the first law with Hawking's result for the temperature:

$$S = \frac{A}{4} \,. \tag{2.2.8}$$

2.3 Extended thermodynamics

In the thermodynamics we have considered to this point, there is a significant deviation from terrestrial thermodynamics: the first law for black holes lacks a term involving pressure and volume. In recent years, an approach to more closely align the first law of black hole thermodynamics and a typical Clausius-Clapeyron relation has been investigated by considering the cosmological constant to exert a vacuum pressure of the form familiar to cosmologists. To exert a positive pressure P on

spacetime, in this thesis we consider only the case of negative cosmological constant:

$$P = -\frac{\Lambda}{8\pi} > 0\,. \tag{2.3.1}$$

This may then be related to the anti-de Sitter length scale ℓ by

$$P = \frac{(D-1)(D-2)}{16\pi\ell^2}\,. \tag{2.3.2}$$

By embedding the gravitational theory in some more complete theory, one can envisage the cosmological constant arising as an expectation value from some set of dynamical fields. In this way, the cosmological constant can evolve in time, providing a varying pressure for the spacetime. One should then expect such variations to impact the first law, to providing a novel additive term in the first law. The first attempts at incorporating the cosmological constant dynamically were performed in [56, 57], who induced it from a three-form gauge potential coupled to the gravitational field. This mechanism can be derived from a Kaluza-Klein compactification [58] of M-theory on S^7. The dynamical cosmological constant was then incorporated into the first law in [59][2]. The interpretation of pressure's conjugate quantity was then uncovered in [62], wherein a first law and Gibbs–Duhem equation were written down for static black holes. These results were later generalised to rotating black holes with electric charge[3] [59, 63, 64]. This *extended first law* reads

$$\delta M = T\delta S + V\delta P + \Omega\delta J + \Phi\delta Q\,, \tag{2.3.3}$$

where, in the spirit of a typical Clausius-Clayperion relation the conjugate quantity to pressure

$$V = \left.\frac{\partial M}{\partial P}\right|_{S,J,Q} \tag{2.3.4}$$

has the dimensions of a spatial volume. The form of (2.3.3) indicates that, while traditionally associated with the black hole's internal energy U, M should more correctly be identified as a kind of spacetime *enthalpy*

$$M(S,P) = U(S,V) + PV\,. \tag{2.3.5}$$

In constructing a black hole, there is an additional amount of work which need to be done creating the cosmological environment in which it resides. The two quantities M and U are, of course, related by a Legendre transformation which allows one to work with whatever fundamental thermodynamic relation one prefers.

The novel pressure-entropy terms in the state function widen the thermodynamic

[2]See also [60, 61] for a similar investigation with a modern perspective.

[3]Such black holes may possess up to $\lfloor (D-1)/2 \rfloor$ independent rotations; we include only one.

phase spaces of black holes significantly, aligning them much more closely with the familiar phase spaces of chemical reactions. The field of examining black holes from this perspective was hence christened *black hole chemistry* [65, 66]. To date, a number of novel behaviours have been found within this framework. Notably, charged, static black holes with anti-de Sitter asymptotics obey an equation of state qualitatively similar to the van der Waals equation, and exhibit a first-order phase transition between small and large black holes [67, 68]. There is a critical point at one end the coexistence curve between the two phases, at which the transition becomes second-order and which possesses mean-field exponents. The system closely mimics the liquid-gas transition of an interacting fluid[4].

One might reasonably wonder if the enthalpy is the "true" energy of the black hole. Indeed, Gwak [70] argued that dropping electrically charged test particles into a near-extremal electrically charged black hole violates the second law of thermodynamics. Similar contradictions were subsequently acknowledged in a number of scenarios [71–79]. Gwak assumed that, in the extended thermodynamics framework, the energy of the particle should be converted to internal energy within the black hole. The issue was rectified by Hu et al. [80], who argued that—since it is the quantity calculated as a conserved charge at the boundary—the enthalpy M is the true measure of the energy of the spacetime and matter or radiation which imparts energy to the black hole should contribute it to the enthalpy of the geometry. When this is the case, there is no guaranteed violation of the second law; the area of the horizon should increase in accordance with Hawking's area theorem. A review of this argument is given in appendix A. We return to this point in chapter 4 where we argue similarly that a Penrose process must extract enthalpy from spacetime. These arguments give a clear indication that the true measure of a system's gravitational energy is it's enthalpy.

One straightforward way to see that the thermodynamic pressure and volume must enter the laws of black hole thermodynamics is to consider the Gibbs–Duhem relation, which in the context of black hole thermodynamics is usually referred to as the "Smarr relation" [81]. The following argument was proposed in [82]. A function f, dependent on some set of parameters Q_i, is homogeneous if it satisfies

$$\alpha^{a_0} f(Q_i) = f(\alpha^{a_i} Q_i) \tag{2.3.6}$$

for all non-zero scalars a_0 and a_i with $i \in \{1, \ldots, N\}$. By taking the derivative with

[4]It is even possible to reverse engineer a black hole, coupled to well-behaved matter, which obeys exactly the van der Waals equation of state [69].

respect to α, we see that f satisfies the scaling relation

$$a_0 f(Q_i) = \sum_{i=1}^{N} a_i \left(\frac{\partial f}{\partial Q_i}\right) Q_i \,. \tag{2.3.7}$$

Assuming the back hole mass to be a homogeneous function of the entropy, pressure, and charges $M = M(S, P, J, Q)$, Considering the dimensionalities of the various quantities leads one to conclude that

$$\begin{aligned}(D-3)\, M = &+ (D-2)\left(\frac{\partial M}{\partial S}\right) S + (-2)\left(\frac{\partial M}{\partial P}\right) P \\ &+ (D-2)\left(\frac{\partial M}{\partial J}\right) J + (D-3)\left(\frac{\partial M}{\partial Q}\right) Q \,. \end{aligned} \tag{2.3.8}$$

The usual definitions of conjugate quantities, $T = \frac{\partial M}{\partial S}\big|_{P,J,Q}$, $\Omega = \frac{\partial M}{\partial J}\big|_{S,P,Q}$, $\Phi = \frac{\partial M}{\partial Q}\big|_{S,P,J}$, then give the Smarr relation

$$M = \left(\frac{D-2}{D-3}\right)(TS + \Omega J) - \left(\frac{2}{D-3}\right) VP + \Phi Q \,. \tag{2.3.9}$$

Though the argument just given relies on the assumption that M is homogeneous of degree one half, it has been shown to hold directly for a wide variety of gravitational theories and solutions, including typical rotating, charged black holes with compact horizons [82], eternal black holes with a positive cosmoligcal constant [83], black holes evolving in cosmological enviroments [84], and three-dimensional topological black holes [85, 86]. Further, for theories with Killing vectors, it is possible to argue the Smarr relation from a geometric perspective. The argument is cleanest in the language of differential forms; we follow [87].

Consider a stationary, axisymmetric vacuum black hole with horizon generated by the vector field

$$\eta = k + \Omega m \,, \tag{2.3.10}$$

where m is a Killing vector generating rotations in some spatial two-plane, k is a Killing vector which is timelike at infinity, and Ω is the angular velocity of the horizon. The vector field η is Killing so satisfies $\nabla \cdot \eta = 0$ and $\nabla^2 \cdot \eta = -\mathcal{R}(g) \cdot \eta$.

Consider first the Ricci-flat case. Translating the relation for a Killing vector that we just wrote down, the horizon generator's dual one-form $\eta^\flat$ satisfies $d \star d\eta^\flat = 0$. After integration over some spacelike hypersurface Σ extending between the horizon and infinity, one can apply Stokes' theorem to find

$$0 = \int_{\partial\Sigma} \star d\eta^\flat = \int \star d\eta^\flat - \int_{S_\infty} \star d\eta^\flat \,, \tag{2.3.11}$$

where H is a spacelike slice of the horizon and S_∞ is the $(D-2)$-sphere at spatial

infinity. The integrals over S_∞ define two quantities conserved under translations in time [88, 89], the mass M and angular momentum J:

$$M = -\frac{(D-2)}{16\pi(D-3)}\int_{S_\infty} \star dk^\flat\,, \quad J = \frac{1}{16\pi}\int_{\mathrm{H}} \star dm^\flat\,. \tag{2.3.12}$$

It was shown in [36] that the integral over H gives a product of the horizon surface gravity and area, which we identify as the temperature and entropy by the arguments of the previous section:

$$\frac{1}{16\pi}\int_{\mathrm{H}} \star d\eta^\flat = TS\,. \tag{2.3.13}$$

Combining these results brings (2.3.11) straightforwardly into the form of the Smarr relation

$$(D-3)\,M = (D-2)\,(TS + \Omega J)\ . \tag{2.3.14}$$

The preceding argument extends to the case of a negative comological constant [62]. As we stated, η is Killing and so satisfies $d\star\eta^\flat = 0$. Hence, locally there exists a two-form ω_η such that $\eta^\flat = \star d\star\omega_\eta$. This two-form may be added to the integrands of (2.3.12) to form similar conserved charges in an asymptotically anti-de Sitter space [90, 91]. In the presence of a cosmological constant, the Einstein equations imply $\mathcal{R}(g) = 2(D-2)^{-1}\Lambda g$ so the horizon generator now satisfies $d\star d\eta^\flat + 2\Lambda\star\eta^\flat = 0$. Employing the definition of ω_η we get

$$d\star d\eta^\flat + 2\Lambda d\star\omega_\eta = 0\,. \tag{2.3.15}$$

Integrating similarly to the Ricci-flat case, we may break the integral up into four terms:

$$0 = \int_{S_\infty}\left(\star dk^\flat + 2\Lambda\star\omega_\eta\right) + \Omega\int_{S_\infty} dm^\flat + \int_{\mathrm{H}}\star d\eta - 2\Lambda\int_{\mathrm{H}}\star\omega_\eta\,, \tag{2.3.16}$$

Of course, ω_η is not unique. There exist translations by a one-form $\omega_\eta \to \omega_\eta + \nu$ which leave the right hand side of (2.3.16) invariant. Firstly, if ν is co-exact, $\nu = \star d\star\xi$ for any three-form ξ, then the integral of $\star\omega_\eta$ over either S_∞ or H is invariant by Stokes' theorem. Secondly, if ν is co-closed, $d\star\nu = 0$, then although each of the integrals $\int_{S_\infty}\star\omega_\eta$ and $\int_{\mathrm{H}}\star\omega_\eta$ are altered, their difference remains invariant, since

$$\int_{S_\infty}\star\omega_\eta - \int_{\mathrm{H}}\star\omega_\eta = \int_\Sigma d\star\nu = 0\,. \tag{2.3.17}$$

We seek to interpret the four terms in (2.3.16) similarly to those in (2.3.11). Firstly, the solution's angular momentum may be defined as in (2.3.12). The result (2.3.13) may also be used. On the other hand, the integral $\int_{S_\infty}\star dk^\flat$ is divergent so we cannot define mass as we did for the Ricci flat black hole. However, the integral $\int_{S_\infty}\star\omega_\eta$ is also divergent. The relation (2.3.16) guarantees that the two conspire in such a

way that the combination $\int_{S_\infty}\left(\star dk^\flat - 2\Lambda \star \omega_\eta\right)$ is finite. However, as we remarked, this combination is not invariant under gauge transformations of ω_η; the best be can do is to choose a gauge in which $-\frac{(D-2)}{16\pi(D-3)}\int_{S_\infty}\left(\star dk^\flat - 2\Lambda \star \omega_\eta\right)$ is coincident with the correct mass, which must be determined by another method, typically holographically as we discuss in section 2.3.1. In this gauge, a definition of the thermodynamic volume is

$$V = \frac{2-D}{16\pi}\int_{\mathrm{H}} \star\omega_\eta\,. \tag{2.3.18}$$

2.3.1 Calculating gravitational mass

Although the Komar integral may be used to calculate gravitational mass in Ricci-flat spacetimes possessing a Killing vector which is timelike at spatial infinity, in section 2.3 we described how this process can fail in the presence of a negative cosmological constant. Fortunately, in asymptotically (locally) anti-de Sitter spacetimes we have another route to the black hole mass. This technique has its roots in the "holographic correspondence" which posits an equivalence between the partition functions of (certain) theories of quantum gravity in D dimensions and an ordinary quantum field theory in $D-1$ dimensions [52, 53].

As mentioned in section 2.2, the addition of counterterms is necessary to ensure finiteness of the Euclidean action

$$I = \frac{1}{16\pi}\int_M d^4x\sqrt{g}\left[\mathcal{R}(g) + \frac{6}{\ell^2}\right] + \frac{1}{8\pi}\int_{\partial M} d^3x\sqrt{|h|}\,\mathcal{K} - \frac{1}{8\pi}I_{\mathrm{ct}}\,. \tag{2.3.19}$$

Here, $\mathcal{K}$ is the trace of the extrinsic curvature of the boundary metric h. The counterterms I_{ct} necessary to remove the divergences are quantities constructed from the intrinsic geometry h of the conformal boundary.

We assume that the manifold we are dealing with is the interior of a manifold with boundary, and that the bulk metric g has a second order pole at the boundary. We then assume there exists a *defining function* z which is positive in the interior, vanishing at the boundary, and for which the exterior derivative of which is non-vanishing at the boundary, such that $z^2 g$ smoothly extends to the boundary and is non-degenerate there. We call such a manifold "asymptotically locally anti-de Sitter" [92]. There are infinite possible defining functions z, and so the boundary is equipped with a family of conformally equivalent metrics, known as a conformal structure.

The minimal counterterm action, in various bulk dimensions D, is given by [55]

$$I_{\rm ct} = \begin{cases} \int_{\partial M} d^2x\sqrt{-h}\left(\frac{1}{\ell}\right), & D=3\,, \\ \int_{\partial M} d^3x\sqrt{h}\left(\frac{2}{\ell}+\frac{\ell}{2}\mathcal{R}(h)\right), & D=4\,, \\ \int_{\partial M} d^4x\sqrt{-h}\left(\frac{3}{\ell}+\frac{\ell}{4}\mathcal{R}(h)\right), & D=5\,, \\ \int_{\partial M} d^{D-1}x\sqrt{|h|}\left(\frac{D-1}{\ell}+\frac{\ell}{2\,(D-3)}\mathcal{R}(h)+\ldots\right), & D>5\,. \end{cases} \tag{2.3.20}$$

In the above, ellipses denote additional counterterms which are higher-than-first-order in the boundary Ricci curvature.

Variation of the complete counterterm action in the usual way defines a stress-energy tensor [93] from which a conserved charge associated to a given Killing vector of the boundary theory may be calculated [51]. Explicitly, the stress tensors relevant for our purposes in later chapters are:

$$T_{\mu\nu} = \frac{1}{8\pi}\begin{cases} -\left(\mathcal{K}_{\mu\nu}-\mathcal{K}h_{\mu\nu}\right)-\ell^{-1}h_{\mu\nu}\,, & D=3\,, \\ -\left(\mathcal{K}_{\mu\nu}-\mathcal{K}h_{\mu\nu}\right)-2\ell^{-1}h_{\mu\nu} & \\ \qquad\qquad +\ell\left(\mathcal{R}(h)_{\mu\nu}-\frac{1}{2}\mathcal{R}(h)h_{\mu\nu}\right), & D=4\,. \end{cases} \tag{2.3.21}$$

Note that the metric h diverges as z^{-2} as the conformal boundary is approached $z\to 0$. We may multiply through by the defining function squared to define a finite stress tensor associated with the manifold's conformal structure. A conserved charge [51] associated with a killing vector η is given by [93]

$$Q[\eta] = \int_\Sigma d^{D-2}x\sqrt{\sigma}\,(u\cdot T\cdot\eta)\,, \tag{2.3.22}$$

where σ is the induced metric on, and u is the future-pointing unit normal to, a time-slice Σ of the boundary geometry. Once a suitable generator η of a timelike isometry of the boundary geometry has been identified, one attains a mass.

It should be noted that other means of calculating conserved quantities in asymptotically anti-de Sitter spaces have been attempted. In particular, in the literature surrounding the four-dimensional accelerating black hole we discuss in chapter 3, a definition of mass exploiting the conformal structure of the boundary due to Ashtekar and Das [94] is sometimes encountered. While this may be viewed as an alternative (equivalent) approach for a theory with an odd dimensional boundary, for black holes with even dimensional conformal boundaries it has been shown to fail to reproduce the appropriate conserved charge [95, 96]. This is due to the counterterms breaking conformal invariance in the boundary theory in these cases.

2.3.2 The Reverse Isoperimetric Inequality

The nature of thermodynamic volume is not well understood. A number of attempts at relating thermodynamic volume to a purely geometric quantity have been attempted, including attempts to compute the volume by integrating "inside the horizon" [97–99], attempts at defining an internal volume of the black hole using quantities defined outside the horizon [100], and attempts based on dynamical considerations [101]. None of these are particularly compelling; they all fail to reproduce the thermodynamic volume of desirable spacetimes, in particular that of Kerr-AdS. The best definition we have available is the one utilising the Killing co-potential (2.3.18), which is not entirely geometric as it relies on one's ability to define the spacetime mass. That said, there is some understanding of the *behaviour* of the thermodynamic volume. We now discuss a conjecture relating it to the area of the horizon.

The Isoperimetric Inequality states that the area of a two-dimensional shape is maximised when its perimeter forms a circle. The higher-dimensional analogue of this statement is that a $(D-1)$-dimensional closed volume V and the $(D-2)$-dimensional volume A of its boundary are related by

$$\Pi \equiv \left((D-1)\frac{V}{v_{D-1}}\right)^{\frac{1}{D-1}} \left(\frac{v_{D-1}}{A}\right)^{\frac{1}{D-2}} \leq 1\,, \tag{2.3.23}$$

where v_n is the volume of an n-dimensional unit ball:

$$v_n = \frac{\pi^{\frac{n}{2}+1}}{\Gamma\left(\frac{n}{2}+1\right)}\,. \tag{2.3.24}$$

It was noticed in [87] that, at fixed thermodynamic volume, compact black holes seem to have maximal entropy when static. This led to the conjecture that for asymptotically anti-de Sitter black holes, the *Reverse Isoperimetric Inequality* holds between the thermodynamic volume V and horizon area A:

$$\Pi \geq 1\,. \tag{2.3.25}$$

The conjecture has been shown to hold in a variety of contexts, including compact black holes with spherical horizon topology [87], and ultraspinning black rings with toroidal horizon topology [64]. Even apparent exceptions to the hypothesis [102, 103], for which the black hole horizon is non-compact, have since had their incongruity resolved [104]. We will return to this conjecture in chapter 4, where we shall prove it for accelerating black holes.

Chapter 3

Accelerating black holes in four dimensions

3.1 Overview

In order to investigate the effects of accelerating a black hole, one requires a suitable model. This is provided by the C-metric, the prototypical model of a stationary black hole undergoing acceleration. The C-metric, in its most simple form, consists of a compact black hole horizon with the topology of a two-sphere less two points. At these antipodal points, one finds conical singularities which extend outwards in opposing directions. These topological defects are under tension, and an imbalance in the two provides a force of acceleration and distorts the horizon. The C-metric also has generalisations which include rotational and electromagnetic charges. In this chapter we will refer to a number of these as "the C-metric"; the geometry under consideration should be clear from context.

The conical singularities may be considered first-order approximations to physical objects, such as finite-width cosmic strings [105] and magnetic flux tubes [106]. These physical objects are examples of *topological defects*, solitonic solutions to field theories which can arise when the vacuum manifold possesses a non-trivial fundamental group [107]. Specifically, a (local) cosmic string is an approximately two-dimensional object (with local support in the transverse directions), which may arise when one couples the gravitational field to other matter.

The prototypical model of such a string is the Nielsen-Olesen vortex [108], a solution to the Abelian-Higgs model in which the phase of the Higgs scalar field winds around a line-like "core". Both the $U(1)$-gauge and Higgs modes are strongly localised, decaying rapidly in directions orthogonal to the core. This decay is exponential in the absence of a cosmological constant, with a rate set by the mass of the Higgs

[109, 110]. The spacetime away from these localised matter fields is curvature-free, (save for a possible contribution from a cosmological constant). However, the proper circumference of a circle enclosing the string is found to be in proportion to its proper radius from the core by a factor not-equal to 2π. For a string of positive energy density, the circumference is found to be "shortened" by a quantity proportional to that energy density. The core is thus referred to as a *conical deficit*.

When observed from a distance, the key attributes of a cosmic string are then encapsulated in the behavior of the conical defect. Thus, by constructing models of spacetimes containing cosmic strings, one can begin to understand the interactions between strings and black holes. In particular, one can gain insight into the thermodynamic behavior of these objects. Further support for this approach arrived with the discovery of solutions of Einstein-Maxwell theory for which the Nielsen-Olesen vortex passes through the horizon of a black hole without incident [111–113]. The C-metric is one such solution [105].

In the rest of this chapter, we introduce the C-metric in its generalised form. We present its basic attributes in section 3.2, before specialising to the case of negative cosmological constant in section 3.3. We explain the existence of a phase in which the acceleration of the black hole is low enough that the solution exhibits a single, isolated, compact horizon, and review some recent success in understanding the thermodynamic behaviour of the solution in this phase.

3.2 The Plebański-Demiański solution

Though the static form of the C-metric has been known for over a century [114], it has more recently been shown by Plebański and Demiański [115] (and independently by Debever [116]) that a broader class of solutions exhibiting both electromagnetic and rotational charges exists. In fact, this generalised solution accommodates the existence of a non-zero cosmological constant. This possibility of forming a C-metric-like solution with Anti-de Sitter asymptotics [92] later proved invaluable in formulating a consistent thermodynamic description of such systems. We will discuss these developments in section 3.3.

We wish to understand the interplay between acceleration and other charges so we take the Plebański-Demiański metric [115] as our starting point. It reads

$$ds^2 = \frac{1}{(x-y)^2}\left\{\frac{P(y)}{1+(xy)^2}\left[d\tau + x^2 d\sigma\right]^2 - \frac{1+(xy)^2}{P(y)}dy^2 \right. \\ \left. - \frac{1+(xy)^2}{Q(x)}dx^2 - \frac{Q(x)}{1+(xy)^2}\left[y^2 d\tau - d\sigma\right]^2\right\}, \quad (3.2.1)$$

with metric functions

$$\begin{aligned} P(y) &= -\left(\frac{\Lambda}{3}+\kappa\right) + 2ny + \varepsilon y^2 + 2my^3 + \left(\kappa + e^2 + g^2\right) y^4 \,, \\ Q(x) &= \kappa - 2nx - \varepsilon x^2 - 2mx^3 - \left(\kappa + e^2 + g^2 + \frac{\Lambda}{3}\right) x^4 \,, \end{aligned} \tag{3.2.2}$$

and associated gauge field

$$B = \frac{ey}{1+(xy)^2}\left[d\tau + x^2 d\sigma\right] + B_\tau d\tau + B_\sigma d\sigma + \frac{gx}{1+(xy)^2}\left[y^2 d\tau - d\sigma\right] . \tag{3.2.3}$$

We have chosen to parametrise the metric functions slightly differently to the original form [115]. However, the salient point is that P and Q are each are fourth order polynomials. Note that any choice of B_t and B_σ will solve the equations of motion in some region, though there is no choice of both which makes B globally well defined for non-zero magnetic charge. Though x and y are dimensionless coordinates, the Plebański-Demiański form of the solution has the unfavourable attribute that both τ and σ have dimensions of length squared. One may resolve this by introducing two length scales to the system via new parameters, a and A. These possesses dimensions of length and inverse length, respectively, and we refer to them as the rotational and acceleration scales. One may now form dimensionless coordinates

$$x \to (aA)^{\frac{1}{2}} x \,, \qquad y \to (aA)^{\frac{1}{2}} y \,, \qquad \tau \to \left(\frac{a}{A^3}\right)^{\frac{1}{2}} \tau \,, \qquad \sigma \to \left(\frac{a}{A^3}\right)^{\frac{1}{2}} \sigma \,, \tag{3.2.4}$$

and introduce dimensionless parameters and metric functions

$$\begin{aligned} &m \to \left(\frac{A}{a}\right)^{\frac{3}{2}} m \,, \quad n \to \left(\frac{A}{a}\right)^{\frac{1}{2}} n \,, \quad e \to \left(\frac{A}{a}\right) e \,, \quad g \to \left(\frac{A}{a}\right) g \,, \\ &\varepsilon \to \left(\frac{A}{a}\right) \varepsilon \,, \qquad \kappa \to A^2 \kappa \,, \qquad P \to A^2 P \,, \qquad Q \to A^2 Q \,. \end{aligned} \tag{3.2.5}$$

The line element then takes the form [117]

$$\begin{aligned} ds^2 = \frac{1}{A^2 (x-y)^2} \Bigg\{ &\frac{P(y)}{1+(aAxy)^2}\left[d\tau + aAx^2 d\sigma\right]^2 - \frac{1+(aAxy)^2}{P(y)} dy^2 \\ &- \frac{1+(aAxy)^2}{Q(x)} dx^2 - \frac{Q(x)}{1+(aAxy)^2}\left[aAy^2 d\tau - d\sigma\right]^2 \Bigg\} , \end{aligned} \tag{3.2.6}$$

with metric functions

$$\begin{aligned} P(y) &= \left(\frac{1}{A^2\ell^2} - \kappa\right) + \frac{2n}{A} y + \varepsilon y^2 + 2mAy^3 + A^2\left(\kappa a^2 + e^2 + g^2\right) y^4 \,, \\ Q(x) &= \kappa - \frac{2n}{A} x - \varepsilon x^2 - 2mAx^3 + \left(\frac{a^2}{\ell^2} - A^2\left(\kappa a^2 + e^2 + g^2\right)\right) x^4 \,. \end{aligned} \tag{3.2.7}$$

The gauge field must also be updated:

$$B = \frac{ey}{1+(aAxy)^2}\left[d\tau + aAx^2 d\sigma\right] + B_\tau d\tau + B_\sigma d\sigma \\ + \frac{gx}{1+(aAxy)^2}\left[aAy^2 d\tau - d\sigma\right] . \quad (3.2.8)$$

Again, any reasonable choices of B_τ and B_σ solve the equations of motion in some region.

This general metric has two disjoint Killing horizons at $x = \pm 1$. These are known as Misner strings—massless, singular sources of angular momentum [118–120]—and introduce significant complications to the thermodynamic analysis [121, 122]. As we are interested in understanding acceleration only, we will consider only the case for which this "NUT charge" vanishes [115]. This in general requires a particular choice of n. See [123, 124] for studies of accelerating black holes possessing NUT charge. After removing the NUT charge, the parametrisation above is in keeping with [125] and, as we will see later when the true physical quantities of the solution are calculated, allows one to interpret m, A, a, e, and g as measures of mass, acceleration, rotational charge, electric charge, and magnetic charge respectively [126, 127].

One will note that there are two parameters we have not yet discussed: κ and ϵ. In fact, by examining the curvature invariants of the spacetime, one finds that these are entirely gauge. There are two common choices of these parameters. The most obvious is to take

$$\kappa = 1\,, \qquad\qquad \varepsilon = 1\,. \quad (3.2.9)$$

In this case we must set $n = 0$ to remove the Misner strings [117]. Upon taking the limit $a \to 0$, this gives the (non-rotating) C-metric in a form familiar to most relativists: the one originally written down by Kinnersley and Walker [128] in Ricci-flat space and subsequently generalised to the case of non-zero cosmological constant by Griffiths and Podolsky [126]:

$$ds^2 = \frac{1}{A^2(x-y)^2}\left\{P(y)d\tau^2 - \frac{dy^2}{P(y)} - \frac{dx^2}{Q(x)}dx^2 - Q(x)d\sigma^2\right\}, \quad (3.2.10)$$

with metric functions

$$Q(x) = 1 - x^2 - 2mAx^3 - A^2\left(e^2+g^2\right)x^4\,, \\ P(y) = \frac{1}{A^2\ell^2} - Q(y)\,. \quad (3.2.11)$$

While common in the literature, the form of the C-metric using the gauge (3.2.9) is less than intuitive, in part due to the unwieldy structure functions. It was shown by

Hong and Teo that for the non-rotating case $a = 0$, an alternative gauge fixing allows the structure function $Q(x)$ to be (at least partially) factorised [129]. This result has since been generalised to the cases of rotation without cosmological constant [130], rotation with cosmological constant [125], and rotation without cosmological constant but with NUT parameter [124]. It seems probable that factorisation of $Q(x)$ will soon be achieved for the general Plebański-Demiański solution. We quote the second of these results, as it is general enough for our purposes:

$$\kappa = 1\,, \qquad\qquad \varepsilon = 1 + \frac{a^2}{\ell^2} - A^2\left(a^2 + e^2 + g^2\right)\,. \tag{3.2.12}$$

To remove the NUT charge in this instance, one must set $n = -mA^2$. The metric takes the form (3.2.6) with the metric functions

$$\begin{aligned} Q(x) &= \left(1 - x^2\right)\left(1 + 2mAx + \left(A^2(a^2 + e^2 + g^2) - \frac{a^2}{\ell^2}\right)x^2\right)\,, \\ P(y) &= \frac{1 + a^2A^2y^4}{A^2\ell^2} - Q(y)\,. \end{aligned} \tag{3.2.13}$$

The discovery of this factorisation of $Q(x)$ also had the unforeseen consequence that one can now easily recognise that the geometry forms an extension of a well-known family of black holes by making the following transformation to *Boyer-Lindquist coordinates* (t, r, θ, φ) [115, 125, 128]:

$$\tau = A\left(\frac{t}{\alpha} - a\frac{\varphi}{K}\right)\,, \qquad y = -\frac{1}{Ar}\,, \qquad x = \cos\theta\,, \qquad \sigma = \frac{\varphi}{K}\,. \tag{3.2.14}$$

Here, α is some as yet undetermined dimensionless quantity which we may insert by exploiting the isometry generated by the Killing vector ∂_t. A particular value will prove necessary for the discussion of thermodynamics later in the chapter; at this point it is immaterial. We have also introduced a dimensionless parameter K such that the period of φ is 2π. K typically tracks the presence of conical deficits in the spacetime and thus has physical content. The line element is now

$$\begin{aligned} ds^2 = \frac{1}{H^2}\Bigg\{ &\frac{f(r)}{\Sigma}\left[\frac{dt}{\alpha} - a\,\sin^2\theta\frac{d\varphi}{K}\right]^2 - \frac{\Sigma}{f(r)}dr^2 \\ &- \frac{\Sigma}{g(\theta)}r^2d\theta^2 - \frac{g(\theta)}{\Sigma}\frac{\sin^2\theta}{r^2}\left[a\frac{dt}{\alpha} - (r^2 + a^2)\frac{d\varphi}{K}\right]^2\Bigg\}\,, \end{aligned} \tag{3.2.15}$$

with metric functions given by

$$\begin{aligned} f(r) &= (1-A^2r^2)\left[1-\frac{2m}{r}+\frac{a^2+e^2+g^2}{r^2}\right]+\frac{r^2+a^2}{\ell^2}\,, \\ g(\theta) &= 1+2mA\cos\theta+(\Xi-1)\cos^2\theta\,, \\ \Sigma &= 1+\frac{a^2}{r^2}\cos^2\theta\,, \qquad H = 1+Ar\cos\theta\,, \\ \Xi &= 1+\left(e^2+g^2\right)A^2-\frac{a^2}{\ell^2}(1-A^2\ell^2)\,. \end{aligned} \tag{3.2.16}$$

Notice that a limit $A \to 0$ of the geometry exists. By the translational symmetry of φ, one may then choose $K = \Xi$ to recover the Kerr-Newmann geometry with a cosmological constant [131], describing a charged and rotating black hole. Of course, by setting either or both of a and the pair e and g to zero, one can recover the Kerr [131–134], Ressiner-Nordström, or Schwarzschild solutions with a cosmological constant. One may then formally take the AdS length scale to infinity to attain their asymptotically-flat counterparts. Given this limit, it seems appropriate to consider a, e, and g to be rotational, electric, and magnetic parameters respectively. We will soon calculate the true conserved charges and show that this is justified. The gauge field associated with the line-element (3.2.15) is

$$B = -\frac{e}{\Sigma r}\left[\frac{dt}{\alpha}-a\sin^2\theta\frac{d\varphi}{K}\right]+\Phi_t dt+\frac{g\cos\theta}{\Sigma r^2}\left[a\frac{dt}{\alpha}-(r^2+a^2)\frac{d\varphi}{K}\right]. \tag{3.2.17}$$

For concreteness, we now choose to make specific choices of B_τ and B_σ, encoded in

$$\Phi_t = \frac{er_+}{\alpha\left(a^2+r_+^2\right)}\,, \tag{3.2.18}$$

such that the gauge potential $-\eta\cdot B$ vanishes on the surface $r = r_+$. Here, η is normal to the surface.

3.3 Properties of the C-metric with negative cosmological constant

We now examine the properties of the charged, rotating, C-metric with a negative cosmological constant, described by equations (3.2.15), (3.2.16), and (3.2.17). We require the solution to describe a compact black hole horizon, disjoint from the boundary. As we will see, there may also be a non-compact "acceleration horizon" in the space, for certain choices of parameters.

As is common, and without loss of generality, we take a non-negative acceleration parameter A. Similarly, we also consider e and g non-negative. A change in the sign

of a may be compensated by a change in the sign φ; we have the freedom to choose $a \geq 0$. Finally, flipping the sign of m may be compensated by similar redefinitions of the coordinates r and θ. We thus have the freedom to take $m \geq 0$.

The metric (3.2.15) has coordinate singularities at $\theta = 0, \pi$. These dictate the north and south poles of our black hole; we thus require $g(\theta) > 0$ on $(0, \pi)$. The non-zero components of the Weyl and Ricci curvature tensors are [125]

$$\begin{aligned} \Psi_2 &= \left(\frac{H(e^2+g^2)}{r - ia\cos\theta} - (1+iaA)\right)\left(\frac{H}{r+ia\cos\theta}\right)^3, \\ \Phi_{11} &= \frac{e^2+g^2}{2}\left(\frac{H^2}{r^2\Sigma}\right)^2, \\ \Lambda &= -\frac{3}{\ell^2}. \end{aligned} \tag{3.3.1}$$

There is thus a Kerr-like ring singularity at $r = 0, \theta = \pi/2$. The maximal range of r is then

$$0 < r < r_\infty \quad \text{where} \quad \begin{cases} -\frac{1}{A\cos\theta} & \text{if } \theta > \frac{\pi}{2}, \\ \infty & \text{otherwise}. \end{cases} \tag{3.3.2}$$

Positivity of the conformal factor H, constrains $Ar\cos\theta < 1$ and sets the location of the conformal boundary $r_{\text{bd.}} = -1/A\cos\theta$. In some sense, for $\theta \leq \pi/2$, the conformal boundary is situated "beyond infinity" in these coordinates. The true location of the boundary is more clearly expressed in the coordinates (3.2.6), for which the boundary is defined by the surface $x = y$. Since we require a black hole, we demand that f have a root r_+ for $r_+ > 0$ for which $f'(r_+) > 0$. Roots of f define null hypersurfaces in the spacetime; the surface $r = r_+$ is the black hole horizon and has normal $\eta = \partial_t + \Omega_{r_+}\partial_\varphi$, where

$$\Omega_{r_+} = \frac{aK}{\alpha\,(r_+^2 + a^2)} \tag{3.3.3}$$

is the angular velocity of an observer at the horizon moving on an orbit of η with respect to a stationary observer. The region between r_+ and either a larger root of f or the conformal boundary is then the immediate black hole exterior.

These constraints restrain the metric parameters significantly. First, $g(\theta) \geq 0$ gives a bound on the possible values of the dimensionless mass:

$$mA < \begin{cases} \Xi/2, & \text{for } \Xi \in (0, 2], \\ \sqrt{\Xi - 1}, & \text{for } \Xi > 2. \end{cases} \tag{3.3.4}$$

However, the fact that the black hole horizon does not intersect the boundary requires $Ar_+ < 1$, hence the Kerr-Newman potential multiplying $(1 - A^2r_+^2)$ in $f(r_+) = 0$

must be negative. This in turn requires

$$m^2 > a^2 + e^2 \qquad \Rightarrow \qquad m^2 A^2 > \Xi - 1 + \frac{a^2}{\ell^2} > \Xi - 1\,. \tag{3.3.5}$$

Thus, by comparison with (3.3.4), we see that $\Xi > 2$ is not allowed. Hence

$$mA \leq \frac{\Xi}{2} < 1. \tag{3.3.6}$$

Another significant constraint one can impose is that the black hole be *slowly accelerating*. Usually, an object under uniform acceleration will have an acceleration horizon, as ultimately the object will asymptote the speed of light. In particular this is true for the Ricci-flat C-metric attained by formally taking the $\ell \to \infty$ limit of (3.2.15). However, in AdS spacetime, the negative curvature of the space means that an isolated black hole held a fixed finite displacement from the centre of the spacetime can actually undergo uniform acceleration, if the parameter A is small enough. This means its (Boyer-Lindquist) time coordinate is proportional to the asymptotic time for an observer near the conformal boundary. This régime of accelerating black hole solutions that are truly static with respect to an observer at the boundary are called *slowly accelerating* black holes [135]. For the black hole to be isolated in this way (i.e. the only event horizon being that of the black hole) we require no zeros of f on the boundary. Define a function

$$\Upsilon(x) = 1 + a^2 A^2 x^4 - A^2 \ell^2 Q(x)\,, \tag{3.3.7}$$

where $Q(x)$ is given by equation (3.2.13). The slow acceleration condition is then the straightforward algebraic bound

$$\Upsilon(x) > 0\,. \tag{3.3.8}$$

This condition must of course be satisfied in conjunction with the existence of a black hole horizon. This is a rather involved set of constraints which are most easily examined numerically. This has been done in considerable detail in the literature [136]. We make some general comments here. Roughly speaking, the criterion for slow acceleration is that the scale set by acceleration A^{-1} is much larger than the AdS radius: $A\ell \lesssim 1$. The true limit is dependent on the mass, charge, and angular momentum of the black hole. As the acceleration increases, the position of the suspended black hole moves closer to the boundary until at $A\ell \sim 1$ there is a shift in the global structure of the spacetime and for $A\ell \gtrsim 1$, the black hole now accelerates in from, and out to, the AdS boundary. See [137] for a discussion of the causal structure of the C-metric.

In this slowly accelerating régime, one can make a straightforward argument that

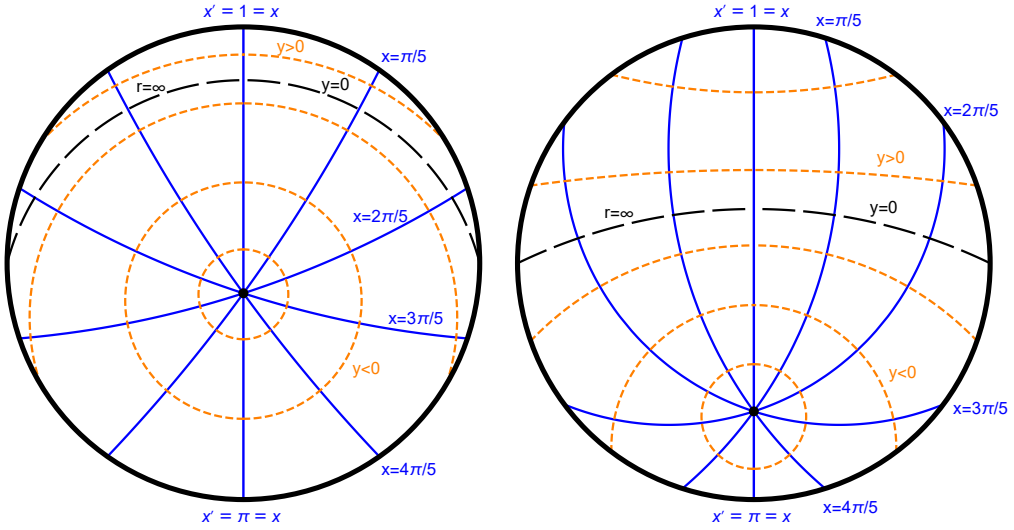

(a) $A\ell = 0.3$ (b) $A\ell = 0.9$

Figure 3.1: Anti-de Sitter space in slowly accelerating coordinates. Lines of constant x (equivalently θ) are shown in solid blue. Lines of constant y (equivalently r) are shown in dashed orange. $y \to -\infty$ ($r = 0$) is shown as an off-centre point, while $y = 0$ ($r \to \infty$) is denoted in dashed black.

the black hole is accelerating [135]. Consider the non-rotating, vacuum black hole, defined by $a = 0$, $e = 0$, and $g = 0$. Consider making the horizon radius incredibly small by taking the limit $m \to 0$. A particle at a fixed radius $r = r_0$ then follows a well-defined worldline with normalised four-velocity

$$u^\mu = \left(\frac{\alpha H}{\sqrt{f(r)}}, 0, 0, 0 \right)^\mu \Bigg|_{r=r_0} . \tag{3.3.9}$$

Calculating the magnitude of the associated four-acceleration $a^\nu = u^\mu \nabla_\mu u^\nu$ at the black hole's location yields $|a| = A$ [135]. We see that the local acceleration of the small black hole is exactly given by the acceleration parameter. The geometry of this argument is shown in figure 3.1, where we show the extent of Boyer-Lindquist coordinates. The small black hole is drawn closer to the boundary as A increases. As $A \to 1$, the black hole merges with the boundary and black hole ceases to be slowly accelerating.

Though we have established that the black hole is accelerating, we have not yet provided a mechanism for the acceleration. The acceleration in the C-metric is provided by two line-like topological defects. There exist other mechanisms—for example immersion of the black hole in an external electromagnetic field [138–144]—however such solutions typically exhibit undesirable behaviour at infinity. The

C-metric possess up to two topological defects: one lying along the North pole $\theta = \theta_+ \equiv 0$ and the other along the South pole $\theta = \theta_- \equiv \pi$. As remarked earlier, such deficits are interpreted as cosmic strings emerging from the black hole [145], as the conical deficits can be smoothed out by a typical cosmic string core [105, 111–113]. A conical deficit betrays a ratio of (proper) circumference about a point to the (proper) radius to that point which differs from 2π. The presence (or not) of conical deficits is revealed by expanding the angular components of the metric near each axis:

$$d\theta^2 + (h(\theta)\sin\theta)^2 \frac{d\varphi^2}{K^2} \sim d(\theta-\theta_\pm)^2 + (\Xi \pm 2mA)^2 (\theta-\theta_\pm)^2 d\varphi^2 \,. \tag{3.3.10}$$

The ratio of proper circumference to radius is then

$$\frac{\mathcal{C}}{\mathcal{R}} = \frac{2\pi}{(\Xi \pm 2mA)K} \left(\frac{h(\theta)\sin\theta}{\theta - \theta_\pm} \right) , \tag{3.3.11}$$

This quantity is then demonstrably not equal to 2π at the points $\theta = \theta_\pm$. The deviation from the expected result, $\delta = 2\pi - \mathcal{R}^{-1}\mathcal{C}$ dictates the tension μ in the string via $\delta = 8\pi\mu$. Calculating the deficits along the North and South axes gives:

$$\mu_\pm = \frac{\delta_\pm}{8\pi} = \frac{1}{4}\left[1 - \frac{\Xi \pm 2mA}{K}\right] . \tag{3.3.12}$$

Often in the literature, K is chosen such that μ_+ vanishes. This regularises the North axis. Note that for $A \neq 0$, no choice of K is possible which regularises both poles simultaneously. We do not wish to entangle the physics of deficits with the physics of acceleration so will not restrict ourselves thus and instead allow both tensions to vary. There is clearly a sense in which $K = \Xi(1-4\bar{\mu})^{-1}$ tracks the average tension $\bar{\mu}$ between the two deficits, while the acceleration parameter tracks the difference in tensions via $mA = (\mu_- - \mu_+)K$.

3.3.1 Thermodynamics of the C-metric in anti-de Sitter space

We now turn a discussion of the thermodynamics of the system. Given that increasing the acceleration parameter from zero distorts the event horizon, it is clear that the thermodynamic parameters of the solution must change. In fact, even the simple act of adding an average deficit through the Kerr-Newmann-AdS solution alters the horizon area, and thus the entropy, of the black hole by a factor of K. This suggests a question: after determining how all of the thermodynamic charges should be modified by the introduction of parameters K and A, does the first law of thermodynamics still hold? This question was first posed for static black holes in [146] with the

answer in the affirmative if the conical defects remain fixed. This breakthrough owed its success to the existence of the slowly accelerating phase of the C-metric with negative cosmological constant. As we remarked, in this phase there is a single, compact, black hole horizon and there are no acceleration horizons. This renders all thermodynamic quantities calculable with current technologies; there is no consensus in the literature regarding the correct way to calculate thermodynamic quantities for solutions with non-compact horizons [147]. In fact, choosing to fix the conical deficits obscured the more general result that the first law still still holds when the tensions are allowed to vary [148, 149]. In this case, each string tension acts like a thermodynamic charge in the first law, with an associated conjugate quantity: the *thermodynamic length*. A similar conjugate quantity with dimensions of length was later shown to hold for more general stationary solutions [150, 151]. We now review this general result for the geometry (3.2.15) in its slowly accelerating phase.

The entropy of the solution is the easiest quantity to calculate, being simply given by one quarter of the area of the black hole horizon:

$$S = \frac{\pi\left(r_+^2 + a^2\right)}{(1 - A^2 r_+^2)\, K}\,. \tag{3.3.13}$$

The temperature of the black hole is also straightforward, due to the trick of imposing regularity on the Wick-rotated geometry. To attain the Euclidean section, we perform the Wick rotation $t_E = it$ and introduce real variables $a_E = -ia$ and $e_E = -ie$. We then transform to new coordinates (τ, φ) via

$$t_E = \tau\,, \qquad\qquad \phi = \varphi - i\Omega_{r_+}\tau\,. \tag{3.3.14}$$

These variables are such that the horizon generator becomes $\eta = i\left(\partial_\tau - i\Omega_{r_+}\partial_\varphi\right)$. The Euclidean geometry is regular at $r = r_+$ provided we identify $(\tau, \varphi) \sim (\tau + \beta, \varphi)$ together with $(\tau, \varphi) \sim (\tau, \varphi + 2\pi)$. We may identify (the reciprocal of) the periodicity β of τ with the temperature T:

$$T = \beta^{-1} = \frac{r_+^2 f'(r_+)}{4\pi\alpha\,(r_+^2 + a^2)}\,. \tag{3.3.15}$$

In the (t_E, ϕ) coordinates, the identification becomes twisted and one finds that traversing a complete orbit of the time circle effects a shift in ϕ proportional to the horizon's angular velocity:

$$(t_E, \phi) \sim (t_E + \beta, \phi + i\beta\Omega_{r_+})\,. \tag{3.3.16}$$

Many of the other thermodynamic quantities are most reliably calculated by holographic techniques [149] (see also [150–152]). The first step in this process is to

transform the metric to Fefferman-Graham gauge

$$ds^2 = -\frac{\ell^2}{z^2}dz^2 + \frac{\ell^2}{z^2}\left(g_{(0)} + z^2 g_{(2)} + z^3 g_{(3)} + \mathcal{O}(z^4)\right) . \tag{3.3.17}$$

Here, $g_{(0)}$, $g_{(2)}$, and $g_{(3)}$ are covariant two-tensors. One may achieve this Fefferman-Graham gauge near the boundary using a systematic expansion [149]. This is most easily performed from the coordinates (3.2.6), from which the entire boundary is accessible.

$$y = \xi + \sum_{m=1}^{\infty} F_m(\xi)\left(\frac{z}{\ell}\right)^m , \qquad x = \xi + \sum_{m=1}^{\infty} G_m(\xi)\left(\frac{z}{\ell}\right)^m . \tag{3.3.18}$$

Expanding the metric in this way, and enforcing Fefferman-Graham gauge at successive orders in z, one may determine $g0$, $g_{(2)}$,and $g_{(3)}$ perturbatively. The resulting representative of the conformal structure is found to be

$$\begin{aligned} g_{(0)} = \frac{\Upsilon^2(\xi)}{A^2 F_1 \Sigma^3}\Bigg(&Q(\xi)\left[aA\xi^2\left(\frac{Adt}{\alpha}\right) - \left(1 + a^2A^2\xi^2\right)\frac{d\varphi}{K}\right]^2 \\ &- \Upsilon(\xi)\left[\frac{a}{\ell}\left(1-\xi^2\right)\frac{d\varphi}{K} - \frac{1}{A\ell}\left(\frac{Adt}{\alpha}\right)\right]^2 - \frac{\Sigma^3}{\Upsilon(\xi)Q(\xi)}\Bigg) . \end{aligned} \tag{3.3.19}$$

One may then define a stress-energy tensor T_z at some surface of constant z, by the method of section 2.3.1. In the Fefferman-Graham gauge, this definition (2.3.21) is written

$$\begin{aligned} T_z = -\frac{\ell}{8\pi}\Bigg(&-\left(\mathcal{R}(g_{(0)}) - \frac{1}{2}g_{(0)}\,\mathrm{Tr}[g_{(0)}^{-1}\mathcal{R}(g_{(0)})]\right) \\ &+ \left(g_{(2)} - g_{(0)}\,\mathrm{Tr}[g_{(0)}^{-1}g_{(2)}]\right) + \frac{3z}{2}\left(g_{(3)} - g_{(0)}\,\mathrm{Tr}[g_{(0)}^{-1}g_{(3)}]\right)\Bigg) + \mathcal{O}(z^2) . \end{aligned} \tag{3.3.20}$$

To attain the expectation value of the holographic stress tensor $\langle T\rangle$, one then takes the limit approaching the boundary

$$\langle T\rangle = \lim_{z\to 0}\left(\frac{T_z}{z}\right) . \tag{3.3.21}$$

The terms involving g_2 act to regulate divergences arising from the intrinsic curvature terms; the resulting stress is completely determined by $g_{(0)}$ and $g_{(3)}$. With rotation included, evaluation of (3.3.21) yields an incredibly unwieldy expression. However, in the static case $a = 0$ the result is much more tractable:

$$\langle T\rangle = \frac{1}{A^2}\left(\frac{Q'''(\xi)\Upsilon^{\frac{3}{2}}}{96\pi\alpha^3\omega^3}\right)\Bigg[\left(-2 + 3A^2\ell^2 Q(\xi)\right)\partial_t \otimes dt$$

$$+\,\partial_\xi \otimes d\xi + \Big(1 - 3A^2\ell^2 Q(\xi)\Big)\,\partial_\varphi \otimes d\varphi\Bigg]\,. \quad (3.3.22)$$

It is straightforward to define the expected boundary gauge field and field strength

$$\langle B\rangle = \lim_{z\to 0} B\,, \qquad\qquad \langle dB\rangle = \lim_{z\to 0} dB\,, \quad (3.3.23)$$

together with an associated boundary electric current one-form

$$\langle j\rangle = \lim_{z\to 0}\left(\frac{n\cdot dB}{z^3}\right)\,. \quad (3.3.24)$$

The stress tensor and electromagnetic quantities satisfy a pair of Ward identities,

$$\Big\langle \bar\nabla\cdot j\Big\rangle = 0\,, \qquad\qquad \Big\langle \bar\nabla\cdot T\Big\rangle = -\,\langle j\cdot dB\rangle\,. \quad (3.3.25)$$

The fact that the boundary theory is odd-dimensional also procludes the existence of a trace anomaly [153]:

$$\Big\langle \mathrm{Tr}[g_{(0)}^{-1}T]\Big\rangle = 0\,. \quad (3.3.26)$$

Given a Killing vector $\bar\eta$ of the boundary theory, one may construct an operator

$$T\cdot\bar\eta + (B\cdot\bar\eta)\,j \quad (3.3.27)$$

which is conserved

$$\Big\langle \bar\nabla\cdot\Big(T\cdot\bar\eta + (B\cdot\bar\eta)\,j\Big)\Big\rangle = 0\,. \quad (3.3.28)$$

This operator ensures the existence of a conserved charge defined by

$$Q[\bar\eta] \equiv \int_{\partial M}\sqrt{\gamma}\Big(u\cdot T\cdot\bar\eta + (u\cdot j)\,(B\cdot\bar\eta)\Big)\,, \quad (3.3.29)$$

where the integral is taken over a spacelike surface of constant time with future-directed unit normal u and induced metric γ. There are two linearly independent Killing vectors of the boundary geometry (3.3.19), given by linear combinations of ∂_t and ∂_φ. The vector ∂_ϕ is the obvious choice from which to calculate a rotational conserved charge:

$$J \equiv Q[\partial_\varphi] = \frac{ma}{K^2}\,. \quad (3.3.30)$$

On the other hand, when rotation is present the choice of vector to generate a mass is a little more subtle. In [151] the choice $\partial_t + \Omega_{\text{bdy.}}\partial_\varphi$ was taken as an ansatz, where

$$\Omega_{\text{bdy.}} = -\frac{aK\,(1 - A^2\ell^2\Xi)}{\alpha\,(1 + a^2A^2)\,\ell^2\Xi}\,. \quad (3.3.31)$$

The mass is then

$$M \equiv Q[\partial_t + \Omega_{\text{bdy.}}\partial_\varphi] = \frac{m\left(\Xi + \frac{a^2}{\ell^2}\right)(1 - A^2\ell^2\Xi)}{\alpha\Xi\,(1 + a^2A^2)\,K}\,. \tag{3.3.32}$$

Indeed, the ansatz (3.3.31) gives a result matching the one attained from the action calculation we will outline in a moment. It also recovers the known non-accelerating result [82] in the $A \to 0$ limit. Some justification for (3.3.31) was given in [150]. The angular-velocity of a zero angular momentum observer in the bulk is given by the ratio of the $t - \varphi$ and $\varphi - \varphi$ components of the four-dimensional metric g:

$$\Omega_r = -\frac{g_{t\varphi}}{g_{\varphi\varphi}} = \frac{a\Big((r^2 + a^2)\,g(\theta) - r^2 f(r)\Big)}{\alpha\Big((r^2 + a^2)^2\,g(\theta) - a^2r^2 f(r)\sin^2\theta\Big)}\,. \tag{3.3.33}$$

We have already made use of the value of this expression at the horizon, Ω_{r_+}. Unlike a Ricci-flat black hole, a typical black hole in an anti-de Sitter universe exhibits rotation at the boundary [82]. Unlike the case $A = 0$, the expression at the boundary must be handled carefully since Ω_r is θ-dependant there. The authors of [149] chose to evaluate (3.3.33) in the limit $m \to 0$ (and $\cos\theta = 1$ when electromagnetic charge is present), giving (3.3.31). In some sense, $\Omega_{\text{bdy.}}$ is the angular velocity of the boundary theory. Incidentally, this also identifies the chemical potential Ω which should enter the first law conjugate to J [82]:

$$\Omega = \Omega_{r_+} - \Omega_{\text{bdy.}}\,. \tag{3.3.34}$$

The conserved total electromagnetic charges are also holographic quantities, attained by integrating the electric and magnetic charge densities over the boundary:

$$Q_e = \frac{1}{4\pi}\int_{\partial M} \star dB = \frac{e}{K}\,, \qquad\qquad Q_{\text{m}} = \frac{1}{4\pi}\int_{\partial M} dB = \frac{g}{K}\,. \tag{3.3.35}$$

The appropriate way to calculate the associated electrostatic potential in the canonical (or Gibbs) ensemble is via the Hawking-Ross prescription [154]. One should determine the difference between the electric potential at the horizon $-\eta\cdot B|_{r=r_+}$ and the zero-mode of the potential at the boundary, defined by

$$\Phi_e = \frac{1}{4\pi Q_e\beta}\int_{\partial M}\sqrt{h}\,n_\mu (dB)^{\mu\nu}B_\nu\,, \tag{3.3.36}$$

where $h_{\mu\nu}$ is the induced boundary metric and n_μ is the outwards-pointing unit normal. In our gauge, the potential at the horizon vanishes, so we will have Φ_e entering the first law conjugate to Q_e. Explicitly,

$$\Phi_e = \frac{e\,r_+}{4\pi\alpha\,(r_+^2 + a^2)}\,. \tag{3.3.37}$$

A similar integral may be performed for the magnetic potential, although it is simpler to exploit electromagnetic duality to exchange the electric parameter for the magnetic one [151]:

$$\Phi_{\rm m} = \frac{g\, r_+}{4\pi\alpha\,(r_+^2 + a^2)}\,. \tag{3.3.38}$$

As a check of the quantities calculated, one may re-employ the Wick rotation used to find the temperature and compute the action

$$I = \frac{1}{16\pi}\int_M d^4x\sqrt{g}\,\left[\mathcal{R}(g) + \frac{6}{\ell^2} - (dB)_{\mu\nu}\,(dB)^{\mu\nu}\right] + \frac{1}{8\pi}\int_{\partial M} d^3x\sqrt{h}\,\left[\mathcal{K} - \frac{2}{\ell^2} - \frac{\ell}{2}\mathcal{R}(h)\right]\,. \tag{3.3.39}$$

Here, h is the induced boundary metric, $\mathcal{K}$ is the extrinsic curvature of the boundary giving the Gibbons-Hawking boundary term, and $\mathcal{R}(g)$ and $\mathcal{R}(h)$ are the intrinsic curvatures of the bulk and boundary respectively. The addition of the boundary counterterms cancels the divergences from the bulk, resulting in a finite action [55, 93]. Upon evaluation, the action is [149, 151]

$$\beta^{-1}I \;=\; \frac{m\,(1 - a^2A^2 - 2A^2\ell^2\Xi)}{2\alpha\,(1 + a^2A^2)\,K} - \frac{r_+\left(r_+^2 + a^2\right)}{2\alpha\ell^2\,(1 - A^2r_+^2)^2\,K} - \frac{(e^2 - g^2)\,r_+^2}{2\alpha\,(r_+^2 + a^2)}\,, \tag{3.3.40}$$

which satisfies the quantum statistical relation:

$$\beta^{-1}I = M - TS - \Omega J - \Phi_e Q_e\,, \tag{3.3.41}$$

This allows us to interpret $\mathcal{G} = \beta^{-1}I$ as the Gibbs free energy of an ensemble at fixed temperature, pressure, and chemical potential [155] and indicates that the expression (3.3.32) has the interpretation of spacetime enthalpy. It also indicates that the somewhat mysterious choice of $\Omega_{\rm bdy.}$ is correct.

The pressure is of course given by the usual extended thermodynamics value $P = 3(8\pi\ell^2)^{-1}$.

As mentioned at the start of this section, the key to attaining the first law was to understand that the string tensions behave like thermodynamic charges. One seeks a first law of the form

$$\delta M = T\delta S + \Omega\delta J + \Phi_e\delta q_e + \Phi_{\rm m}\delta Q_{\rm m} - \lambda_+\delta\mu_+ - \lambda_-\delta\mu_- + V\delta P\,, \tag{3.3.42}$$

where λ_+ and λ_- are the thermodynamic lengths of the strings and V is the thermodynamic volume. On dimensional grounds we should also expect a Smarr relation of the form

$$M = 2\,(TS + \Omega J - PV) + \Phi_e Q_e + \Phi_{\rm m}Q_{\rm m}\,. \tag{3.3.43}$$

To acquire the values of V, λ_+, and λ_-, one examines the definition of the horizon radius, $f(r_+) = 0$, and examines its variation:

$$0 = \left.\frac{\partial f}{\partial r_+}\right|_{r=r_+} \delta r_+ + \left.\frac{\partial f}{\partial m}\right|_{r=r_+} \delta m + \left.\frac{\partial f}{\partial a}\right|_{r=r_+} \delta a + \left.\frac{\partial f}{\partial e}\right|_{r=r_+} \delta e + \left.\frac{\partial f}{\partial g}\right|_{r=r_+} \delta g + \left.\frac{\partial f}{\partial A}\right|_{r=r_+} \delta A + \left.\frac{\partial f}{\partial K}\right|_{r=r_+} \delta K \,. \quad (3.3.44)$$

The variation δr_+ may be easily written in terms of δS, δa, δA, and δK. One may then use the expressions for M, J, Q_e, $Q_{\rm m}$, μ_+, and μ_- to massage the equation into the form of the first law. One finds the following thermodynamic lengths and volume:

$$\lambda_\pm = \frac{r_+}{\alpha(1 \pm A r_+)} - \frac{m\left(\Xi + \frac{a^2}{\ell^2}\left(2 - A^2\ell^2\Xi\right)\right)}{\alpha\left(1 + a^2A^2\right)\Xi^2} \mp \frac{A\ell^2\left(\Xi + \frac{a^2}{\ell^2}\right)}{\alpha\left(1 + a^2A^2\right)}\,, \quad (3.3.45)$$

$$V = \frac{4\pi}{3\alpha K}\left(\frac{r_+\left(r_+^2 + a^2\right)}{\left(1 - A^2 r_+^2\right)^2} + \frac{m\left(a^2\left(1 - A^2\ell^2\Xi\right) + A^2\ell^4\Xi\left(\Xi + \frac{a^2}{\ell^2}\right)\right)}{\Xi\left(1 + a^2A^2\right)}\right), \quad (3.3.46)$$

with the process being consistent if

$$\alpha = \frac{\sqrt{\left(1 - A^2\ell^2\Xi\right)\left(\Xi + \frac{a^2}{\ell^2}\right)}}{1 + a^2A^2}\,. \quad (3.3.47)$$

These values then also satisfy the Smarr relation (3.3.43). In chapter 4 we will show that the mass may be written entirely in terms of the thermodynamic quantities which do not depend upon α in such a way that the well-known Christodoulou-Ruffini formula for the non-accelerating case are recovered in the appropriate limit. Firstly, this indicates that the value of α, and therefore mass, used above is the correct one. Secondly, it will demonstrate that all of the potentials we have derived are indeed the appropriate partial derivatives of the enthalpy when the other charges are held fixed. For example, $\Omega = \left.\frac{\partial M}{\partial J}\right|_{S,P,Q_e,Q_{\rm m},\mu_\pm}$.

At this stage, the value of α may seem mysterious. The need for a particular normalisation of the time coordinate when calculating mass was first acknowledged, (following [156]), for the (non-accelerating) rotating black hole with anti-de Sitter asymptotics by Caldarelli, Cognola, and Klemm [82], who noted that it was required to ensure that the appropriate $\mathfrak{so}(3,2)$ Lie algebra was generated asymptotically [157]. In more physical language, the Boyer-Lindquist time coordinate must coincide with the asymptotic time for an observer near the conformal boundary.

The story is similar for the accelerating black hole. Consider a small ($m \to 0$), uncharged, non-rotating, slowly accelerating black hole. The geometry is one we discussed earlier and is depicted in figure 3.1. The space described by the Boyer-

Lindquist coordinates is (a portion of) AdS_4 with a conical defect[1], although the coordinate system does not make this fact clear. Upon performing the coordinate transformation [149]

$$1+\frac{R^2}{\ell^2}=\frac{1+(1-A^2\ell^2)\,\frac{r^2}{\ell^2}}{\Omega^2(r,\theta)\,(1-A^2\ell^2)}\,,\qquad\qquad R\sin\vartheta=\frac{r\sin\theta}{\Omega(r,\theta)}\,, \tag{3.3.48}$$

one finds more familiar coordinates which one can easily extend to the complete global space:

$$ds^2_{\mathrm{AdS}_4}=\left(1+\frac{R^2}{\ell^2}\right)dt^2-\frac{dR^2}{\left(1+\frac{R^2}{\ell^2}\right)}-R^2\left(d\vartheta^2+\sin^2\vartheta\frac{d\varphi^2}{K^2}\right)\,. \tag{3.3.49}$$

This transformation works if and only if $\alpha=\sqrt{1-A^2\ell^2}$, which coincides with (3.3.47). A similar mapping to global space may be made in the uncharged, rotating case by first transforming to a rotation subtracted frame $\varphi'=\varphi-\Omega_{\mathrm{bdy.}}t$. We refer the interested reader to [150] for details.

[1] less a point at the location of the small black hole.

Chapter 4

Accelerating black hole chemistry

4.1 Overview

Over the past decade, an interpretation of the cosmological constant as a thermodynamic pressure has been explored [56, 62, 63, 66, 67, 87, 158, 159]. A key conceptual development was understanding that the mass term in the first law of thermodynamics, related to the mass parameter m in the Newtonian potential of the black hole, was not in fact the internal energy of the black hole, but rather its enthalpy [62], i.e. the natural first law for a black hole with a cosmological constant includes not only the charges of electromagnetism and rotation, but also the impact of the non-zero energy coming from the cosmological constant in the volume inside the black hole:

$$\delta M = T\delta S + V\delta P + \Omega\delta J + \Phi\delta Q\,. \tag{4.1.1}$$

Once one includes the possibility of a varying pressure, black hole thermodynamics more naturally resembles conventional thermodynamics, not only in its differential sense, but also in its integrable sense: the ideal gas relations $dU = TdS - PdV$ and $U = c_V PV$ have their counterpart in the differential first law (4.1.1) and an integral Christodoulou-Ruffini [82, 160] relation, that for four-dimensional Kerr-Newman-AdS black holes reads

$$M^2 = \frac{S}{4\pi}\left[1 + \frac{\pi Q^2}{S} + \frac{8PS}{3}\right]^2 + \frac{4\pi^2 J^2}{S}\left[1 + \frac{8PS}{3}\right]. \tag{4.1.2}$$

This can be massaged into an ideal-gas like relation at large volume/entropy[1]. Although the formulae for the enthalpy, charges and potentials are naturally derived

[1]That is, for large black holes the Schwarzschild contributions dominate and we find $M \propto PS^{3/2}$ at leading order. The entropy scales with horizon radius squared while the thermodynamic volume scales with the horizon radius cubed, so we have $M \propto PV$.

from the black hole geometry, and written in terms of the metric parameters and horizon radius, expressing the thermodynamic potentials and enthalpy purely in terms of extensive quantities (as in [63, 159]) allows a natural identification with classic thermodynamics, and elucidates the *chemical* nature of the phase space of black holes.

There is another reason to specify the closed form of the black hole charges and enthalpy. While it is possible for material systems to have many charges and chemical potentials, the black hole is typically believed to carry only mass, charge, and angular momentum, due to the *no-hair theorems* [161, 162] . While these theorems are now understood in a broader context to be somewhat limited, the basic picture from the perspective of classic black hole thermodynamics is that thermodynamic potentials are still narrowly restricted to be functions of entropy, rotational and magnetic charges, and thermodynamic pressure. Recently however, a new type of "charge" for a black hole has been explored and added to this stable: a conical deficit [146, 148–150, 163], often interpreted as a cosmic string, that can either run symmetrically along the axis of the black hole [111–113, 145], or have different values along the North and South axes, leading to an *accelerating* black hole. This accelerating black hole is encoded by the C-metric (with negative cosmological constant) [115, 128], which we reviewed in chapter 3. We are interested in the effects of acceleration in particular, and so choose to consider the case where there is neither NUT parameter nor magnetic charge. The geometry we consider is given by the metric (3.2.15). We restate it here,

$$ds^2 = \frac{1}{H^2}\left\{\frac{f(r)}{\Sigma}\left[\frac{dt}{\alpha} - a\,\sin^2\theta\frac{d\varphi}{K}\right]^2 - \frac{\Sigma}{f(r)}dr^2 \right. \\ \left. - \frac{\Sigma}{g(\theta)}r^2 d\theta^2 - \frac{g(\theta)}{\Sigma}\cdot\frac{\sin^2\theta}{r^2}\left[\frac{a dt}{\alpha} - (r^2+a^2)\frac{d\varphi}{K}\right]^2\right\}, \quad (4.1.3)$$

with g set to zero, so that now

$$f(r) = (1 - A^2 r^2)\left[1 - \frac{2m}{r} + \frac{a^2+e^2}{r^2}\right] + \frac{r^2+a^2}{\ell^2} \quad (4.1.4)$$

$$g(\theta) = 1 + 2mA\cos\theta + (\Xi - 1)\cos^2\theta\,, \quad (4.1.5)$$

$$\Sigma = 1 + \frac{a^2}{r^2}\cos^2\theta\,, \qquad H = 1 + Ar\cos\theta\,, \quad (4.1.6)$$

$$\Xi = 1 + e^2A^2 - \frac{a^2}{\ell^2}(1 - A^2\ell^2)\,. \quad (4.1.7)$$

Note that the black hole is assumed to spin on its axis, the acceleration term modifying the angular parts of the metric and distorting the sphere to a teardrop, with a conical deficit at (at least) one of the poles. This deficit is revealed by taking

the limit of the metric as we approach each pole, and is encoded by the *tension*

$$\mu_{\pm} = \frac{1}{4}\left[1 - \frac{\Xi \pm 2mA}{K}\right]. \tag{4.1.8}$$

(with '+' corresponding to the North Pole, and '−' the South) interpreted as a cosmic string emerging from the black hole, causing it to accelerate.

In this chapter, we consider only the case where the black hole is slowly accelerating; there is no acceleration horizon. We discussed the structure of the solution and the bounds imposed by this constraint in section 3.3. This assumption allowed the thermodynamics of conical deficits and slowly accelerating black holes was explored [146, 148–150, 163] (see also [142, 164]). The key insight was to use tools from holographic renormalisation to properly calculate the various charges of the slowly accelerating black hole spacetime [149, 150]. The net result is a set of thermodynamic variables for the black hole, expressed in terms of the black hole metric parameters and the horizon radius r_+, that include the conical deficit as a charge, and introduce the conjugate chemical potential, a *thermodynamic length*. For reference, we restate the thermodynamic parameters we reviewed in section 3.3:

$$\begin{aligned}
M &= \frac{m}{K\Xi}\left(\Xi + \frac{a^2}{\ell^2}\right)^{\frac{1}{2}}\left(1 - A^2\ell^2\Xi\right)^{\frac{1}{2}}, \\
T &= \frac{r_+^2 f'(r_+)}{4\pi\alpha\left(r_+^2 + a^2\right)}, \\
S &= \frac{\pi\left(r_+^2 + a^2\right)}{\left(1 - A^2 r_+^2\right)K}, \\
J &= \frac{ma}{K^2}, \\
\Omega &= \left(\frac{aK}{\alpha\left(r_+^2 + a^2\right)}\right) - \left(-\frac{aK\left(1 - A^2\ell^2\Xi\right)}{\alpha\ell^2\Xi\left(1 + a^2A^2\right)}\right), \\
Q &= \frac{e}{K}, \\
\Phi &= \frac{e\, r_+}{4\pi\alpha\left(r_+^2 + a^2\right)}, \\
P &= \frac{3}{8\pi\ell^2}, \\
V &= \frac{4\pi}{3\alpha K}\left(\frac{r_+\left(r_+^2 + a^2\right)}{\left(1 - A^2 r_+^2\right)^2} + \frac{m\left(a^2\left(1 - A^2\ell^2\Xi\right) + A^2\ell^4\Xi\left(\Xi + \frac{a^2}{\ell^2}\right)\right)}{\Xi\left(1 + a^2A^2\right)}\right), \\
\lambda_{\pm} &= \frac{r_+}{\alpha(1 \pm Ar_+)} - \frac{m\left(\Xi + \frac{a^2}{\ell^2}\left(2 - A^2\ell^2\Xi\right)\right)}{\alpha\left(1 + a^2A^2\right)\Xi^2} \mp \frac{A\ell^2\left(\Xi + \frac{a^2}{\ell^2}\right)}{\alpha\left(1 + a^2A^2\right)}.
\end{aligned} \tag{4.1.9}$$

As we are only considering electrically charged black holes, we have dropped the subscripts from the electric charge and potential. The first law satisfied by these

quantities has full cohomogeneity:

$$\delta M = T\delta S + \Phi\delta Q + \Omega\delta J - \lambda_+\delta\mu_+ - \lambda_-\delta\mu_- + V\delta P\,, \tag{4.1.10}$$

with all the physical parameters of the geometry corresponding to a thermodynamic charge. One of the key difficulties in determining the correct enthalpy was in properly identifying the timelike Killing vector for determining the mass of the black hole. The slowly accelerating black hole, being at a fixed point from the boundary, has the same time coordinate (up to a factor) as the asymptotic AdS spacetime, and the mass can be found via a holographic renormalisation procedure. The resulting enthalpy thus contains factors dependent on this acceleration parameter that then propagate throughout the expressions for thermodynamic volume and length. The accelerating black hole also obeys a Smarr relation [81]

$$M = 2(TS + \Omega J - PV) + \Phi Q\,, \tag{4.1.11}$$

that does not contain any trace of acceleration or tension.

While the expressions (4.1.9) are perfectly adequate for the implicit study of black hole thermodynamics, the "chemical" nature of the black hole is less transparent, and typically has to be studied numerically, and parametrically in terms of the horizon radius r_+.

4.2 Chemical expressions for the accelerating black hole

To elucidate the *chemical* nature of the black hole, and to allow a more general analytic analysis of the phase space our aim is therefore to have closed-form expressions, such as (4.1.2), i.e. an integral expression of the form $M^2(S, P, Q, J, \mu_\pm)$, together with expressions for the chemical potentials in the form $\phi_i = \partial M/\partial q_i$, where q_i stands for a charge, $S, P, Q, J, \mu_\pm$ and ϕ_i its corresponding potential $T, V, \Phi, \Omega, \lambda_\pm$. Given that the Smarr relation is a statement about scaling dimension, and is given in terms of charges and potentials, it does not preclude an expression for M that includes the tensions.

The new physics in the accelerating black hole is that of the conical deficit(s), and while the individual tensions are natural geometric variables, they do not distinguish between an overall conical deficit, such as the cosmic string threading a black hole (that does not have issues with a slow acceleration limit) and a differential conical deficit that produces a net force on the black hole, inducing acceleration. From the

perspective of black hole chemistry, it turns out that the conical deficits are more conveniently encoded in the average and differential conical deficits of the spacetime:

$$\Delta = 1 - 2(\mu_+ + \mu_-) = \frac{\Xi}{K}\,, \tag{4.2.1}$$

$$C = \frac{(\mu_- - \mu_+)}{\Delta} = \frac{mA}{K\Delta} = \frac{mA}{\Xi}\,. \tag{4.2.2}$$

The tensions are bounded below by requiring positivity of energy (or tension) and above by the fact that the maximal conical deficit is 2π. With $A \geq 0$, so that $0 \leq \mu_+ \leq \mu_- \leq 1/4$, this translates into $0 \leq C \leq \text{Min}\left\{\frac{1}{2}, \frac{1-\Delta}{2\Delta}\right\}$. Although Δ and C are not unconstrained – introducing an acceleration necessarily also introduces an overall average deficit – it proves to be the best way to express the impact of the conical deficit on the thermodynamics. Often, when considering an accelerating black hole, the deficit on one axis (here μ_+) is set to zero, in this case $C = (1-\Delta)/2\Delta$, thus the upper bound is saturated and $\Delta \in [\frac{1}{2}, 1]$. We are interested more generally in how conical deficits impact thermodynamics, so will keep C and Δ arbitrary, within their allowed ranges.

Now turn to the mass formula (4.1.2). A check of the thermodynamic expressions (4.1.9) shows that M, S, and Q all scale as K^{-1} while J scales as K^{-2}. This suggests that scaling each by Δ^{-1} (or Δ^{-2} in the case of J) is a promising starting point. Some manipulations then reveal the appropriate remaining modifications, and give the mass formula

$$M^2 = \frac{\Delta S}{4\pi}\left[\left(1 + \frac{\pi Q^2}{\Delta S} + \frac{8PS}{3\Delta}\right)^2 + \left(1 + \frac{8PS}{3\Delta}\right)\left(\left(\frac{2\pi J}{\Delta S}\right)^2 - \frac{3\Delta C^2}{2PS}\right)\right]. \tag{4.2.3}$$

Note that all of the quantities on the right-hand side of equation (4.2.3) are independent of the normalisation α. Given that we have attained the known expression for the mass of the Kerr-Newmann-AdS black hole [165] supplemented by an additive term accounting for acceleration, (and simple rescalings accounting for the average deficit) we take this as compelling evidence that the normalisation (3.3.47) written in chapter 3 (and thus the mass of the black hole) is the correct one.

It is now a matter of algebra to confirm that the thermodynamic potentials conjugate

to the charges, $T = \frac{\partial M}{\partial S}\big|_{P,J,Q,\mu_\pm}$ etc. correspond to the expressions (4.1.9) and are:

$$\begin{aligned}
V &= \frac{2S^2}{3\pi M}\left[\left(1+\frac{\pi Q^2}{\Delta S}+\frac{8PS}{3\Delta}\right)+\frac{2\pi^2 J^2}{(\Delta S)^2}+\frac{9C^2\Delta^2}{32P^2S^2}\right], \\
T &= \frac{\Delta}{8\pi M}\left[\left(1+\frac{\pi Q^2}{\Delta S}+\frac{8PS}{3\Delta}\right)\left(1-\frac{\pi Q^2}{\Delta S}+\frac{8PS}{\Delta}\right)-\frac{4\pi^2 J^2}{(\Delta S)^2}-4C^2\right], \\
\Omega &= \frac{\pi J}{SM\Delta}\left(1+\frac{8PS}{3\Delta}\right), \\
\Phi &= \frac{Q}{2M}\left(1+\frac{\pi Q^2}{S\Delta}+\frac{8PS}{3\Delta}\right), \\
\lambda_\pm &= -\frac{S}{4\pi M}\left[\left(\frac{8PS}{3\Delta}+\frac{\pi Q^2}{\Delta S}\right)^2+\frac{4\pi^2 J^2}{(\Delta S)^2}\left(1+\frac{16PS}{3\Delta}\right)\right. \\
&\qquad\left.-(1\mp 2C)^2\pm\frac{3\Delta C}{2PS}\right].
\end{aligned} \tag{4.2.4}$$

Since everything is now written in terms of the charges, this elucidates the "chemical" structure of the accelerating black hole, and allows for a more intuitive and natural analysis of the thermodynamics, as well as clarifying some of the new phenomenology of accelerating thermodynamics. We will now illustrate this by making some general observations on the impact of conical deficits, before concluding by presenting a new entropy bound for black holes with conical deficits.

The conical structure of the spacetime appears in two ways: the 'overall' conical deficit, encoded in Δ, that can be present whether or not there is acceleration. $\Delta < 1$ means that the spacetime contains a conical deficit, and if $C = 0$, the deficit cuts through the whole spacetime, piercing the black hole. Acceleration appears via the parameter C. This is now more interesting, as, unlike angular momentum and charge, that contribute to the enthalpy positively, C contributes negatively, indicating an exothermic nature to this particular property. This now opens the possibility of new phenomena in phase space, as, apart from the extremal limit, $T \to 0$, we also potentially have a limit $M \to 0$ that signals a breakdown in the thermodynamic description. This breakdown occurs approximately, though not precisely, at the breakdown of the slow acceleration régime.

4.2.1 The free energy and the Hawking-Page transition

Let us begin by exploring the impact of an overall conical deficit, setting $C = 0$ and allowing Δ to vary. It might seem that as Δ simply enters as a rescaling parameter, it does not change the qualitative thermodynamics, but the story is more subtle.

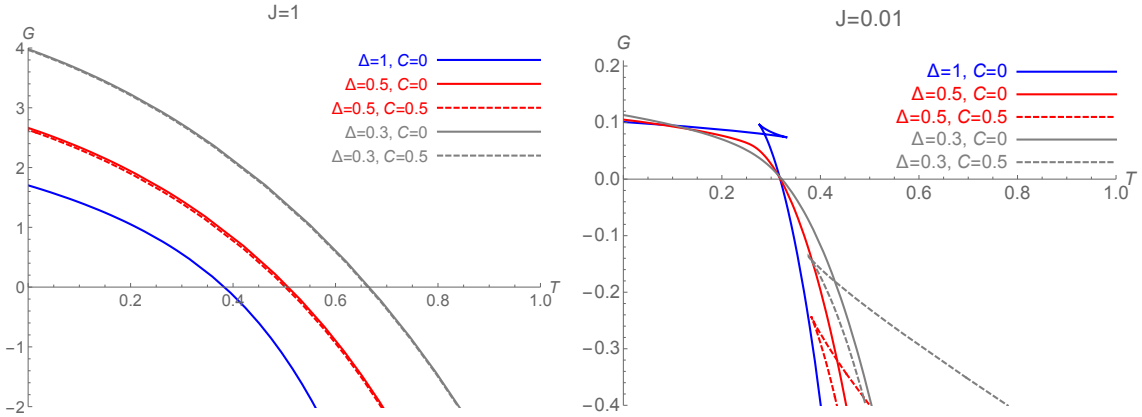

Figure 4.1: The impact of the conical deficit (Δ), and acceleration (C) on the free energy for large and small values of J as labelled, relative to the AdS lengthscale, ℓ, set to unity in these plots.

For example, consider the free energy $G = M - TS$, which in full is

$$G = \frac{\Delta S}{8\pi M}\left[\left(\frac{2\pi J}{\Delta S}\right)^2\left(3+\frac{16PS}{3\Delta}\right) - 4C^2\left(1+\frac{3\Delta}{4PS}\right)\right.$$
$$\left. + \left(1+\frac{8PS}{3\Delta}+\frac{\pi Q^2}{\Delta S}\right)\left(1-\frac{8PS}{3\Delta}+\frac{3\pi Q^2}{\Delta S}\right)\right]. \quad (4.2.5)$$

For an uncharged, non-accelerating black hole, the magnitude of the free energy is decreased by adding a conical deficit. The Hawking-Page transition [166] therefore still occurs at $T_{HP} = \sqrt{8P/3\pi} = 1/\pi\ell$, and the critical point at which the specific heat of the black hole becomes positive (i.e., the minimal temperature that a black hole can have) also remains at $T_m = \sqrt{3}T_{HP}/2$, however, the free energy curves are strongly modified with Δ, and the entropy, or size, of the black hole at each of these critical points is lowered: $S_c = \Delta/8P$, $S_{HP} = 3\Delta/8P$. With the addition of charge and/or rotation, the behaviour is not as simple and depends on the magnitude of the charges Q and J. Increasing the deficit lowers Δ, thus amplifying the positive contributions of J and Q to G, on the other hand, the contribution from the negative PS/Δ term is also amplified. Put together, the general effect of adding a deficit is to make the behaviour of the free energy that of a 'larger' black hole, where 'large' is defined relative to the AdS length scale ℓ. Thus, for large charges the free energy is increased by the addition of a deficit, whereas for a smaller charges the effect is more nuanced, as seen in figure 4.1.

Now consider adding acceleration, via the C term. For large black holes with or without charge, the presence of acceleration in itself does not impact strongly on the thermodynamics, rather, it is the fact that acceleration requires an average deficit

that modifies the thermodynamics. However, as the charge, or size of the black hole drops, things become much more interesting. From (4.2.5), this clearly lowers the free energy, and for sufficiently low charge and overall deficit, can eliminate any regions of positive G. The lack of a Hawking-Page transition (for the simple reason that there is no spacetime with 'half' a cosmic string without a black hole) was discussed in [146].

4.2.2 The snapping swallowtail

With acceleration there is also a novel phase transition, first noticed numerically in [167] and subsequetly explored numerically in [168]. This occurs precisely because of the exothermic nature of acceleration, and so is not present for non-accelerating black holes.

Recall that the third law usually provides a lower bound on the entropy, corresponding to the size of the extremal black hole at which $T = 0$. However, in the presence of acceleration, we have a new limit coming from the positivity of M^2. To explore this, abbreviate notation by writing

$$x = \frac{8PS}{\Delta}\,, \qquad \frac{\pi Q^2}{\Delta S} = q\frac{C^2}{x}\,, \qquad \frac{\pi J}{\Delta S} = j\frac{C^2}{x}\,, \tag{4.2.6}$$

so that

$$M^2 = \frac{\Delta S}{4\pi}\left[\left(1 + x - q_+\frac{C^2}{x}\right)\left(1 + x - q_-\frac{C^2}{x}\right) + 4j^2C^4\frac{(1+x)}{x^2}\right], \tag{4.2.7}$$

where $q_\pm = 2 - q \pm 2\sqrt{1-q}$. If $q \leq 1$, then the roots $q_\pm$ are real, and there is a range of j for which $M \to 0$ at some x_0. Further, since $T = \frac{1}{2M}\frac{\partial M^2}{\partial S} \propto \frac{1}{M}\frac{\partial M^2}{\partial x}$, this occurs before the extremal limit is reached. For this range of low charge/rotation to acceleration ratios, small black holes are no longer cold, but instead, like their uncharged counterparts, are hot, and have a negative specific heat as the enthalpy tends to zero. As the charge/rotation increases, a critical limit is reached, $q_c(j)$ for which M^2 has a repeated zero, at which T is finite, and above the critical values of charge/rotation, the black hole once again exhibits a swallowtail. These behaviours of the enthalpy and free energy of a non-rotating accelerating black hole are shown in figure 4.2 to demonstrate the phenomenon. This "snapping" of the swallowtail was discovered in [167], although the snapping point could not be determined analytically from the implicit expressions (4.1.9) for the thermodynamic variables.

Using the chemical variables, we can analytically find the one-parameter family of critical charged, rotating, and accelerating black holes that have infinite enthalpy, but finite temperature at the snapping point of the swallowtail. These critical entropies

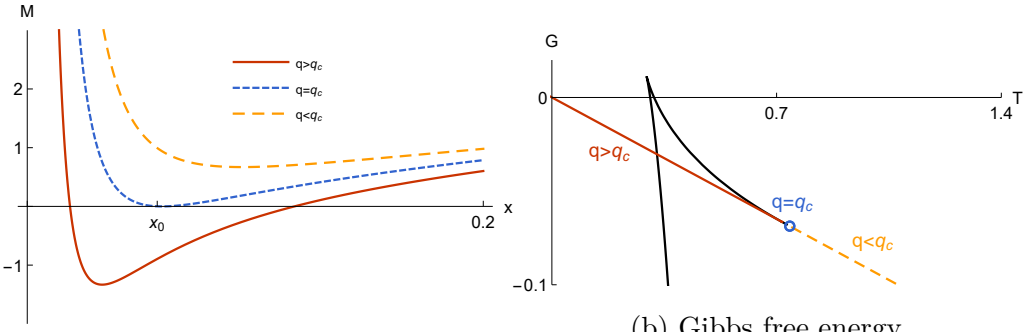

(a) Enthalpy

(b) Gibbs free energy

Figure 4.2: The behaviour of the mass and Gibbs free energy of a non-rotating black hole with $\Delta = 0.5$, $C = 0.25$. Three curves are drawn, demonstrating charges below, at, and above the critical snapping charge.

and temperatures are given implicitly by the value of x at which the mass becomes zero, x_0, and C:

$$\begin{aligned} Q_{\rm S}^2 &= \frac{3\Delta^2}{8\pi P}(1+x_0)\left[1+x_0-\sqrt{(1+2x_0)^2-4C^2}\right], \\ J_{\rm S}^2 &= \frac{1}{2}\left(\frac{3\Delta^2}{8\pi P}\right)^2(1+2x_0)\Big[2C^2 \\ &\qquad -(1+x_0)\left(1+2x_0-\sqrt{(1+2x_0)^2-4C^2}\right)\Big], \\ T_{\rm S} &= \sqrt{\frac{2P}{3\pi x_0}}\Big[(4x_0+3)(1+2x_0)-4C^2 \\ &\qquad -2(1+x_0)\sqrt{(1+2x_0)^2-4C^2}\Big]^{1/2}, \end{aligned} \tag{4.2.8}$$

where $x_0 \in [\frac{\sqrt{1+4C^2}-1}{2}, \frac{\sqrt{1+12C^2}-1}{3}]$. The lower limit has $J = 0$, $Q^2 = \Delta^2 C^2 \ell^2$, as noted in [167], and the upper limit corresponds to $Q = 0$, $J = \Delta^2 \ell^2 x_0 \sqrt{1+2x_0}/2$. What is interesting here is how the overall deficit plays a role in the critical values of Q and J, except for the pure charge snapped swallowtail, where it seems to be the acceleration that is primary driver. As the acceleration decreases, $C \to 0$, and the range and size of x_0 correspondingly decreases, thus the critical temperature for the snapping point also becomes higher, with the critical temperature increasing as x_0 moves towards the lower end of the range (zero angular momentum). The maximum value of acceleration, $C = 1/2$, corresponds to a deficit of 2π along the South axis, and has the lowest values of critical temperature and the largest range of q and j. The absolute lowest critical snapping temperature occurs for $Q = 0$, and is $T = \sqrt{2}/\pi$. A snapping swallowtail for an electrically charged, accelerating black hole is shown in figure 4.3, while one for a rotating, electrically neutral black hole is shown in figure 4.4.

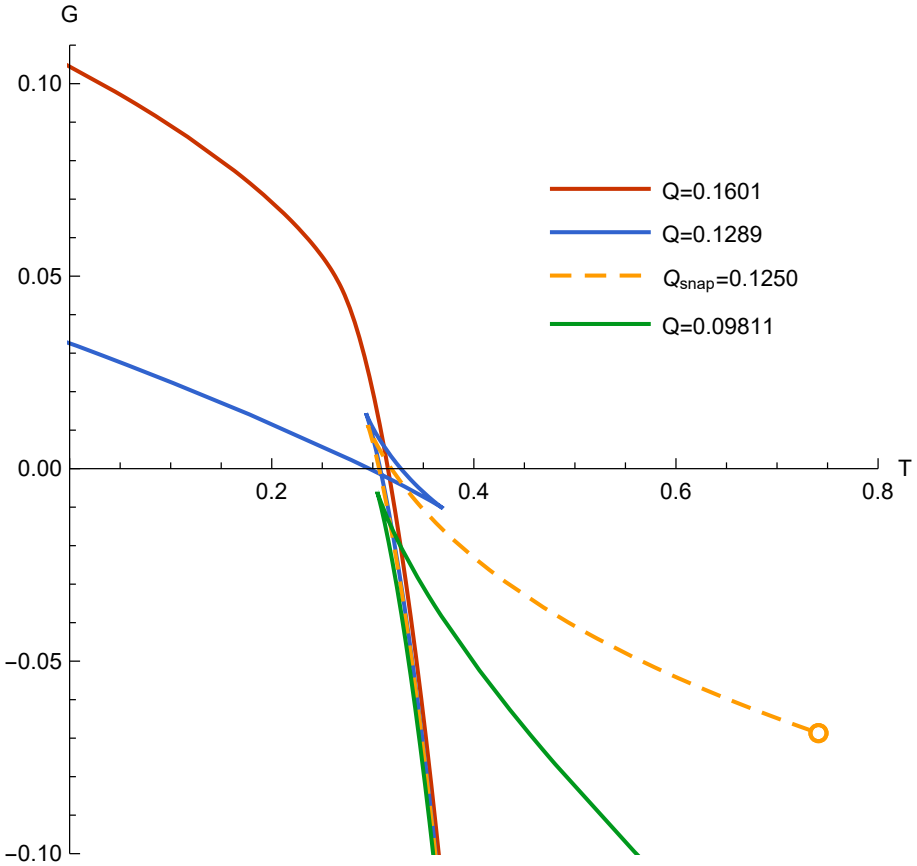

Figure 4.3: The snapping swallowtail for $J = 0$, $\Delta = 0.5$, $C = 0.25$, $P = 3(8\pi)^{-1}$. Various values of electric charge Q are shown. The critical value of charge $Q = \Delta C = 0.125$ is shown in dashed orange. The critical point is $(T_c, G_c) = \left(\frac{1+2x_0}{2\pi\sqrt{x_0}}, -\frac{\Delta\sqrt{x_0}}{2}(1+2x_0)\right)$, indicated by a circle at the end of the coexistence curve.

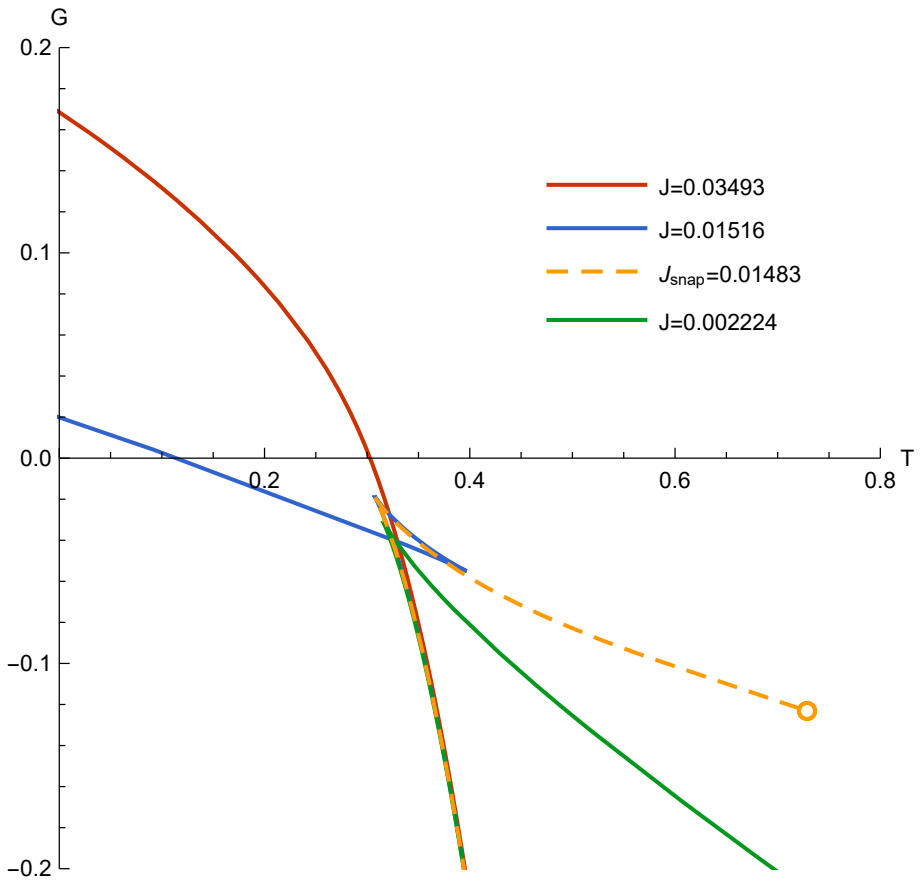

Figure 4.4: The snapping swallowtail for $Q = 0$, $\Delta = 0.5$, $C = 0.25$, $P = 3(8\pi)^{-1}$. Various values of rotation J are shown. The critical rotational charge $J = \Delta^2 x_0 \sqrt{1+2x_0}/2$, where $x_0 = (\sqrt{1+12C^2}-1)/3$, is shown in dashed orange. The critical point is indicated by a small circle at the end of the coexistence curve.

4.3 The Reverse Isoperimetric Inequality

We now consider the *Reverse Isoperimetric Inequality* [87] for this family of black holes. The Isoperimetric Inequality is the simple geometric statement that the largest surface area enclosed by a loop of string is when the string is circular (or its higher-dimensional analogue): $(\mathcal{A}/\mathcal{A}_0)^D \geq (\mathcal{V}/\mathcal{V}_0)^{D-1}$, where the subscript 0 indicates the volume or area of a unit sphere. However, for the black hole, the area directly determines the entropy, thus we would expect that for a given volume, a black hole would want to maximise its entropy, which runs counter to the standard inequality that would mean a spherical black hole would be the lowest entropy for that volume, and hence unstable. Analysing a wide range of solutions, Cvetic et al. [87] discovered that black holes always seemed to satisfy the *inverse* of this inequality:

$$\left(\frac{\mathcal{A}}{\mathcal{A}_0}\right)^D \leq \left(\frac{\mathcal{V}}{\mathcal{V}_0}\right)^{D-1} \tag{4.3.1}$$

leading to their *Reverse Isoperimetric Inequality* conjecture.

Let us now explore this inequality in the context of black holes with conical deficits. Note that

$$\frac{4\pi M^2}{\Delta S} = \left(1 + \frac{\pi Q^2}{\Delta S} + x\right)^2 + 4\,(1+x)\left(\frac{\pi^2 J^2}{\Delta^2 S^2} - \frac{C^2}{x}\right) \tag{4.3.2}$$

$$= \left(\frac{3\pi MV}{2S^2} - \frac{2C^2}{x^2}\right)^2 - 4\left(\frac{\pi Q^2}{\Delta S}\right)\left(\frac{\pi J}{\Delta S}\right)^2 - 4\left(\frac{\pi J}{\Delta S}\right)^4 - 4\frac{(1+x)}{x}C^2\,. \tag{4.3.3}$$

At this point, we spot that the term in brackets on the right-hand side contains the seed of the isoperimetric ratio:

$$M^2\left(\frac{3V}{4\pi}\right)^2\left(\frac{\pi}{S}\right)^4 \geq \left(\frac{3\pi MV}{4S^2} - \frac{C^2}{x^2}\right)^2 \geq \frac{\pi M^2}{\Delta S} \tag{4.3.4}$$

from which we may conclude a *new Reverse Isoperimetric Inequality*, appropriate for spacetimes with a conical deficit:

$$\left(\frac{3V}{4\pi}\right)^2 \geq \frac{1}{\Delta}\left(\frac{\mathcal{A}}{4\pi}\right)^3 \tag{4.3.5}$$

with equality if and only if $C = J = 0$. The larger the conical deficit, the smaller the entropy is with respect to the volume, thus conical defects appear to render black holes sub-entropic.

4.4 Evidence for the exchange of enthalpy during gravitational interaction

For an asymptotically flat solution, the usual definition of the efficiency of a Penrose process would be

$$\eta_U = \frac{U(J = J_{\text{ext.}}) - U(J = 0)}{U(J = J_{\text{ext.}})}\,, \tag{4.4.1}$$

where we slow a maximally spinning black hole to a ron-rotating phase by passing one or more test particles through the ergoregion. We expect the particles to each collect some of the internal energy from the black hole and carry it to infinity. We then define the efficiency as the percentage of the black hole's initial internal energy U extracted. The problem with this definition is that the denominator, which expresses the initial amount of energy in the system available to be used in the process, only accounts for the amount of energy stored within the black hole. Within the extended thermodynamics framework, the system is not an isolated black hole, but rather the complete gravitational solution in which the black hole resides. This includes a contribution to the total available energy from the pressure (and associated conjugate volume) induced by the cosmological constant. As is canon in the thermodynamics of chemical reactions, this energy "budget" is the enthalpy of the system, $M = U + PV$. Such an argument has led previous authors [159] to consider an updated definition for the efficiency of the maximum-energy extracting Penrose process:

$$\eta = \frac{U(J = J_{\text{ext.}}) - U(J = 0)}{M(J = J_{\text{ext.}})}\,. \tag{4.4.2}$$

However, as we will see, both of these attempts at definitions for the efficiency of a Penrose process result in pathological behaviour for accelerating black holes. The difference in internal energy between the initial and final states may exceed both the initial internal energy and the initial enthalphy, implying a superefficient process. We will argue that such pathologies may be removed if one no longer assumes that the Penrose process extracts internal energy from the black hole, instead assuming the extraction of *enthalpy* from the spacetime. In other words, the correct formula for efficiency is

$$\eta_M = \frac{M(J = J_{\text{ext.}}) - M(J = 0)}{M(J = J_{\text{ext.}})}\,. \tag{4.4.3}$$

For simplicity, let's consider a rotating black hole without electric charge. Then the

three relevent thermodynamic potentials [1] are

$$\begin{aligned} V &= \frac{2S^2}{3\pi M}\left[\left(1+\frac{8PS}{3\Delta}\right)+2\left(\frac{\pi J}{\Delta S}\right)^2+2\left(\frac{3\Delta C}{8PS}\right)^2\right], \\ T &= \frac{\Delta}{8\pi M}\left[\left(1+\frac{8PS}{3\Delta}\right)\left(1+\frac{8PS}{\Delta}\right)-4\left(\frac{\pi J}{\Delta S}\right)^2-4C^2\right], \\ M^2 &= \frac{\Delta S}{4\pi}\left[\left(1+\frac{8PS}{3\Delta}\right)^2+4\left(1+\frac{8PS}{3\Delta}\right)\left\{\left(\frac{\pi J}{\Delta S}\right)^2-\frac{3\Delta C^2}{8PS}\right\}\right]. \end{aligned} \tag{4.4.4}$$

The internal energy is given by

$$U = \frac{1}{2\pi M}\left[\frac{1}{2}\Delta S(1+x)+\frac{(\pi J)^2}{\Delta S}(2+x)-C^2\Delta S\left(2+\frac{3}{x}\right)\right], \tag{4.4.5}$$

where

$$x = \frac{8PS}{\Delta}. \tag{4.4.6}$$

We can calculate the value of J for the extremal solution, for which temperature vanishes:

$$J_{\text{ext.}} = \frac{S}{2\pi}\sqrt{\frac{32}{3}PS\left(2PS+\Delta\right)+\Delta^2(1-4C^2)}. \tag{4.4.7}$$

In the final state of the complete Penrose process, where rotation vanishes, M has a single positive root given by

$$PS = \frac{3\Delta}{16}(-1+\sqrt{1+16C^2}). \tag{4.4.8}$$

As discussed earlier in this chapter, for vanishingly small accelerations the massless solution satisfying (4.4.8) is unobtainable for black holes of finite size.

For context, first consider the Penrose process around a rotating black hole with a conical deficit but without induced acceleration. It is straightforward to write down both η_U and η_M:

$$\eta_U = \left(\frac{2PS+\Delta}{4PS+\Delta}\right)-\frac{\Delta^{\frac{3}{2}}}{(8PS+3\Delta)(4PS+\Delta)^{\frac{3}{2}}}\left(6\sqrt{2}PS+3\Delta/\sqrt{2}\right), \tag{4.4.9}$$

$$\eta_M = 1-\frac{\sqrt{2\Delta(4PS+\Delta)}}{8PS+2\Delta}. \tag{4.4.10}$$

Neither of these seem desperately exciting, giving efficiencies in the range $(0,1)$ for all legal values of Δ and for all sizes of black hole. The efficiencies are plotted against horizon size for a range of string tensions in figure 4.5. In particular, the $\Delta = 1$ case was examined by Dolan [159] who did not find unphysical behaviour.

Once we introduce acceleration, the story changes. Pathological behaviour becomes manifest if one relies on η_U for the definition of efficiency. Consider an extremal

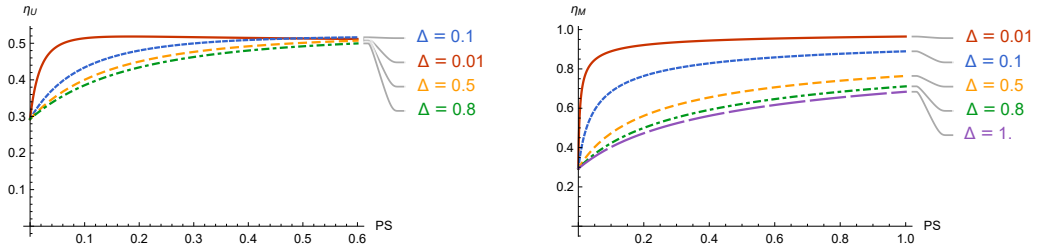

Figure 4.5: Efficiency of the maximum-energy extracting Penrose process for the Kerr geometry pierced by a conical deficit. *Left:* assuming the process extracts internal energy. *Right:* assuming the process extracts enthalpy.

rotating black hole of a fixed horizon size, average deficit Δ, and fixed non-zero C. Consider slowing the rotation of this black hole via a Penrose process, until the black hole is effectively static. If the passing test particles extract internal energy from the black hole, one should compare the internal energies of the initial and final black hole states. If the hole the process is applied to is small (that is, its horizon area is only slightly larger than the minimal value for which the mass vanishes) any non-zero acceleration results in a process with $\eta_U > 1$. This is shown in figure 4.6. One would conclude that the test particles can extract more internal energy than the black hole initially possessed. Similar pathologies apply if one assumes that the internal energy is extracted from an "available budget" of the initial enthalpy, as in (4.4.2).

We propose a resolution of this by instead assuming that is is in fact the enthalpy of the spacetime which is transferred to the deflected particles during scattering. Looking at the proposed definition (4.4.3) of η_M, one sees that roots of $M(J = 0)$ precisely give the points at which the efficiency becomes unity. For $M(J = 0) > 0$, (and less than $M(J = J_{\text{ext.}})$, which will always be the case), η_M lies between unity and zero. This is demonstrated in figure 4.7. The pathologies for positive mass black holes are no-longer observed, with the process becoming perfectly efficient only for spacetimes of vanishing mass. A superefficient process could only attained for non-physical solutions obtaining negative mass (not shown in figure 4.7). Black holes undergoing uniform acceleration are seen to give a minimally efficient Penrose process for moderately sized black holes, and the presence of slow acceleration is seen to become negligible in the large black hole limit, where efficiency approaches $1/2$ regardless of the value of C.

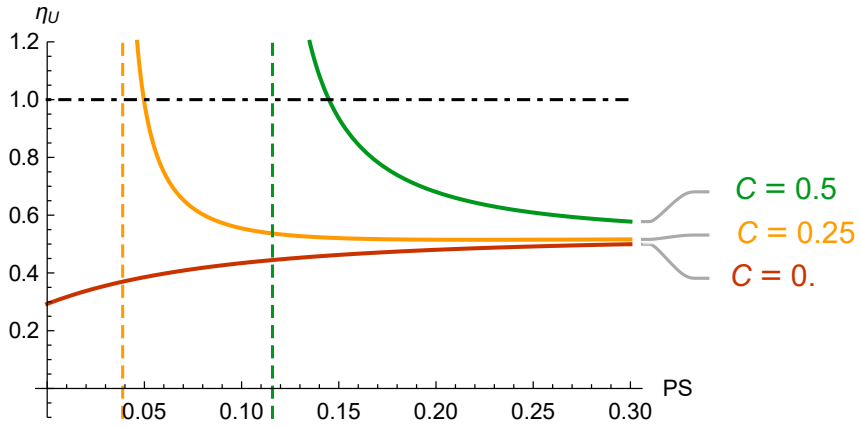

Figure 4.6: η_U for the maximum-energy extracting Penrose process applied to the rotating C-metric, with $\Delta = 1/2$ and at various values of acceleration. The efficiencies are given by solid coloured curves. The process becomes super-efficient ($\eta_U > 1$, indicated by the black, dot-dashed, horizontal line) as the horizon area of the black hole is lowered. A vertical dashed line of the corresponding colour denotes the lower bound on PS at which the black hole becomes massless.

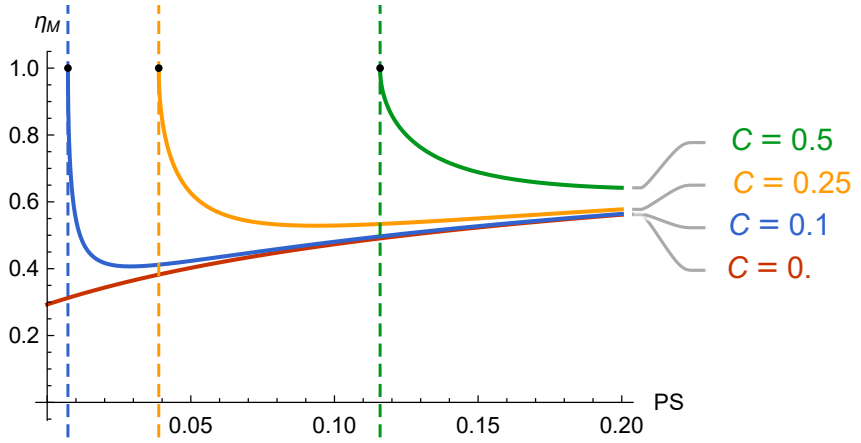

Figure 4.7: The efficiency of maximum-energy extracting Penrose process, as prescribed by the new definition η_M, for the rotating C-metric, with $\Delta = 1/2$, at various values of acceleration. The efficiencies are given by solid coloured curves, with the associated $M = 0$ limit for each value of C given by a vertical dashed line of the same colour. The process is never superefficient.

4.5 Conclusions

We have established "chemical" expressions for the thermodynamic potentials of the accelerating black hole, expressing them as functions of the thermodynamic charges varied in the first law. In particular, we have found a Christodoulou-Ruffini-like formula for the mass. The mass is expressed entirely in terms of thermodynamic charges which do not scale with the normalisation α of the time-coordinate of the solution and thus the formula provides compelling evidence that the value of α (3.3.47) used to define the mass in [150] is the correct one. Using these formulae, we were able to easily show that the potentials are the appropriate partial derivatives of the enthalpy.

The string tensions naturally form two variables, governing the thermodynamic effects due to average deficit and acceleration respectively. We used these variables to understand the effects of acceleration on the phase space. We were able to analytically find the set of black holes which can exhibit a snapping swallowtail, and explained this as a consequence of the fact that, unlike any of the usual charges, the addition of acceleration is an exothermic process. This allows for the existence of non-extremal black holes of vanishing mass. It would be interesting to find other examples of gravitational solutions with exothermic charges; they may also exhibit the snapping phenomenon.

We were also able to prove the Reverse Isoperimetric Inequality for this class of black holes.

Finally, we considered the efficiency of a Penrose process for a rotating, accelerating black hole. Using the "chemical" expressions (4.2.3) and (4.2.4), we showed that, within the extended thermodynamics framework, defining the efficiency of the process by assuming an extraction of internal energy from the black hole leads to inconsistencies. This argument mirrored that of Gwak [70], who argued that dropping electrically charged test particles across the horizon of a near-extremal electrically charged black hole violates the second law of thermodynamics. Similar contradictions were subsequently acknowledged in a number of scenarios [71–73, 75–79]. Gwak's issue was rectified by Hu et al. [80], who showed that by instead assuming that the absorbed particles increase the enthalpy of the black hole, no such violation of thermodynamics exists. We reviewed this in chapter 2. We resolved our issue in a similar manner: the Penrose process is well-behaved if one assumes an exchange of enthalpy between the black hole and the scattered particles. Our argument provides further evidence that the black hole mass should be considered a true thermodynamic enthalpy.

Chapter 5

Thermodynamics of accelerating black holes with vanishing cosmological constant

5.1 Overview

As discussed in chapter 2, the thermodynamic charges of a black hole such as entropy and temperature, while intrinsically quantum in nature, are related to classical attributes such as horizon area and surface gravity [38, 48, 50, 169]. Indeed, it was considering the classical response of a black hole to infalling matter that led Bardeen, Carter, and Hawking to make the link between black hole variations and the first law of thermodynamics in their seminal paper [36]. More recently, our understanding of black hole thermodynamics and the interpretation of the various parameters has also been improving. The first law of thermodynamics in gravitational systems has been more comprehensively understood as an extended thermodynamic law by including pressure in the guise of variations in vacuum energy [56, 62, 67, 158, 159], and a more complete understanding of the nature of "M" for the black hole has emerged as the enthalpy of the system [62]; see [66] for a review.

These attempts at understanding the first law have largely considered single, isolated, black holes, as in the Kerr-Newman family of solutions. Indeed, it was from this perspective that we analysed the thermodynamic behaviour of individual accelerating black holes in chapter 4. However, there are more complex, and therefore more interesting, multi-black hole systems for which exact solutions are known. Such geometries are thus amenable to thermodynamic analysis. For example, the Israel-Khan solution [170] is an asymptotically flat geometry consisting of two black holes kept apart by a "strut"—a conical defect with an angular excess—corresponding to

a negative tension cosmic string. More generally, one can sacrifice global asymptotic flatness to remove the unphysical negative-tension defect by running a positive tension cosmic string through the spacetime [111, 112, 145]. In doing so, one retains local asymptotic flatness away from the core. Generalising further, the *accelerating black hole*, encoded in the C-metric [115, 128], consists of a black hole with a protruding cosmic string [105] (or an imbalance between antipodal strings) that provides an accelerating force. In this case, not only is asymptotic flatness lost near the string extending to spatial infinity, but a non-compact *acceleration horizon* forms. Such systems beg the question: how does one define thermodynamics for a geometry which is neither asymptotically flat, an isolated black hole, nor (in the case of the Israel-Khan solution) stable?

Early thermodynamic investigations of black holes with conical defects focused on a fixed deficit threading the horizon [145, 171–174], or a deficit "variation" during the capture of a cosmic string [175]. The thermodynamic consequences of a truly varying deficit, were worked out in [146, 148]. In particular, an accelerating, asymptotically locally anti-de Sitter black hole has provided a context within which one maintains excellent computational control. This is owing both to one's ability to accelerate a black hole without forming an acceleration horizon, and the availability of the holographic dictionary [92]. A fully general first law was hence derived [146, 148], accounting for a variation in a string's tension μ:

$$\delta M = T\delta S - \lambda\delta\mu + \cdots . \tag{5.1.1}$$

This tension comes paired with a conjugate thermodynamic potential λ, christened the *thermodynamic length* of the string [148]. These results were later generalised to accelerating black holes carrying rotational and $U(1)$ gauge charge [149, 150]. We reviewed these advances in understanding the thermodynamics of the AdS C-metric in chapter 3, and explored their physical consequences in chapter 4. Interestingly, the expression for thermodynamic tension parallels that of the gravitational tension of Kaluza-Klein black strings [176–178], a set-up with no conical deficits.

Some understanding of the origin of thermodynamic length has also arisen. Considering a system of two black holes coupled by a strut, Krtouš and Zelnikov [179] have found a thermodynamic length corresponding to the strut worldvolume evaluated at some fixed time. This has since been verified for similarly coupled Kerr-Newman black holes [180, 181].

As stated above, much of the progress in formulating the first law of thermodynamics for accelerating black holes has been assisted by endowing the system with a negative cosmological constant. Though the system's accessibility allowed us to identify the novel thermodynamic features introduced by acceleration, (see chapter

4), from an astrophysical perspective such a set-up is not ideal. In that context, one should be interested in solutions with vanishing cosmological constant, for which holographic technology is unavailable and the formation of an acceleration horizon is unavoidable. Some attempt at calculating a mass for the C-metric without cosmological constant has been attempted in the literature. Specifically, since in this case the horizon generators behave as boosts at infinity, one can find an associated dimensionless charge by performing a background subtraction with the background taken to be Minkowski space with a conical deficit [173]. This charge can then be promoted by hand to a dimensionful mass by multiplication by a dimensionful quantity. However, the C-metric possesses two length scales – the horizon radius and the acceleration – rendering this definition ambiguous. Further, this definition obscures the connection to non-accelerating black holes: the Schwarzschild solution's horizon generators do not behave as boosts at infinity and so there does not exist a suitable "non-accelerating limit" of the C-metric's mass. In this chapter we address this shortcoming, showing how to correctly identify the mass in a manner consonant by the holographic calculations.

Taking a step back, one should also expect that if gravitational solutions are truly representatives of a first law of thermodynamics in the classical limit, then one will find common features no matter the number of black holes involved. We demonstrate this here, by calculating variations of an array of collinear black holes – connected by strings – which may be accelerated by external strings so as to form an acceleration horizon. We allow all parameters in the solution to vary and thereby prove a general first law,

$$\delta M = \sum_I T_I \delta S_I - \sum_J \lambda_J \delta \mu_J \,, \tag{5.1.2}$$

wherein the temperatures T_I and entropies S_I of the compact black hole horizons contribute together with the thermodynamic lengths λ_J and tensions μ_J of the strings. We justify the quantities appearing in (5.1.2), and consider its implications in a number of instructive cases, including a triple black hole system and the C-metric geometry. A key feature of our result is that the system behaves as a composite; the individual black holes are not thermodynamically isolated, but each interacts with the other, a variation of one having implications for all the rest.

Note also that the first law (5.1.2) further supports the notion of M as enthalpy [62], even though there is no cosmological constant present here. The energy momentum of the conical deficit, or cosmic string, takes the form of a worldsheet cosmological constant: the string has a tension equal in magnitude and opposite in sign to its energy density. Thus, the "$-\delta\mu_J$" term in (5.1.2) is in fact a "$+\delta p_J$" term, or pressure term, for the cosmic string. That the first law contains a $\lambda\delta p$, rather than $p\delta\lambda$ is indicative that M truly represents an enthalpy, and not an internal energy as

previously imagined.

The outline of the chapter is as follows: In section 5.2, we review the construction of black hole arrays and acceleration horizons in Weyl gauge [114]. In section 5.3 we formulate a first law for such systems, justifying the charges and potentials involved. Section 5.4 discusses implications of the result via some instructive examples and demonstrates a novel Christodoulou-Ruffini mass formula [160] for the C-Metric.

5.2 Four-dimensional Weyl metrics: black hole arrays

In this section we briefly review the multi-black hole solutions we will be analysing. We will largely follow the presentation of [182], with minor notational changes. The main new result in this section is a discussion of the determination of the acceleration scale for an array of accelerating black holes in (5.2.31). The black holes are aligned along an axis, and are static in the sense of possessing a time-like Killing isometry in the region between the black hole and acceleration horizons. Though an Israel-Khan-like solution for two rotating black holes is known analytically [183, 184], exact solutions for three or more Kerr black holes remain elusive[1]. To make the investigation of the system's thermodynamics accessible, we sidestep any discussion of rotation here. One expects that rotational charges may be included in the obvious way, once an appropriate family of geometries is written down.

With temporal and axial symmetry, the metric can be written in a block diagonal (Weyl) form, with metric functions $\gamma, \nu,$ and α depending only on transverse coordinates r and z:

$$ds^2 = e^{2\gamma}dt^2 - e^{2(\nu-\gamma)}(dr^2 + dz^2) - \alpha^2 e^{-2\gamma}d\phi^2 \,. \tag{5.2.1}$$

The Einstein equations are:

$$\Delta\alpha = -8\pi\alpha e^{2(\nu-\gamma)}\left[T^r_r + T^z_z\right] \tag{5.2.2}$$

$$\Delta\gamma + \frac{\nabla\gamma\cdot\nabla\alpha}{\alpha} = 4\pi e^{2(\nu-\gamma)}\left[T^t_t - T^r_r - T^z_z - T^\phi_\phi\right] \tag{5.2.3}$$

$$\Delta\nu + (\nabla\gamma)^2 = -8\pi e^{2(\nu-\gamma)}T^\phi_\phi \tag{5.2.4}$$

$$\frac{\partial^2_\pm\alpha}{\alpha} + 2(\partial_\pm\gamma)^2 - 2\partial_\pm\nu\frac{\partial_\pm\alpha}{\alpha} = 8\pi[T_{rr} - T_{zz} \pm 2iT_{rz}] \tag{5.2.5}$$

[1]The existence of arrangements of more than two aligned Kerr black holes (with or without intermediating objects) has, however, been demonstrated; see for example [185] and references therein.

where T^b_a is the energy momentum tensor of bulk matter, Δ is the two-dimensional Laplacian ($\partial_r^2 + \partial_z^2 = \partial_+\partial_-$), with $\partial_\pm = \partial_r \mp i\partial_z$ the derivatives with respect to the complex coordinates $(r \pm iz)/2$.

In the absence of matter or a cosmological constant, these have a very elegant solution: one simply fixes the conformal gauge freedom remaining in the metric (5.2.1) by setting $\alpha \equiv r/K$, which is consistent with (5.2.2). Note, we introduce the parameter K here to maintain a 2π periodicity of the $\phi-$coordinate; this will become relevant when we discuss conical sources. With $\alpha \propto r$, (5.2.3) becomes a cylindrical Laplace equation for γ in vacuo, with solution

$$\gamma = -2 \int \frac{S(\mathbf{r}')d^3\mathbf{r}'}{|\mathbf{r} - \mathbf{r}'|} \tag{5.2.6}$$

for a source with energy density $S(\mathbf{r})$. Note then that the metric component γ is nothing but the Newtonian source of axial symmetry. In turn, ν is determined from γ via (5.2.5). Since the equation for γ is linear, its solutions can be superposed; the nonlinearity of Einstein gravity shows up in the solution of ν. Note that, since regularity of the r-axis requires $\nu(0, z) = -\log K$, in general there will be conical singularities when regular solutions for γ are superposed. These can be interpreted as strings or struts supporting the static sources in equilibrium.

5.2.1 The Schwarzschild solution

As described in [182], a black hole may be represented by a finite-length line source[2], $8\pi S(\mathbf{r}) = \delta(r)/r$ for $z \in [-m, m]$, yielding

$$\gamma_S = -\frac{1}{2}\int_{-m}^{m} \frac{dz'}{[r^2 + (z - z')^2]^{1/2}} = \frac{1}{2}\log\frac{R_- - Z_-}{R_+ - Z_+}\,, \tag{5.2.7}$$

where

$$Z_\pm = z \mp m \qquad , \qquad R_\pm^2 = r^2 + Z_\pm^2\,. \tag{5.2.8}$$

Integration of (5.2.5) then gives

$$\nu_S = \frac{1}{2}\log\frac{E_{+-}}{2R_+R_-}\,, \tag{5.2.9}$$

where

$$E_{+-} = R_+R_- + Z_+Z_- + r^2\,. \tag{5.2.10}$$

[2]We make the gauge choice to centre the rod at $z = 0$.

Although this does not look like the familiar Schwarzschild black hole, the simple transformation

$$z = (\rho - m)\cos\theta \quad , \quad r^2 = \rho(\rho - 2m)\sin^2\theta \tag{5.2.11}$$

in fact returns the metric to its standard spherical form, with $2m = 2M_S$ representing the Schwarzschild radius.

5.2.2 Rindler space

Interestingly, one can formally introduce an acceleration horizon by adding a semi-infinite line source (SILM) [186], where $8\pi S(\mathbf{r}) = \delta(r)/r$ for $z > z_0$:

$$\gamma_R = -\frac{1}{2}\int_{z_0}^{\infty} \frac{dz'}{[r^2 + (z - z')^2]^{1/2}} \to \frac{1}{2}\ln\frac{R_0 - Z_0}{\ell_\gamma}\,, \tag{5.2.12}$$

where $Z_0 = (z - z_0)$, $R_0 = \sqrt{r^2 + Z_0^2}$, and the infinite integral has been regulated by the lengthscale ℓ_γ. Solving for ν yields the Rindler metric in Weyl coordinates:

$$ds^2 = \frac{(R_0 - Z_0)}{\ell_\gamma}dt^2 - \frac{\ell_\gamma}{2R_0}[dr^2 + dz^2] - \frac{\ell_\gamma r^2}{(R_0 - Z_0)}d\phi^2\,. \tag{5.2.13}$$

Since Rindler spacetime is simply flat spacetime as observed by an accelerating observer, we can transform (5.2.12) to Minkowski spacetime (in cylindrical polars) via the transformation

$$t = \frac{\ell_\gamma}{2}\log\left(\frac{\zeta + \tau}{\zeta - \tau}\right) \quad , \quad r = \frac{\rho}{\ell_\gamma}\sqrt{\zeta^2 - \tau^2} \quad , \quad z - z_0 = \frac{\tau^2 + \rho^2 - \zeta^2}{2\ell_\gamma}\,. \tag{5.2.14}$$

The origin of Minkowski corresponds to $z = z_0$, $r = 0$, (i.e. the start of the SILM), as expected. The origin of the Weyl system corresponds to $\zeta = \sqrt{2\ell_\gamma z_0}$, which gives a natural choice of gauge for the Weyl system. Note that the values of z_0 and ℓ_γ are independent from the perspective of solving the Einstein equations, the former is a gauge choice—the origin of the z-coordinate—and the latter because the same Rindler horizon can apply to observers with differing accelerations $A = 1/\ell_\gamma$; see figure 5.1. Interpreting the origin of the Weyl system as the location of the accelerating observer, thus fixing the gauge, gives $z_0 = 1/2A$ from $\zeta = 1/A$.

5.2.3 Many black holes

Now we can consider superposing solutions for γ, to build up multi-black hole solutions as described in [182]. We will briefly review these solutions, using a slightly different notation to [182] that is more suited to our argument. Each black hole is represented by a rod of length $2m_I$, $I = 1 \ldots N$, and acceleration is represented

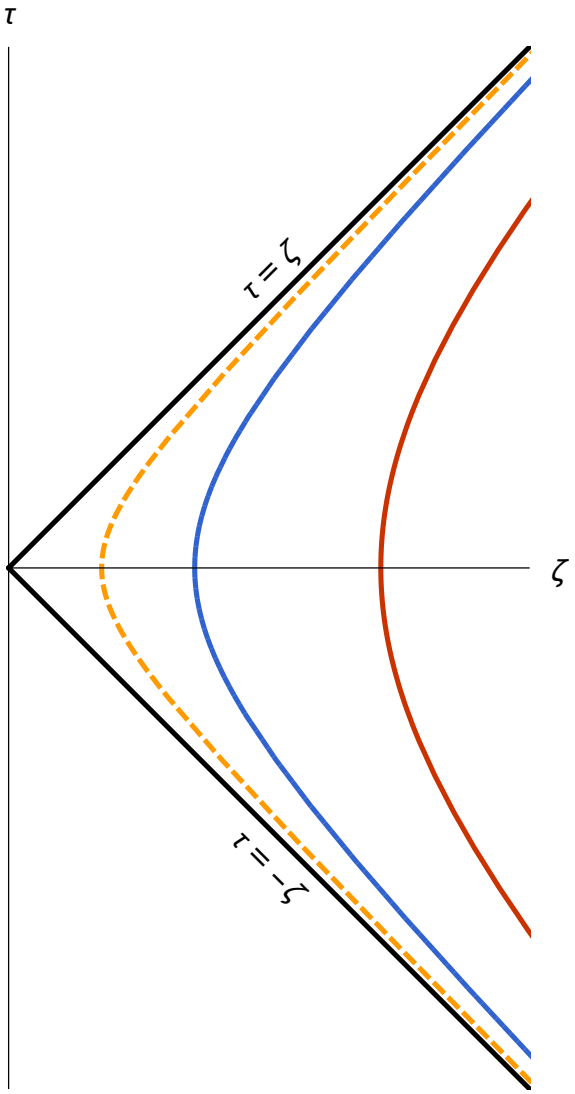

Figure 5.1: Rindler worldlines of observers with differing accelerations asymptoting the same horizon.

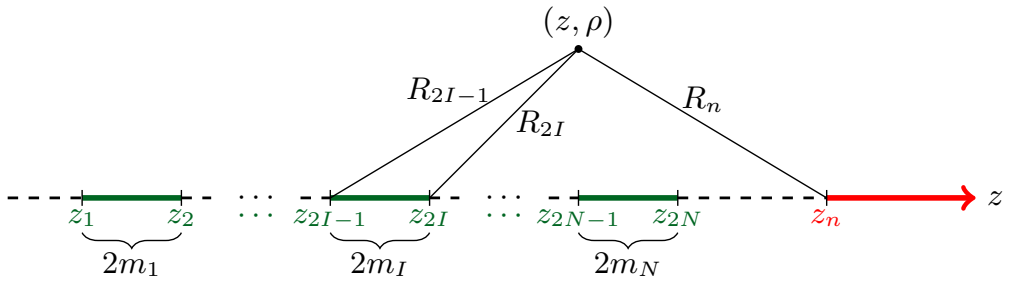

Figure 5.2: The source arrangement for the multi-black hole system of section 5.2.3. In the non-accelerating case, the point z_n, representing the start of the SILM (thick red arrow), and the SILM itself are absent; its neighbouring string (dashed black) instead extends to $z \to \infty$.

by a SILM as described above. We will label the rod ends at z_i, where $i = 1..n$ and $z_1 < z_2 < ...$ If we have an array of accelerating black holes, $n = 2N + 1$, and the SILM begins at z_n, if we have an array of (non-accelerating) black holes, then $n = 2N$ is even. This arrangement is depicted in figure 5.2

A natural generalisation of previous notation is

$$\begin{aligned} Z_i &= z - z_i\,, & R_i^2 &= r^2 + Z_i^2\,, \\ X_i &= R_i - Z_i\,, & E_{ij} &= R_i R_j + Z_i Z_j + r^2\,. \end{aligned} \tag{5.2.15}$$

The solution for γ is simply the superposition of the general potentials from (5.2.7), with ν then obtained by quadrature:

$$\begin{aligned} \gamma &= \frac{1}{2}\sum_{i=1}^{n}(-1)^{i+1}\log\frac{X_i}{\ell_\gamma}\,, \\ \nu &= \frac{1}{4}\sum_{i,j=1}^{n}(-1)^{i+j+1}\log\frac{E_{ij}}{\ell_\nu^2} + O_n\gamma\,. \end{aligned} \tag{5.2.16}$$

Here, the ℓ's are integration constants that cancel only if n is even, and O_n acts as a "switch" for additional terms when n is odd:

$$O_n = n - 2\left\lfloor\frac{n}{2}\right\rfloor = \begin{cases} 1 & n \text{ odd} \\ 0 & n \text{ even} \end{cases}\,. \tag{5.2.17}$$

As we move to the thermodynamics of the system, we will need the limit of these functions as we approach the axis, $r \to 0$. We therefore conclude this subsection by finding the behaviour of (5.2.16) as $r \to 0$, and discussing the conical deficits on the

axis. Noting that $R_i \to |Z_i|$ as $r \to 0$, we see that

$$X_i \sim |Z_i| - Z_i + \frac{r^2}{2|Z_i|} = \begin{cases} 2|Z_i| & z < z_i \\ \frac{r^2}{2Z_i} & z > z_i \end{cases} , \tag{5.2.18}$$

hence

$$\gamma \sim \frac{1}{2}\sum_{i=1}^{p}(-1)^{i+1}\log\frac{r^2}{2|Z_i|\ell_\gamma} + \sum_{i=p+1}^{n}(-1)^{i+1}\log\frac{2|Z_i|}{\ell_\gamma} \quad : \quad z \in (z_p, z_{p+1}) \tag{5.2.19}$$

where $p = 0$ if $z < z_1$ leaving only the second sum, and conversely the first sum for $z > z_n$.

Next,

$$E_{ij} \sim \begin{cases} 2Z_iZ_j & z < \mathrm{Min}[z_i, z_j]\ , \quad z > \mathrm{Max}[z_i, z_j] \\ \frac{r^2(z_i-z_j)^2}{2|Z_iZ_j|} & \mathrm{Min}[z_i, z_j] < z < \mathrm{Max}[z_i, z_j] \end{cases} . \tag{5.2.20}$$

Hence if we approach the axis at the I^{th} black hole, for which $z \in (z_{2I-1}, z_{2I})$,

$$\begin{aligned} \nu \sim & \frac{1}{4}\sum_{i,j=1}^{2I-1}(-1)^{i+j+1}\log\left(\frac{2Z_iZ_j}{\ell_\nu^2}\right) + \frac{1}{4}\sum_{i,j=2I}^{n}(-1)^{i+j+1}\log\left(\frac{2Z_iZ_j}{\ell_\nu^2}\right) \\ & + \frac{1}{2}\sum_{i=1}^{2I-1}\sum_{j=2I}^{n}(-1)^{i+j+1}\log\left(\frac{r^2(z_i-z_j)^2}{2|Z_iZ_j|\ell_\nu^2}\right) + O_n\gamma\,. \end{aligned} \tag{5.2.21}$$

Away from the black holes, writing $\nu_0 = \frac{1}{2}\log\left(\frac{\sqrt{2}\ell_\nu}{\ell_\gamma}\right)$, we have:

$$\begin{aligned} \nu(0,z) &= O_n\nu_0 && z < z_1 \\ &= \sum_{i=1}^{2I}\sum_{j=2I+1}^{n}(-1)^{i+j+1}\log(z_j - z_i) + O_n\nu_0 && z_{2I} < z < z_{2I+1} \\ &= O_n\left[\sum_{i=1}^{n-1}(-1)^i\log(z_n - z_i) + \nu_0\right] && z_{2N} < z < z_n\,. \end{aligned} \tag{5.2.22}$$

Notice that $z_j - z_{i+1} < z_j - z_i < z_{j+1} - z_i$, thus $\nu(0,z) < \nu_0$ for the first string tension, and (for accelerating black holes) $\nu_N < \nu_0$.

We can now identify the conical structure on the axis. The axis will have a conical defect if the circumference of circles of proper radius Δr around it are not $2\pi\Delta r$. For small r, $\Delta r \sim e^{\nu(0,z)-\gamma(0,z)}$ and the circumference is $2\pi r e^{-\gamma(0,z)}K^{-1}$, hence the deficit angle δ is

$$\delta = 2\pi\lim_{r\to 0}\left[1 - \frac{e^{-\nu(0,z)}}{K}\right] , \tag{5.2.23}$$

which is related to the cosmic string tension via $\delta = 8\pi\mu$. (5.2.22) dictates how the deficit angle changes as we move between the black holes. The tension between the

I^{th} and $(I+1)^{\text{th}}$ black hole is

$$\mu_I = \frac{1}{4}\left(1 - \frac{e^{-O_n\nu_0}}{K}\prod_{i=1}^{2I}\prod_{j=2I+1}^{n}(z_j - z_i)^{(-1)^{i+j}}\right) . \tag{5.2.24}$$

The final black hole has μ_N as the deficit for $z > z_{2N}$,

$$\mu_N = \begin{cases} \frac{1}{4}\left(1 - \frac{1}{K}\right) & n = 2N \\ \frac{1}{4}\left(1 - \frac{e^{-\nu_0}}{K}\prod_{i=1}^{N}\frac{(z_n - z_{2i-1})}{(z_n - z_{2i})}\right) & n = 2N+1 \end{cases} , \tag{5.2.25}$$

and for the incident tension, $z < z_1$, we have

$$\mu_0 = \frac{1}{4}\left(1 - \frac{e^{-O_n\nu_0}}{K}\right) . \tag{5.2.26}$$

We now see the interpretation of K. For the non-accelerating black hole array, there is an ambient tension running through the system, as the deficit outside the array ($z < z_1$ and $z > z_{2N}$) have the same conical deficit of

$$\mu_0 = \mu_N = \frac{1}{4}\left(1 - \frac{1}{K}\right) . \tag{5.2.27}$$

Equation (5.2.22) shows that $e^{\nu(0,z)} < 1$ between the black holes. Hence, if we did not insert the parameter K, instead retaining a 2π periodicity of ϕ for $z < z_1$ and $z > z_{2N}$, the conical singularity between any two of the black holes would be an excess $\delta < 0$, corresponding to a negative tension "cosmic strut" as in [179]. Although one can consider such systems [172, 179–181], we prefer to keep physical sources. We therefore take K large enough that all the conical singularities are deficits and correspond, in principle, to physical cosmic strings [111, 112]. Note however that if $K > 1$, there is an ambient conical deficit through the spacetime, irrespective of whether there is acceleration.

For an accelerating black hole array, we follow the convention of [1, 149] that K measures the ambient deficit, i.e.

$$\mu_0 + \mu_N = \frac{1}{2}\left(1 - \frac{1}{K}\right) . \tag{5.2.28}$$

This in turn allows us to determine ν_0:

$$e^{\nu_0} = \left(\frac{\sqrt{2}\ell_\nu}{\ell_\gamma}\right)^{1/2} = \frac{1}{2}\left(1 + \prod_{i=1}^{N}\frac{(z_n - z_{2i-1})}{(z_n - z_{2i})}\right) \equiv \frac{1}{2}\left(1 + V_n\right) . \tag{5.2.29}$$

thus we have

$$\mu_0 = \frac{1}{4}\left(1 - \frac{2}{(1+V_n)K}\right) \quad , \qquad \mu_N = \frac{1}{2}\left(1 - \frac{2V_n}{(1+V_n)K}\right) . \tag{5.2.30}$$

Note however that the choice of K is not unique; this one, (5.2.30), corresponds to the same normalisation as the standard C-metric, however, if one were viewing the metric as a split cosmic string, then an alternate natural choice might be to normalise the "initial" deficit. That is, we could choose $\mu_0 = \frac{1}{4}\left(1 - \frac{1}{K}\right)$, in which case $\mu_N = \frac{1}{4}\left(1 - \frac{V_n}{K}\right)$.

Finally, we are left with the length scale ℓ_γ, which is (only) present in an accelerating array, This parameter represents the net acceleration scale of the spacetime. We expect that for small accelerations (large z_n) this should asymptote the Rindler value $\ell_\gamma \sim 2z_n$. Interpreting the acceleration as the overall mass of the composite black hole system divided by the overall force measured by the differential deficit, we are led to

$$\ell_\gamma = \frac{M}{\mu_0 - \mu_N} = \frac{V_n + 1}{V_n - 1} \sum_1^N (-1)^k z_k \ , \tag{5.2.31}$$

where $M = \sum m_I K^{-1}$ is the total mass of the system (see section 5.3.1). We see that ℓ_γ has the required large z_n limit and a clear physical interpretation in close analogy with its pure Rindler cousin from section 5.2.2.

5.3 Thermodynamics of an array of black holes

We now derive a first law for collinear black holes with varying positive tension strings and a possible acceleration horizon, the solutions for which were presented in section 5.2.3.

5.3.1 Deriving the thermodynamic parameters

First we need to derive these relevant thermodynamic parameters. For the entropy of a given black hole, we compute the area of the relevant horizon

$$S_I = \lim_{r\to 0} \frac{\pi}{2K} \int_{z_{2I-1}}^{z_{2I}} r e^{\nu - 2\gamma} dz = \frac{\pi m_I}{K} \lim_{r\to 0} r e^{\nu - 2\gamma} \,. \tag{5.3.1}$$

For the temperature, the standard techniques apply, yielding

$$T_I = \lim_{r\to 0} \frac{1}{2\pi} \frac{e^{2\gamma}}{r e^{\nu}} = \frac{m_I}{2K S_I} \,. \tag{5.3.2}$$

The limit of $re^{\nu-2\gamma}$ as we approach the axis is given by (5.2.19), (5.2.21), and using (5.2.29), we obtain:

$$\log(re^{\nu-2\gamma}) \to \log 2 + O_n \log\left(\frac{\ell_\gamma e^{\nu_0}}{2}\right) + \sum_{i=1}^{2I-1} \sum_{j=2I}^{n} (-1)^{i+j+1} \log|z_j - z_i| \,. \tag{5.3.3}$$

The most challenging thermodynamic quantity to identify is the total mass. This is in part due to the fact that external strings which extend to infinity prevent global asymptotic flatness[3]and thus render the ADM mass [188] ill-defined. The presence of a non-compact acceleration horizon further complicates matters. Some attempt has been made [173] to redefine ADM mass in the presence of a conical defect by calculating the mass relative to conical Minkowski space, rather than pure Minkowski as one would in the usual construction. However, such a construction gives undesirable results. In particular, one would conclude that the mass of the C-metric is vanishing. This is puzzling from the perspective of having no smooth transition to the non-accelerating black hole. It is also counter to the intuition gained from the slowly accelerating black hole in AdS, for which the mass is $M_{\text{AdS}} = mK^{-1}$. One may be confident in the AdS calculation due to the holographic correspondence.

Although one may struggle to find a useful notion of ADM mass, the existence of the ∂_t isometry means that one still has a Komar construction [88, 89] at one's disposal. Focusing first on the non-accelerating case, the ADM mass for a system of collinear black holes without external strings ($\mu_0 = \mu_N = 0$) has been calculated [172]. One can compute the asymptotic behaviour,

$$e^{2\gamma} \sim 1 - \frac{2(\Sigma_{I=1}^{N} m_I)}{\tilde{r}} + \mathcal{O}(\tilde{r}^{-2})\,, \qquad \nu \sim \mathcal{O}(\tilde{r}^{-2})\,, \tag{5.3.4}$$

where $\tilde{r}$ is a suitable radial coordinate, and simply read off the mass. As discussed above, when we have an ambient conical deficit the ADM mass is undefined. However, we may instead read off the Komar mass as $M = \sum_{I=1}^{N} m_I/K$.

When an acceleration horizon is present, the situation requires more explanation. We take $k = \partial_t$ as our Killing vector field generating time translations. The normalisation of k is implicit in the choice (5.2.31) of ℓ_γ; see the discussion given at the end of section 5.2. The covector associated to k is $k^\flat = e^{2\gamma} dt$. Taking the exterior derivative and Hodge dual, we find

$$\star dk^\flat = \frac{r}{K e^{2\gamma}} \Big[(\partial_r e^{2\gamma}) dz - (\partial_z e^{2\gamma}) dr \Big] \wedge d\phi\,. \tag{5.3.5}$$

The causal structure of the spacetime is now significantly more complicated than in the non-accelerating case, but there is still a well defined spatial infinity [189]. To calculate the total mass, one could, in principle, integrate this form over a two-surface there. That said, it is more instructive to use Gauss' law to rewrite the boundary integral as the sum of integrals over each black hole horizon and a bulk

[3]A misleading notion of "local asymptotic flatness" has led to some incorrect calculations of mass in the literature [187].

integration:

$$\frac{1}{8\pi}\int_{\infty}\star dk^{\flat} = \frac{1}{8\pi}\sum_{I=1}^{N}\int_{\mathcal{H}_I}\star dk^{\flat} + M_{\text{bulk}}\,. \tag{5.3.6}$$

The quantity on the left hand side is the total mass[4] M. From (5.2.19) and (5.2.21), we have the relevant behaviour for the integrand on the right hand side of (5.3.6) near the I^{th} horizon $\mathcal{H}_I$,

$$\partial_r e^{2\gamma} \sim \frac{r}{2\,|z_{2I+1}z_{2I}|}\,, \qquad e^{-2\gamma} \sim \frac{4\,|z_{2I+1}z_{2I}|}{r^2}\,, \tag{5.3.7}$$

making the integrand straightforward:

$$\lim_{r\to 0}\left[\star dk^{\flat}\right]_{z\in(z_{2I},z_{2I+1})} = \frac{2}{K}dz\wedge d\phi + \dots\,. \tag{5.3.8}$$

Hence we conclude that the integral over $\mathcal{H}_I$, which we interpret as the mass of an individual black hole in the array, is

$$M_I \equiv \frac{1}{8\pi}\int_{\mathcal{H}_I}\star dk^{\flat} = \frac{m_I}{K}\,. \tag{5.3.9}$$

Finally, we note that the volume integral M_{bulk} vanishes, and that the strings themselves make no contribution to the above calculation.

The conclusion is that the total Komar mass is directly related to the rod lengths of compact horizons. The same result for the mass of the solitary accelerating black hole has been proposed in [150], albeit with a non-commital attitude to the normalisation of k. We also observe a clear similarity with the holographically calculated mass of a slowly accelerating black hole in AdS [149].

5.3.2 The first law of thermodynamics

We now show how to derive equation (5.1.2), the first law of thermodynamics for an array of collinear black holes. Consider a variation to the array. The solution (5.2.16) describes a coupled system; any variation of one black hole will impact on all the others. Therefore, we do not expect individual first laws for each black hole. Instead, it makes sense to consider a variation of the total mass

$$M = \sum_{I=1}^{N}\frac{m_I}{K}\,, \tag{5.3.10}$$

[4]There is a caveat here that we have divided through to retain only the mass of objects on one side of the acceleration horizon.

as this is a state function of the complete system. Indeed, this is the philosophy for the first law derived in [179]. Thus, to derive a first law, we must compute

$$\delta M = \sum_{I=1}^{N} \frac{1}{K}\delta m_I - m_I \frac{\delta K}{K^2}\,. \tag{5.3.11}$$

We begin by computing the variation in entropies for the individual black holes:

$$\sum_{I=1}^{N} T_I \delta S_I = \frac{1}{2}\sum_{I=1}^{N} \delta\left(\frac{m_I}{K}\right) + S_\Sigma + \frac{O_n M}{2}\left(\frac{\delta \ell_\gamma}{\ell_\gamma} + \delta\nu_0\right)\,, \tag{5.3.12}$$

having replaced $\ell_\nu = e^{2\nu_0}\ell_\gamma/\sqrt{2}$, and where

$$S_\Sigma = \sum_{I=1}^{N}\frac{m_I}{2K}\sum_{i=1}^{2I-1}\sum_{j=2I}^{2N}(-1)^{i+j+1}\frac{\delta(z_j - z_i)}{z_j - z_i} + O_n\sum_{I=1}^{N}\frac{m_I}{2K}\sum_{i=1}^{2I-1}(-1)^i\frac{\delta(z_n - z_i)}{z_n - z_i}\,. \tag{5.3.13}$$

This contains part of what we need for a first law, but has a rather messy sum!

Now we turn to the cosmic strings. We write the thermodynamic lengths for the strings as $\lambda_I = -e^{\nu_I}L_I$, and then vary the tensions in (5.2.24), (5.2.25), and (5.2.26) to obtain the contribution to the first law coming from the tensions:

$$-\sum_{I=0}^{N}\lambda_I\delta\mu_I = \sum_{I=0}^{N}\frac{L_I\delta K}{4K^2} + O_n\sum_{I=0}^{N}\frac{L_I}{4K}\delta\nu_0 + \mu_\Sigma\,, \tag{5.3.14}$$

where

$$\mu_\Sigma = \sum_{I=1}^{N-1}\frac{L_I}{4K}\sum_{i=1}^{2I}\sum_{j=2I+1}^{2N}(-1)^{i+j+1}\frac{\delta(z_j - z_i)}{z_j - z_i} + O_n\sum_{I=1}^{N}\frac{L_I}{4K}\sum_{i=1}^{2I}(-1)^i\frac{\delta(z_n - z_i)}{z_n - z_i}\,. \tag{5.3.15}$$

Putting these two expressions together, we have:

$$\begin{aligned}&\sum_{I=1}^{N}T_I\delta S_I - \sum_{I=0}^{N}\lambda_I\delta\mu_I \\ &\quad = \frac{\delta M}{2} + S_\Sigma + \mu_\Sigma + \sum_{I=0}^{N}\frac{L_I\delta K}{4K^2} + \frac{O_n}{4K}\sum_{I=0}^{N}(L_I + 2m_I)\delta\nu_0 + 2m_I\frac{\delta\ell_\gamma}{\ell_\gamma}\,.\end{aligned} \tag{5.3.16}$$

First, let us deal with the sums S_Σ and μ_Σ in these expressions. Observing that $m_I = (z_{2I} - z_{2I-1})/2$, we can rewrite the entropy sum as

$$S_\Sigma = \sum_{k=1}^{2N}\sum_{i=1}^{2\left[\frac{k+1}{2}\right]-1}\sum_{j=2\left[\frac{k+1}{2}\right]}^{2N}\frac{(-1)^{i+j+k+1}}{4K}z_k\frac{\delta(z_j - z_i)}{z_j - z_i} + \frac{O_n}{4K}\sum_{k=1}^{2N}\sum_{i=1}^{2\left[\frac{k+1}{2}\right]-1}(-1)^{i+k}z_k\frac{\delta(z_n - z_i)}{z_n - z_i} \tag{5.3.17}$$

Generalising [179] for the thermodynamic lengths of strings in between horizons as $L_I = z_{2I+1} - z_{2I}$ (with the exception of L_0 and L_N – see later) gives the tension sum

as

$$\begin{aligned}\mu_\Sigma = &\sum_{k=2}^{2N-1}\sum_{i=1}^{2[\frac{k}{2}]}\sum_{j=2[\frac{k}{2}]+1}^{2N}\frac{(-1)^{i+j+k}}{4K}z_k\frac{\delta(z_j-z_i)}{z_j-z_i}\\ &+\frac{O_n}{4K}\sum_{k=1}^{2N-1}\sum_{i=1}^{2\left[\frac{k}{2}\right]}(-1)^{i+k+1}z_k\frac{\delta(z_n-z_i)}{z_n-z_i}+\frac{L_N}{4K}\sum_{i=1}^{2N}(-1)^i\frac{\delta(z_n-z_i)}{z_n-z_i}\,.\end{aligned} \tag{5.3.18}$$

We now see that many of the terms in S_Σ are cancelled by terms in μ_Σ, leaving just $k=1,2N$ from the entropy sum, and intermediate i,j terms from each when $2[\frac{k+1}{2}]$ differs from $2[\frac{k}{2}]+1$:

$$\begin{aligned}&S_\Sigma+\mu_\Sigma\\ &=\sum_{j=2}^{2N}\frac{(-1)^{j+1}}{4K}z_1\frac{\delta(z_j-z_1)}{z_j-z_1}+\sum_{i=1}^{2N-1}\frac{(-1)^{i+1}}{4K}z_{2N}\frac{\delta(z_{2N}-z_i)}{z_{2N}-z_i}\\ &+\sum_{k=2}^{2N-1}\left[\sum_{j=k+1}^{2N}\frac{(-1)^{j+k}}{4K}z_k\frac{\delta(z_j-z_k)}{z_j-z_k}+\sum_{i=1}^{k-1}\frac{(-1)^{i+k+1}}{4K}z_k\frac{\delta(z_i-z_k)}{z_i-z_k}\right]\\ &+\frac{O_n}{4K}\left(\sum_{i=1}^{2N-1}\left[(-1)^i(L_N+z_{2N})-z_i\right]\frac{\delta(z_n-z_i)}{z_n-z_i}+L_N\frac{\delta(z_n-z_{2N})}{z_n-z_{2N}}\right)\\ &=\sum_{j=2}^{2N}\sum_{i=1}^{j-1}\frac{(-1)^{i+j+1}}{4K}(\delta z_j-\delta z_i)+\frac{O_n}{4K}\sum_{k=1}^{2N}(-1)^k(L_N+z_{2N}-z_k)\frac{\delta(z_n-z_k)}{z_n-z_k}\,.\end{aligned} \tag{5.3.19}$$

We now have to identify L_N (and L_0). We write

$$L_N=z_c-z_{2N}\qquad,\qquad L_0=z_1-z_c \tag{5.3.20}$$

in keeping with the expressions for L_I, where z_c is a normalisation, similar to that of the SILM in γ, to be determined. We can therefore reduce this combination to

$$\begin{aligned}S_\Sigma+\mu_\Sigma&=\sum_{I=1}^{N}\frac{\delta m_I}{2K}+\frac{O_n}{4K}\sum_{k=1}^{2N}(-1)^k\left(\delta(z_n-z_k)+(z_c-z_n)\frac{\delta(z_n-z_k)}{z_n-z_k}\right)\\ &=\sum_{I=1}^{N}\frac{\delta m_I}{2K}\,(1-O_n)+\frac{O_n}{4K}(z_c-z_n)\sum_{k=1}^{2N}(-1)^k\frac{\delta(z_n-z_k)}{z_n-z_k}\\ &=\sum_{I=1}^{N}\frac{\delta m_I}{2K}\,(1-O_n)-\frac{O_n}{4K}(z_c-z_n)\frac{\delta V_n}{V_n}\,.\end{aligned} \tag{5.3.21}$$

Having simplified $S_\Sigma+\mu_\Sigma$, we now turn to the rest of the putative first law, (5.3.16). We note that the sum of the thermodynamic lengths can be related to the sum of the masses:

$$\sum_{I=0}^{N}L_I=\sum_{I=1}^{N-1}(z_{2I+1}-z_{2I})+L_N+L_0=-2\sum_{I=1}^{N}m_I\,. \tag{5.3.22}$$

Hence,

$$\begin{aligned}\sum_{I=1}^{N} T_I \delta S_I - \sum_{\mu' s} \lambda_I \delta \mu_I &= \frac{\delta M}{2} + \sum_{I=0}^{N} \frac{L_I \delta K}{4K^2} + \sum_{I=1}^{N} \frac{\delta m_I}{2K} \\ &\quad + \frac{O_n}{4K}\left[\sum_{I=1}^{N} 2m_I \frac{\delta \ell_\gamma}{\ell_\gamma} - \sum_{I=1}^{N} 2\delta m_I - (z_c - z_n)\frac{\delta V_n}{V_n}\right] \\ &= \delta M + \frac{O_n}{2K}\left[m_{\rm tot}\frac{\delta \ell_\gamma}{\ell_\gamma} - \delta m_{\rm tot} - (z_c - z_n)\frac{\delta V_n}{2V_n}\right],\end{aligned} \tag{5.3.23}$$

where $m_{\rm tot} = \sum_I m_I$ is shorthand for the sum of the individual rod lengthscales. Thus, we have derived the first law (5.1.2) for a general array of black holes, provided we identify

$$z_c = z_n + \frac{2m_{\rm tot}\delta\ell_\gamma/\ell_\gamma - 2\delta m_{\rm tot}}{\delta V_n/V_n} = z_n - \left(\frac{4V_n}{V_n^2 - 1}\right) m_{\rm tot}\,, \tag{5.3.24}$$

for the accelerating black hole. For the non-accelerating black hole, the first law is automatically satisfied and we set $L_0 = L_N = (z_1 + z_{2N})/2$.

5.4 Exploring multi-black hole spacetimes

Having derived these expressions, it is interesting to explore some sample accelerating and non-accelerating black hole arrays to gain an understanding of the interdependency of black hole entropy, and to see how the strings contribute to the thermodynamic system as well as cross-checking against known results.

5.4.1 Non-accelerating arrays

We start by considering non-accelerating black holes. This includes the Schwarzschild case as a basic cross-check of our results, and the two black hole system which has already been considered in the literature [172, 179–181].

Schwarzschild with a string

As discussed in section 5.2, the Schwarzschild solution (with an axial conical defect) has $n = 2$, $N = 1$, and $z_2 - z_1 = 2m$. Conventionally, we set the centre of the rod at the origin so that $z_2 = -z_1 = m$. From (5.3.1) and (5.3.2) we find that the entropy and temperature are $S = 4\pi m^2/K$ and $T = 1/8\pi m$ respectively, as expected. For the cosmic string piercing the horizon, we have $\mu_0 = \mu_1 = \frac{1}{4}\left(1 - \frac{1}{K}\right)$, and $\lambda_0 = \lambda_1 = m$ in agreement with [148].

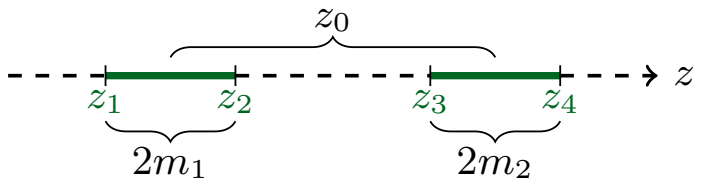

Figure 5.3: The source arrangement for two (non-accelerating) black holes.

Two black holes

The first law for the two black hole system, with $K = 1$, was explored in [179]. The arrangement of Newtonian sources for this solution is shown in figure 5.3. This value of K means that there are no strings running to infinity; instead, the black holes are held apart by a negative tension strut. Nevertheless, for larger K,

$$K \geq \frac{z_0^2 - (m_2 - m_1)^2}{z_0^2 - (m_1 + m_2)^2} \tag{5.4.1}$$

where z_0 is the distance between the centres of the two rods, we find results harmonious with their conclusions: the first law holds with the thermodynamic length of the defect connecting the black holes given by the worldsheet volume of the string per unit time. The thermodynamic lengths of the semi-infinite strings are now

$$\lambda_0 = \lambda_2 = \frac{z_4 - z_1}{2} = \frac{z_0}{2} + \frac{m_1 + m_2}{2}\,. \tag{5.4.2}$$

That is, the system responds to the average mass, and the distance between the black holes. Note that $\lambda_1 = -(z_3 - z_2)e^{\nu_1}$ also has a factor of the separation that is important for consistency in varying the net conical deficit of the system. We discuss this in more detail below for three black holes.

Three black holes

The three black hole system has rods on the intervals (z_1, z_2), (z_3, z_4), and (z_5, z_6); see figure 5.4. We are interested in exploring how the locations of the sources affect entropy and tension, and how a perturbation of one black hole impacts on the others. Hence, we consider a set-up in which the two outer black holes have equal mass and spacing from the middle black hole, which is centred around the origin: $z_6 - z_5 = z_2 - z_1 = 2m_0$, and $z_6 = -z_1 = z_0$, $z_4 = -z_3 = m$. The entropies and

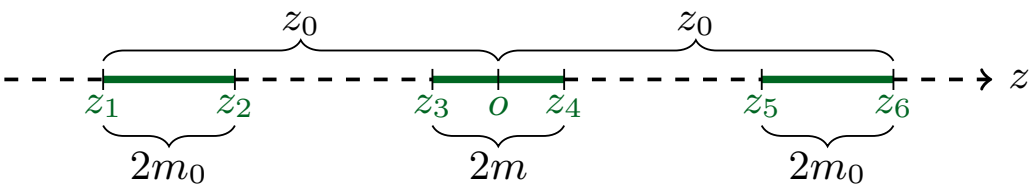

Figure 5.4: A source arrangement for three (non-accelerating) black holes. The two outer holes have equal masses $2m_0$, while the central hole has independent mass $2m$. The origin of coordinates o is marked.

tensions then become:

$$\begin{aligned} S_1 &= \frac{4\pi m_0^2}{K}\frac{(z_0+m_0)(z_0+m_0+m)}{z_0(z_0+m_0-m)} = S_3 \\ S_2 &= \frac{4\pi m^2}{K}\frac{(z_0^2-m_0^2)(z_0+m_0+m)^2}{z_0^2(z_0-m_0+m)^2} \\ \mu_0 &= \frac{1}{4}\left(1-\frac{1}{K}\right) \\ \mu_1 &= \frac{1}{4}\left(1-\frac{z_0^2(z_0^2-(m_0-m)^2)}{(z_0^2-m_0^2)(z_0^2-(m_0+m)^2)K}\right) = \mu_2\,. \end{aligned} \tag{5.4.3}$$

It is easy to see that $\mu_1 < \mu_0$. This is to be expected: in order to retain equilibrium, additional force must be applied on the outer black holes to counterbalance their attraction of the middle one.

For the thermodynamic lengths we have:

$$\begin{aligned} \lambda_0 &= (z_6-z_1)/2 = (z_0+m_0) = \lambda_3\,, \\ \lambda_1 &= -(z_0-m_0-m)\frac{(z_0^2-m_0^2)(z_0^2-(m_0+m)^2)}{z_0^2(z_0^2-(m_0-m)^2)} = \lambda_2\,. \end{aligned} \tag{5.4.4}$$

Thus the thermodynamic length of the ambient deficit—that is, the total from both string 1 and 4—is the distance from the north pole of the topmost black hole to the south pole of the bottom-most black hole. The length associated to the intermediate strings is *minus* the distance between the horizons of adjacent black holes (see figure 5.5).

We have found an interesting phenomenon where the thermodynamic lengths of the outer strings are positive whereas those of interior strings are negative. This is puzzling from the perspective of the individual black holes. However, upon taking the system as a composite it makes sense: if we alter the overall tension, we must account for the contributions from both inner and outer cosmic strings. The negative contribution from the interior lengths then counteracts the positive contribution from

the outer lengths. Explicitly, first set up the three black holes so that there is no deficit between the central and outer black holes. That is, K takes the value

$$K_0 = \frac{z_0^2(z_0^2-(m_0-m)^2)}{(z_0^2-m_0^2)(z_0^2-(m_0+m)^2)}\,. \tag{5.4.5}$$

We now "add" a cosmic string to the system by increasing K to K_0+K_1, so that

$$\delta\mu_0 = \frac{K_1}{4K_0(K_0+K_1)} \quad , \quad \delta\mu_1 = \frac{K_1}{4(K_0+K_1)} = K_0\delta\mu_0\,. \tag{5.4.6}$$

Note that the tension of the ambient cosmic string through the whole spacetime increases from $\mu_0 = (1-1/K_0)/4$ to $\mu_0+\delta\mu_0$. However, the region between the black holes, which initially had no deficit, now exhibits a cosmic string with tension $K_0\delta\mu_0$, i.e., a slightly greater tension than the increase in ambient string tension.

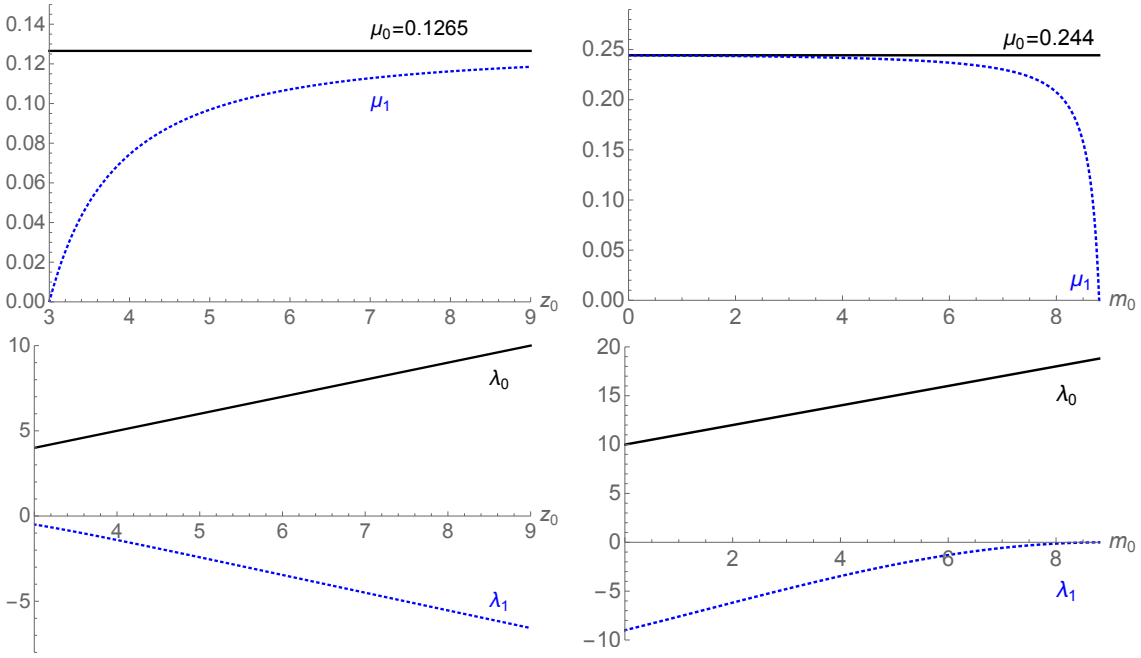

Figure 5.5: The variation of tensions and thermodynamic lengths of the three black hole system: Left: for equal masses as a function of black hole separation, and Right: for fixed black hole separation but varying the mass of the outer black hole. On the left, the tension is set by taking the minimal value consistent with zero tension between the black holes at minimum separation, $z_{min}=3$, giving an ambient tension of $41/324$. On the right the separation is set at $z_0=10$, and the outer black hole mass varies from zero to 8.8, which is very close to the merger limit of maximal tension, $\mu_0 \sim 0.244$.

Now let us look at the overall change in energy:

$$\begin{aligned}\sum_{I=0}^{3}\lambda_I\delta\mu_I &= \lambda_0\delta\mu_0+\lambda_1\delta\mu_1+\lambda_2\delta\mu_2+\lambda_3\delta\mu_3\\ &= 2(z_0+m_0)\frac{K_1}{4K_0(K_0+K_1)}-2\frac{(z_0-m_0-m)}{K_0}\frac{K_1}{4(K_0+K_1)}\\ &= \frac{(4m_0+2m)K_1}{4K_0(K_0+K_1)}\,.\end{aligned}\tag{5.4.7}$$

This is the total length of string captured by the black holes multiplied by the tension. We conclude therefore that the thermodynamic lengths really do behave in concert, combining in such a way that the overall modification of tension has a sensible impact on the overall thermodynamics of the system.

Turning to the entropies, one sees that $S_2/m^2 > S_1/m_0^2$. Essentially, this is saying that the inner black hole has a higher entropy in units of its mass (squared) than the outer ones. We understand this from the impact of the conical deficits: entropy is decreased in general by having a conical deficit, as part of the horizon is "cut out", leaving a rugby, as opposed to soccer, ball shape. We would expect that the entropy of the middle black hole would be relatively higher, as the deficit running through this black hole is less than the deficit emerging from the outer poles of the outer black holes.

The picture is a little more subtle than this broad brush expectation however; the central black hole has a uniform tension, μ_1, running through it, so naively, we might expect that the entropy might be tracked by $4\pi m^2(1-4\mu_1)$, but in fact the entropy is higher than this. For the outer black holes, we might expect the entropy to be tracked by the average tension between the poles, but again, it is higher. Indeed,

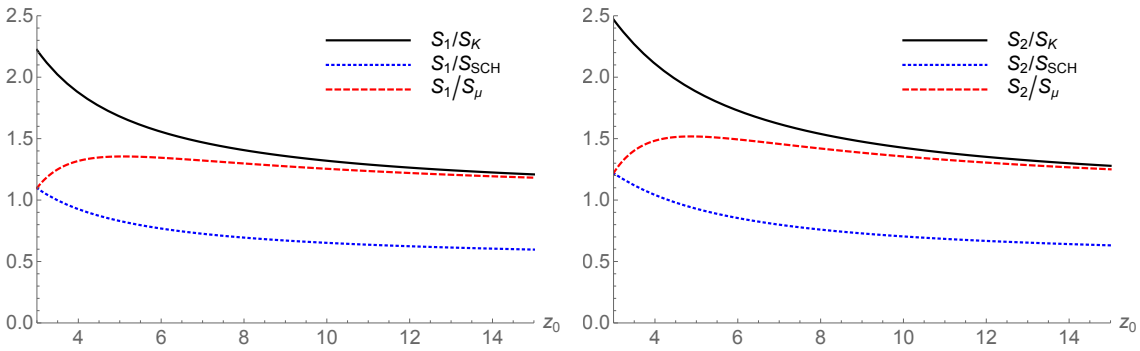

Figure 5.6: The entropy of the outer (left) and middle (right) black holes for equal masses as a function of black hole separation. The black holes all have unit mass, with an ambient tension of 41/324. The tension is set by taking the minimal value consistent with no strut between the black holes at minimum separation, here $z_{min} = 3$.

the entropy is higher even than the Schwarzschild entropy for a range of separation values z_0; see figure 5.6.

Similarly, we can track what happens to the entropy of one black hole as a result of changing the mass of the others. For example, keeping the central black hole at unit mass, and keeping the other two black holes at a given distance, we can see how the entropy of the central black hole

$$S_{\text{central}} = \frac{4\pi}{K}\frac{(1-m^2/z_0^2)(1+m/z_0+1/z_0)^2}{(1-m/z_0+1/z_0)^2} \tag{5.4.8}$$

alters as we change the mass of the outer black holes. The mass of the outer hole m_0 can range from zero to $z_0 - 1$, however at this point the horizons merge and to maintain a non-negative tension between the black holes we would have to have a maximal deficit of 2π. Instead, we choose a maximal mass m_{max}, and set K so that at the maximal mass there is no deficit between the black holes:

$$K = K_c \equiv \frac{z_0^2(z_0^2-(m_{\text{max}}-1)^2)}{(z_0^2-m_{\text{max}}^2)(z_0^2-(m_{\text{max}}+1)^2)}\,. \tag{5.4.9}$$

Figure 5.7 shows the variation of the entropy of the central black hole for a separation $z_0 = 10$, and a mass range up to $m_{\text{max}} = 8.8$. This is very close to the merger limit, giving a large external tension $\mu_0 \sim 0.244$, so a deficit angle of $(2\pi)^{-1}\delta \sim 0.977$. As before, the entropy is normalised by the entropy of a single black hole in a spacetime with both this ambient deficit ($S_K = 4\pi K^{-1}$) as well as that of a black hole with a cosmic string of tension μ_1 running through ($S_\mu = 4\pi(1-4\mu_1)$).

We now see a more nuanced behaviour. Initially, at $m = 0$, the spacetime is precisely that of a single black hole of unit mass pierced by a cosmic string of tension $\mu_0 = \mu_1 = 4^{-1}(1-K^{-1})$. As we switch on the black hole mass at z_0, μ_1 decreases, and this results in an increase in entropy, but this is over and above what we would

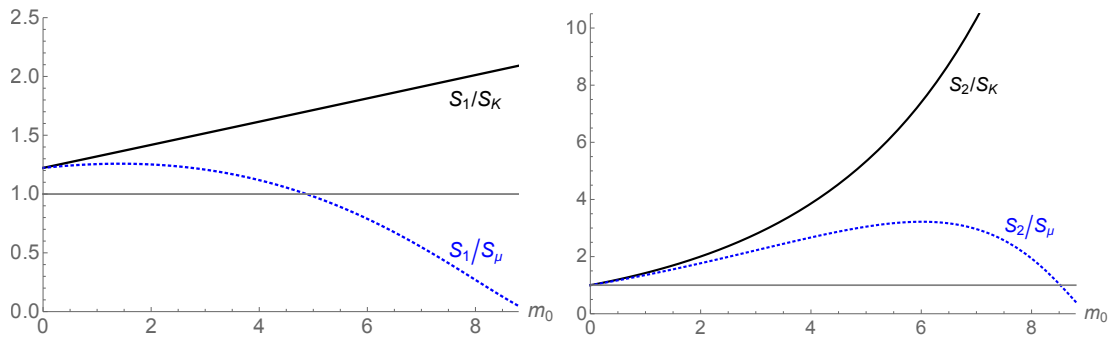

Figure 5.7: The entropies of the outer (Left) and central (Right) black holes as a function of the mass m_0 of the outer black holes. The mass of the central black hole is fixed at 1, and the outer black holes have the same mass m_0.

expect simply from a drop in μ_1. This comes primarily from the m dependence in (5.4.8). As we increase the mass further however, while the function S_2/S_K continues to grow, the ratio S_2/S_μ, of the entropy to that of a black hole with the μ_1 cosmic string starts to drop, eventually becoming less than one. We can understand this as being a consequence of the very large deficit in the majority of the spacetime, even though locally, at the central black hole, there is no cosmic string. The outer black holes are very close (within a Schwarzschild radius) to the central black hole, thus the geometry is strongly distorted there.

5.4.2 Accelerating arrays

Now let us consider accelerating black hole arrays of the type depicted in figure 5.2. The main difference with the non-accelerating array is that we have chosen the parameter K to represent the ambient tension, so that the asymptotic tension in principle varies with the locations of the rod ends. The expressions for entropy, temperature, tension and thermodynamic length are readily worked out from (5.3.1) and (5.3.2), though are not particularly illuminating. However, we can intuit the general behaviour as we vary the black hole masses and positions.

First, note that $\mu_0 > \mu_N$. We expect this because since the black holes are accelerating there must be an imbalance between the tension of the string coming in from infinity and that of the string exiting through the acceleration horizon. Next, as we increase the first black hole mass m_1, the first tension μ_1 will drop, as more of the pulling power of the string will be used to accelerate the increased mass. Whether the subsequent string tensions increase or decrease depends on the masses of the individual black holes: the second black hole will be attracted to the first (and third, if present) which provides an additional attractive force over and above that of the cosmic string. Typically, if the black holes are well separated relative to their size, the string tensions will cascade down in magnitude as one moves along the array, but for large black holes, this need not be the case (see the two black hole case below).

The C-metric

It is worth briefly checking the C-metric results, first proposed in [150]. The C-metric has a single horizon and a SILM so we have $n = 3$ and $N = 1$. This source arrangement is shown in figure 5.8. The metric in Weyl form is

$$ds^2 = \frac{X_1 X_3}{\ell_\gamma X_2} dt^2 - \frac{\ell_\gamma E_{12} E_{23}}{4 R_1 R_2 R_3 E_{13}} \left(\frac{z_3 - z_0}{z_3 - z_2} \right)^2 [dr^2 + dz^2] - r^2 \frac{\ell_\gamma X_2}{X_1 X_3} \frac{d\phi^2}{K^2} \,, \quad (5.4.10)$$

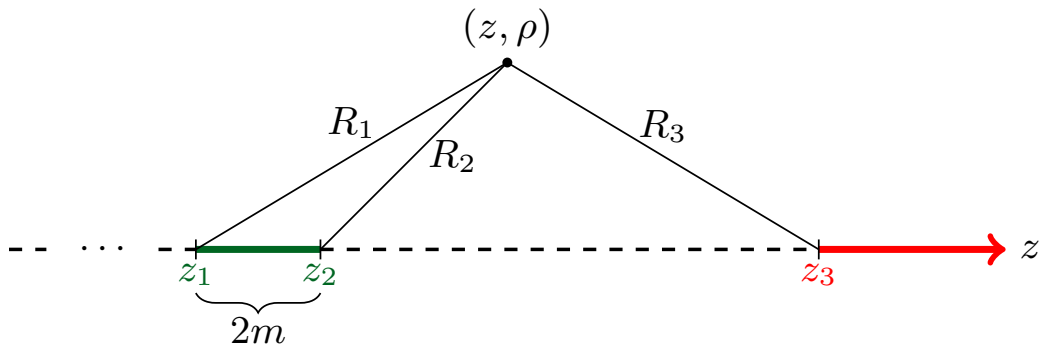

Figure 5.8: The source arrangement for the C-metric.

where $z_0 = (z_1 + z_2)/2$ is the centre of the black hole rod, and we have replaced $V_3 = (z_3 - z_1)/(z_2 - z_2)$. Here, $\ell_\gamma = 2(z_3 - z_0)$ is shown to be the reciprocal of the acceleration of a small black hole in appendix B, where we also note the transformation between this metric and the more familiar spherical coordinates.

Turning to the thermodynamics, we compute z_c as

$$z_c = z_3 - \frac{(z_3 - z_2)(z_3 - z_1)}{(z_3 - z_0)} = \frac{(z_3 z_0 - z_1 z_2)}{(z_3 - z_0)}\,. \tag{5.4.11}$$

Meanwhile, the entropy and thermodynamic lengths are

$$\begin{aligned} S &= \frac{4\pi m^2}{K}\frac{(z_3 - z_0)^2}{(z_3 - z_2)(z_3 - z_1)} &\to \quad & \frac{4\pi m^2}{(1 - 4m^2A^2)} \\ \lambda_0 &= e^{\nu_0}(z_c - z_1) = m\frac{(z_3 - z_1)}{(z_3 - z_2)} &\to \quad & \frac{m(1 + 2mA)}{(1 - 2mA)} \\ \lambda_1 &= e^{\nu_1}(z_2 - z_c) = m\frac{(z_3 - z_2)}{(z_3 - z_1)} &\to \quad & \frac{m(1 - 2mA)}{(1 + 2mA)} \end{aligned} \tag{5.4.12}$$

in agreement with the parameters proposed in [150].

It is also straightforward to write down a Christodoulou-Ruffini-like formula [160] for the C-metric. Following [1], define a quantity Δ characterising the average tension emerging from the black hole horizon, and a quantity C characterising the tension differential:

$$\begin{aligned} \Delta &= 1 - 2(\mu_0 + \mu_1) = \frac{1}{K}\,, \\ C &= \frac{\mu_0 - \mu_1}{\Delta} = \frac{z_2 - z_1}{4\ell_\gamma} \to mA\,. \end{aligned} \tag{5.4.13}$$

Then one finds that

$$M^2 = \frac{\Delta S}{4\pi}\left(1 - 4C^2\right)\,. \tag{5.4.14}$$

Increasing the acceleration of the black hole while maintaining a constant ambient

deficit removes energy from the black hole. This result is not as unsettling as it may first appear, as energy may be lost both across the acceleration horizon and as gravitational radiation at future infinity [137].

Electromagnetic charge Q and rotational charge J fit into the above story in a straightforward manner. By analogy with the asymptotically AdS case [1], one should expect that the Christodoulou-Ruffini formula will take the form

$$M^2 = \frac{\Delta S}{4\pi}\left[\left(1+\frac{\pi Q^2}{\Delta S}\right)^2 + \left(\frac{2\pi J}{\Delta S}\right)^2 - 4C^2\right] . \tag{5.4.15}$$

From the charged, rotating, (asymptotically flat) C-metric written in Boyer-Lindquist type coordinates, one may explicitly calculate the conserved charges using Komar-like integrals. This was done in [150]. One then finds that (5.4.15) holds only if the temporal Killing vector is normalised as it was in [150], (where the choice of normalisation was made in order to make the first law and Smarr relations hold). Since the quantities Q, J, S, Δ, and C are independent of the choice of normalisation, one may interpret (5.4.15) as evidence that the mass proposed in [150] is the correct one.

Two accelerating black holes

As a less trivial example, we present results for the two accelerating black hole system, first explored in [182]. The arrangement of Newtonian sources is shown in figure 5.9. We have

$$\begin{aligned}\ell_\gamma &= 2z_5 - \frac{(z_4^2 - z_3^2 + z_2^2 - z_1^2)z_5 - (z_4 - z_3 + z_2 - z_1)(z_1 z_3 + z_2 z_4)}{(z_4 - z_3 + z_2 - z_1)z_5 + z_1 z_3 - z_2 z_4} \\ &\sim 2(z_5 - z_{\rm com}) + \mathcal{O}\left(z_5^{-1}\right) ,\end{aligned} \tag{5.4.16}$$

where $z_{\rm com} = \frac{z_4^2 - z_3^2 + z_2^2 - z_1^2}{2(z_4 - z_3 + z_2 - z_1)}$ is the centre of mass of the pair of black holes (this formula generalises to any number of accelerating black holes).

Placing the two black holes at $\pm z_b$ fixes the gauge, and we can see how the string tensions and black hole entropies react to changes in black hole mass and distance to the horizon (without loss of generality we can keep z_b fixed as a choice of scale). Writing

$$S_0 = \frac{(m_1+m_2)(m_1+m_2+2z_b)(m_1 m_2 - z_b^2 + z_5^2)^2}{(z_5+z_b+m_1)(z_5-z_b-m_2)(z_5(m_2+m_1)+z_b(m_2-m_1))} , \tag{5.4.17}$$

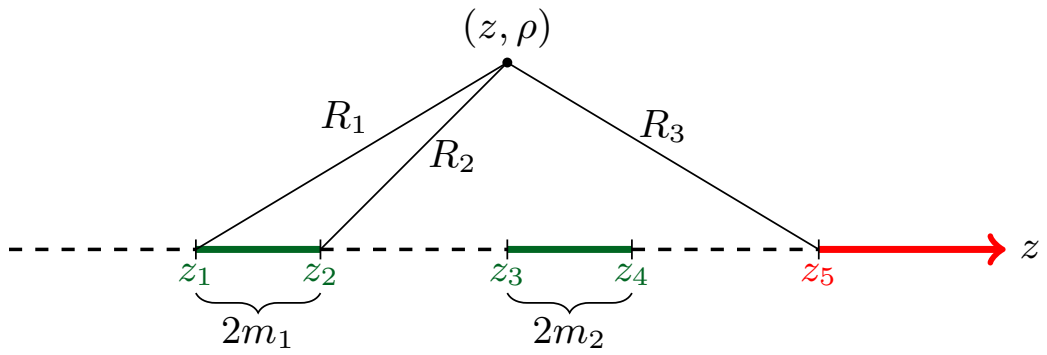

Figure 5.9: The source arrangement for two accelerating black holes
The source arrangement for two accelerating black holes.

the entropies are

$$\begin{aligned} S_1 &= \frac{4\pi m_1^2}{K}\frac{S_0}{(2z_b+m_1-m_2)(z_5+z_b-m_1)}\,, \\ S_2 &= \frac{4\pi m_2^2}{K}\frac{S_0}{(2z_b+m_2-m_1)(z_5-z_b+m_2)}\,. \end{aligned} \tag{5.4.18}$$

We can quickly see that if $m_1 = m_2$, the entropy of the first black hole will always be less than that of the second, which would be expected as the mean deficit through the first black hole is greater than that through the second. However, normalising the entropies with respect to their reference $S_K = 4\pi m_I^2/K$, we can see that the multiplicative factors in (5.4.18) show that both initially decrease as m_2 increases from zero before turning, although S_2/S_K shows a sharper decrease and eventually drops below S_1/S_K. Again, this behaviour is easy to see from the ratios in (5.4.18). Figure 5.10 shows this behaviour with varying m_I.

In order to compare the impact of varying the masses of the black holes and their separation, we first fix the outgoing tension at $z \to -\infty$, so that we are comparing the same conical asymptotics. Figure 5.10 shows the effect of varying the mass of the inner and outer black hole respectively on the entropies and thermodynamic lengths. In each case, we fix one of the masses at unity and vary the other. In both cases, varying the mass of the black hole closer to the acceleration horizon (m_2) causes a "crossover" behaviour.

Figure 5.11 shows how the entropy, length (and tension) are affected by moving the black holes apart. As before, the outgoing tension is fixed at 1/8, and both black hole masses are fixed at $m_1 = m_2 = 1$; the acceleration horizon is at $z_5 = 12$. The normalised entropy of the black hole closer to the acceleration horizon increases as the black holes are moved apart, whereas the entropy of the other black hole

decreases sharply. We can get a rough understanding of this by looking at the string tensions; the tension between the second black hole and the acceleration horizon drops off sharply at large separation, meaning that less of the angular direction is cut out by the deficit, thus increasing entropy. The tension between the black holes, μ_1, in contrast increases, leading to an expectation that the first entropy will decrease. While these statements are broadly true – note that we have already normalised the K factor out of the entropy, indicating that the effect of this geometry is magnified. As expected, the thermodynamic lengths exhibit a scaling with increasing separation, with the intermediate length λ_1 negative and decreasing to compensate the increase in λ_0.

5.5 Conclusions

To sum up: we have proven a thermodynamic first law for a composite system of black holes, both accelerating and isolated. We have allowed the varying of the tensions of

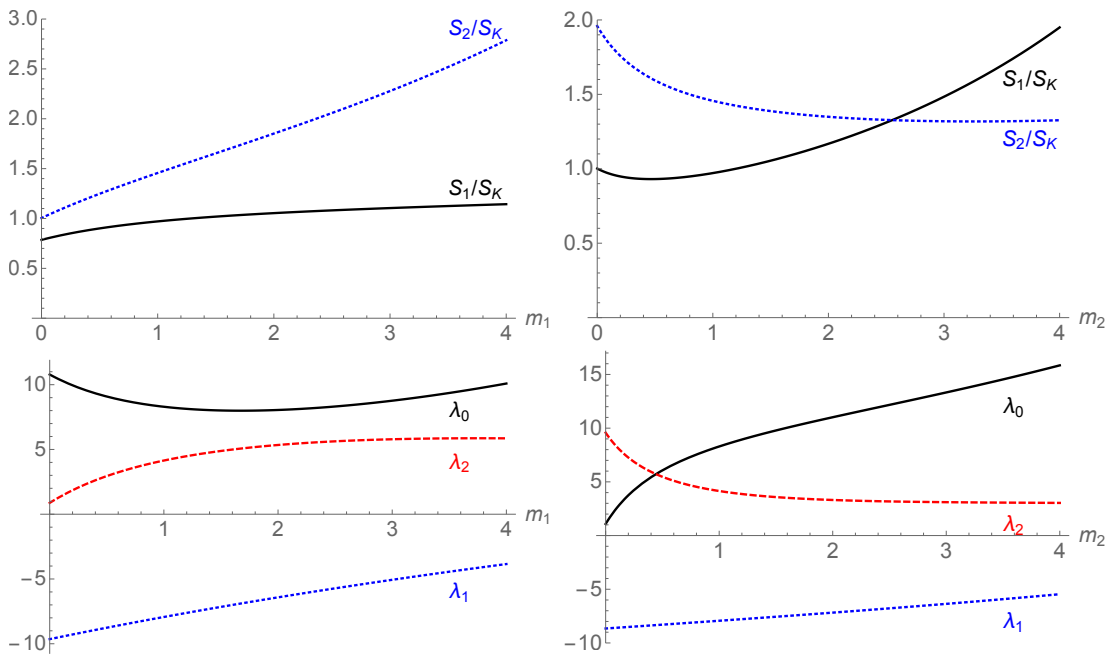

Figure 5.10: The variation of entropies and thermodynamic lengths as a function of mass in a system of two accelerating black holes. The outgoing tension is fixed at $\mu_0 = 1/8$, and the displacement of each rod from the origin at $z_b = 5$. One mass is fixed at unity, with the other mass varying from zero to 4. The upper plots show how the entropies, normalized by $4\pi m_I^2/K$, vary, and the lower plots the thermodynamic length. Note that K varies as m_I varies, in order to keep μ_0 fixed.

the cosmic strings along the axis that are necessary for maintaining the equilibrium configuration. As with the accelerating AdS black hole thermodynamics previously developed, these strings have a corresponding potential, the thermodynamic length, which has a direct specification in terms of the Weyl coordinate parametrising the axis of symmetry of the black hole array.

We have presented a range of accelerating and non-accelerating black hole systems to illustrate the various facets of the thermodynamic parameters. The main point is that the black holes form a fully composite thermodynamic system—the variation of one black hole affects all the others. We also see how the tensions and lengths in a composite system collude in such a way that the overall picture makes intuitive sense, whereas the individual black hole contributions may be less transparent.

Our findings, that the thermodynamic lengths between compact horizons is related to the proper distance along the axis, are in agreement with previous results [179–181]. However, in our construction there are also semi-infinite strings for which this proper distance would be infinite, yet this is not what we would expect thermodynamically. The thermodynamic length represents the contribution to the enthalpy from the tension (negative pressure) of the cosmic string inside the black hole, thus should be finite. We take this into account via a renormalisation process, the z_c, similar to the renormalising of the metric coefficients.

Open questions remain as to the inclusion of electric charge. Explicit solutions to Einstein-Maxwell theory describing two electrically charged black holes connected by a conical singularity, without exterior strings, are known and have been investegated thermodynamically [179, 181]. One could, therefore, proceed as in section 5.3, adding exterior semi-infinite strings to the system and determining the necessary modifications to the resulting thermodynamic lengths. However, since charging the

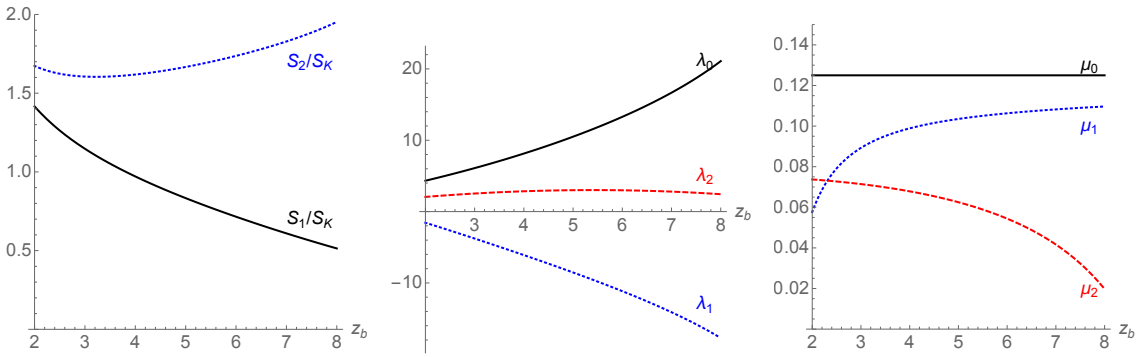

Figure 5.11: The variation of thermodynamic parameters for the double accelerating black hole set-up where the two black holes have equal mass $m_1 = m_2 = 1$ and the distance between them $2z_b$ is varied. The acceleration horizon is fixed at $z_5 = 12$.

black holes destroys the linearity property present in (5.2.3), it is not currently known how to construct arrays containing an arbitrary number of charged objects.

While the system of many black holes is not stable, it is nonetheless interesting that it too displays sensible thermodynamic properties, further supporting the inclusion of cosmic strings in the thermodynamic picture.

Chapter 6

The three-dimensional C-metric

6.1 Overview

As we have established, the four-dimensional C-metric [128] is the prototypical model of an accelerating black hole. It consists of a compact black hole horizon, undergoing uniform acceleration, isolated from a second black hole by a non-compact acceleration horizon. The force of acceleration is provided by a tension or compression in one or two codimension-two topological defects, which connect the horizon either to the second black hole or to infinity.

Similar solutions of the Einstein equations exist in the presence a negative cosmological constant [135, 190] and with the addition of rotational and electromagnetic charges [115, 125]. Such asymptotically (locally) anti-de Sitter solutions exhibit a "slowly accelerating" phase in which there is neither an acceleration horizon nor a second black hole. The drastic simplification which occurs in this phase has led to significant advances understanding the role of acceleration. In particular, the consistency of thermodynamic laws for slowly accelerating black holes has recently been established [146, 148–150]. First laws of thermodynamics have also been established for "rapidly accelerating" black holes [3], which possess an acceleration horizon. In these constructions, the thermodynamic tension of the defect is promoted to a thermodynamic charge [1], with the conjugate quantity being the defect worldvolume [179] renormalised in a suitable manner. We discussed these advances in chapters 3 and 4, wherin we showed how to formulate a first law for such black holes, and investigated the new thermodynamic phenomena which arise as a result of the defect.

Despite these advances in understanding the classical aspects of acceleration, relatively little is known about the quantum properties of the accelerating black hole. There are two apparent approaches towards addressing this shortcoming.

The first is to exploit the holographic correspondence, attempting to understand the quantum gravitational system via its dual description as a quantum field theory [52]. It has recently been shown that particular supersymmetric C-metrics may be realised as Kaluza-Klein truncations of eleven-dimensional supergravity solutions devoid of topological defects [152]. These uplifted solutions give a first step towards a direct holographic understanding of the C-metric. See also [191, 192], for studies investigating the holographic data available from conical defects which have been "smoothed" by matter fields.

The second approach is to exploit the simplification of general relativity in dimensions fewer than four, for which the theory is topological [193]. Lower-dimensional gravity still exhibits many of the interesting features shared by its higher-dimensional sibling, including the admission of black holes [194, 195]. However, from the perspective of the path integral, the lack of dynamics renders the theory radically simpler [196]. In fact, for asymptotically AdS solutions (without defect singularities) the path integral may be evaluated explicitly [197]. Were one able to construct three-dimensional solutions analogous to the C-metric, one may be able to apply similar technology to gain insight into the nature of acceleration. It is this latter approach we follow in this chapter.

Though we have motivated the C-metric as a description of an accelerating black hole, more generally one may select less typical ranges of parameters in the C-metric to find a menagerie of solutions [198]. In this way, one can construct geometries with horizons that extend to the conformal boundary; they are dual to strongly coupled field theories living on black hole backgrounds. Such solutions are known as either black funnels or black droplets [199]. In fact, the acceleration horizon formed in the rapidly accelerating phase of the AdS C-metric is one such droplet. In this chapter we demonstrate that an analogous collection of solutions exists in three dimensions, providing a range of black funnel and droplet solutions. This builds on the work of [40], which presented both a solution describing an accelerating conical deficit [200], and a solution analogous to the C-metric descibing a BTZ black hole [194] with a codimension-one defect emerging from its horizon. This defect is under compression so is commonly referred to as a "strut"; it possesses a negative energy density. We show that not only can a more physical solution be constructed, describing a BTZ black hole with the defect appendage under *tension*, the solution with a strut exhibits a richer phase structure than acknowledged in the literature, possessing a "rapid phase" in which a disconnected black droplet forms. This phase transition to a droplet solution is directly analogous to the formation of an acceleration horizon in the four-dimensional theory. We also construct a solution analogous to the C-metric describing a white hole and one exhibiting a black funnel. We calculate the masses

of our solutions using holographic techniques, and comment on their other physical properties.

The chapter is organised as follows. In section 6.2 we outline the process for constructing solutions from a C-metric-like ansatz, categorizing the resultant possibilities into three classes. In sections 6.3 and 6.4 we construct and analyse accelerating conical defects. In section 6.5 we construct a novel white hole solution, with a domain wall defect under tension, analogous to the C-metric. In section 6.6 we clarify the results of [40], discussing their BTZ-like solution with a domain wall under compression. We show that the solution exhibits a more broad range of behaviours than previously acknowledged, and call into question the author's conclusion that this is an "accelerating" BTZ black hole. In section 6.7 we demonstrate a similar, yet more physical, family of black holes possessing instead a domain wall under tension. We construct a novel three-dimensional black funnel in section 6.8, and conclude in section 6.9.

6.2 C-metric-like solutions in three dimensions

We start with an ansatz similar to the typical form of the four-dimensional C-metric [115, 135], as in [40, 201],

$$ds^2 = \frac{1}{\bar{\Omega}^2}\Big[\bar{P}(y)d\tau^2 - \frac{dy^2}{\bar{P}(y)} - \frac{dx^2}{\bar{Q}(x)}\Big]\,, \tag{6.2.1}$$

with the conformal factor given by

$$\bar{\Omega} = \bar{A}(x-y)\,. \tag{6.2.2}$$

Here, $\bar{A}$ is a parameter with dimensions of inverse-length. The conformal boundary lies at $x = y$. The Einstein equations with negative cosmological constant $\Lambda = -\ell^{-2}$ are explicitly solvable, with solution

$$\bar{Q}(x) = c + bx + ax^2\,, \qquad \bar{P}(y) = \frac{1}{\bar{A}^2\ell^2} - \bar{Q}(y)\,. \tag{6.2.3}$$

All three parameters a, b and c are, in principle, arbitrary real numbers, provided the correct signiture is retained. However, there exist gauge redundancies which allow us to eliminate two of the three. Firstly, eliminate b by noting that the metric is invariant under translation:

$$x \to x + s\,, \qquad y \to y + s\,. \tag{6.2.4}$$

There exists also a dilatation symmetry:

$$\tau \to s\tau\,, \qquad x \to sx\,, \qquad y \to sy\,. \tag{6.2.5}$$

Class	Sgn $\Delta_{\bar{Q}}$	Sgn c
I	+	+
II	+	−
III	−	+

Table 6.1: The three classes of solution and their defining characteristics.

The effect of dilatation is to scale a by a positive factor of s squared. We thus have the freedom to choose $|a| = |c|$. There are two possibilities; either the signs of a and c are the same, or they differ. The upshot of this discussion is that the parameter space consists of 3 possible classes of geometry[1] distinguished by the sign of c and that of the discriminant $\Delta_{\bar{Q}} = b^2 - 4ac$. Their definitions are given in table 6.1.

Symmetry under parity

$$x \to -x\,, \qquad y \to -y\,, \tag{6.2.6}$$

allows us to take $x > y$. This is the same as a choice one can make for the four-dimensional C-metric[2].

Finally, a simple parameter redefinition $A = \bar{A}/\sqrt{|c|}$ shifts all of the dependence on c into the timelike component of the metric which, since the geometry is static, we are free to absorb by a rescaling $\tau \to \tau/|c|$. We have arrived at a set of *canonical gauges* in which all of the dependence on a, b, and c has been removed. The metric in this gauge takes the form

$$ds^2 = \frac{1}{\Omega^2}\Big[P(y)d\tau^2 - \frac{dy^2}{P(y)} - \frac{dx^2}{Q(x)}\Big]\,, \tag{6.2.7}$$

with the conformal factor given by

$$\Omega = A(x - y) \tag{6.2.8}$$

and the metric functions in table 6.2. Also given in table 6.2 are the maximal ranges of x for which $Q(x)$ is positive.

Before giving a procedure to construct solutions with a domain wall, it will be helpful to describe how each solution class may be grouped into phases distinguished by causal structure. Geometries of Class I fall into three possible subclasses: those which satisy the *slow acceleration condition* $A^2\ell^2 < 1$ lack event horizons, wheras

[1] In fact, there is a fourth possible class, with both $c < 0$ and $\Delta_{\bar{Q}} < 0$, for which no range of x gives a Lorentzian signature. We disregard this case.

[2] However, in four dimensions there is an equivalent alternative: the symmetry for the four-dimensional metric is $x \to -x, y \to -y, \mu \to -\mu$, where μ is the coefficient of the y^3 term now present in $P(y)$. This has led some authors [198] to fix $\mu > 0$, which leaves a choice of orderings for x and y. We do not have such an option here since P is quadratic.

Class	$Q(x)$	$P(y)$	Maximal range of x
I	$1-x^2$	$\frac{1}{A^2\ell^2}+(y^2-1)$	$\lvert x\rvert<1$
II	x^2-1	$\frac{1}{A^2\ell^2}+(1-y^2)$	$x>1$ or $x<-1$
III	$1+x^2$	$\frac{1}{A^2\ell^2}-(1+y^2)$	$\mathbb{R}$

Table 6.2: The metric functions in canonical gauge, together with the largest available range of x.

those with $A^2\ell^2>1$ possess two distinct event horizons. Solutions which saturate the bound possess a single event horizon at $y=0$. We christen these subclasses *slow*, *rapid*, and *saturated* respectively. Solutions of Class II have a persistent horizon structure over all values of A and ℓ. However, they may be instead categorised by the choice to take x to live in a particular connected component, with either $x<1$ or $x>1$. We christen these the *left* and *right* subclasses of II respectively. Metrics of Class III attain P positive only if $A^2\ell^2<1$. There are then two event horizons, with the valid range of y between them.

6.2.1 Adding a domain wall

Having identified the largest available range of x in each solution class, we now seek solutions with one regular semi-axis and one domain wall coincident with the oposing semi-axis, where we interpret x as an angular variable. To do so, we take a solution written in canonical form and restrict x to take values in some subset of the maximal range, such that the newly restricted range extends between a root x_1 of Q and some finite value x_2. We then glue two copies of the resulting chart, "mirroring" along the surfaces $x=x_1$ and $x=x_2$. The Israel junction conditions

$$\Pi_{ij}|_{\text{right}}-\Pi_{ij}|_{\text{left}}=8\pi\int_{\text{left}}^{\text{right}}T_{ij} \tag{6.2.9}$$

give the stress induced in the glued surface induced by a discontinuity in canonical momentum $\Pi_{ij}=K_{ij}-Kh_{ij}$ across it. The (inwards pointing) unit normal to the bounding surface $x=$ constant is

$$\mathbf{n}=\pm\Omega^{-1}Q^{-\frac{1}{2}}dx\,. \tag{6.2.10}$$

Equation (6.2.10) takes the $\pm$ sign for $x_1\lesseqgtr x_2$. The extrinsic curvature $K_{ij}=\nabla_i n_j$ is then easily computed:

$$K_{ij}=\mp A\sqrt{Q}h_{ij}\,. \tag{6.2.11}$$

Using this result to evaluate the discontinuity in momenta across x = constant reveals the smeared stress to be proportional to the induced metric

$$\int_{\text{left}}^{\text{right}} T_{ij} = \mu h_{ij} \ , \tag{6.2.12}$$

with induced tension

$$\mu = \pm \frac{A}{4\pi} \sqrt{Q(x)} \ . \tag{6.2.13}$$

As we glue along $x = x_1$ we find smooth spacetime. However, along $x = x_2$, which is not a root of Q, we instead find a non-zero induced stress which signals a domain wall. The domain wall fulfils an analagous role to that of the conical deficit or *cosmic string* found in the four-dimensional C-metric, although in that case the defect has instead a codimension of two.

Throughout this chapter, when μ is positive we will refer to the domain wall as a *tensioned-wall*. Similarly, when μ is negative, we will refer to it as a *strut*. We restrict ourselves to a discussion of solutions containing only one domain wall. We will refer to such geometries either generically as *single-wall solutions*, or more specifically as either *single-tensioned-wall* or *single-strut solutions*.

Note that, since Class III solutions have Q everywhere positive, it is clear from (6.2.13) that this class does not admit a tensionless cutting and gluing of the type described above. Thus, single-defect solutions may be constructed from Class I or II solutions only.

When restricting the range of the x coordinate, it may be that the new range of parameters "avoids" one or more of the event horizons that would have been present, or changes the number of horizons that meet the conformal boundary, had the full range of x been considered. As a concequence, (with t timelike) there are eight qualitatively distinct single-tensioned-wall and seven qualitatively distinct single-strut solutions one can construct through various choices of x_1 and x_2.

Figure 6.1 shows all of the possible distinct single-tensioned-wall solutions constructable from Class I geometries. Figure 6.1a shows the rapidly accelerating subclass I_{rapid}, with three possible single-tensioned-wall solutions: A denotes a choice of $x_+ \in (-1, -y_h)$ with $y < 0$, for which there are no horizons. B denotes a choice of $x_+ \in (-y_h, 1)$ with $y < 0$, for which there is a single horizon. C denotes a choice of $x_+ \in (-y_h, 1)$ with $y > 0$. There are three similar solutions for $\text{I}_{\text{saturated}}$, shown in figure 6.1b. D denotes a solution with $x_+ < 0$ and E one with $x_+ > 0$. Having chosen $x_+ > 0$, one may then constuct single-tensioned-wall solutions with either $y > 0$ or $y < 0$. Figure 6.3a shows the unique single-tensioned-wall solution which can be derived from Class II. Table 6.4 gives a representation of all the possible single-tensioned-wall solutions with $t > 0$.

Similarly, figures 6.2 and 6.3b show all of the possible qualitatively distinct single-strut solutions constructable from Class I and II geometries respectively. The letters A, B, C, and D in figures 6.2a and 6.2b denote choices of x_+ that determine whether the constructed solution has (for B and D), or does not have (for A and C), a horizon. Table 6.5 gives a representation of all the possible single-strut solutions with $t > 0$.

6.3 Class I: A particle pulled by a domain-wall

Upon adding a domain wall to a Class I geometry by the method of the previous section, one can obtain an accelerating conical singularity held a fixed proper distance from the conformal boundary by a "pulling force" exerted by a domain wall.

To construct the accelerating conical defect, we start with the metric (6.2.7) with the Class I metric functions given in table 6.2. Choose some value $x_+ \in (-1, 1)$ and define a patch with $x \in (x_+, 1]$. Glue two copies of this patch, mirroring along both $x = x_+$ and $x = 1$. The identifications are shown in figure 6.6. The $x = 1$ axis of the newly formed spacetime is regular, and the $x = x_+$ axis marks the position of a domain wall of positive tension $\mu = A(4\pi)^{-1}\sqrt{Q(x_+)}$. A conical deficit is present at $y \to -\infty$. If $A^2\ell^2 \geq 1$, two (possibly coincident) horizons are present at $\pm y_h = \pm\sqrt{1 - A^{-2}\ell^{-2}}$. If $A^2\ell^2 < 1$, no horizons are present. One can now see why we call these three possibilities slow, saturated, and rapid; if the acceleration parameter A becomes too large, the geometry forms a Killing horizon at $y = -y_h$, which we refer to as an *acceleration horizon*. If, then, we choose $x_+ < -y_h$, as in the $\mathrm{I}_{\mathrm{rapid,A}}$ and $\mathrm{I}_{\mathrm{saturated,D}}$ geometries, this horizon is non-compact and masks part of the conformal boundary. The domain wall extends between the conical defect and the conformal boundary. If, instead, we choose $x_+ > -y_h$, as in the $\mathrm{I}_{\mathrm{rapid,B}}$ and $\mathrm{I}_{\mathrm{saturated,E},y<0}$ geometries the horizon "wraps around" to mask the entire conformal boundary. In this case the domain wall extends between the conical defect and the horizon. Note that the saturated solution possesses the lowest possible value of A whilst retaining an acceleration horizon. To describe an accelerating conical defect, we restrict ourselves to values of y between $y \to -\infty$ and either the conformal boundary at $y = x$ or the horizon at $y = -y_h$, whichever is encountered first as y is increased.

Following the $(3 + 1)$-dimensional wisdom, intuition can be gained by introducing dimensionful coordinates $r = -(Ay)^{-1}$ and $t = \alpha A^{-1}\tau$. We also introduce an angular coordinate $x = \cos(\phi/K)$. The parameter $K \equiv \pi/\arccos(x_+)$ encodes the range of

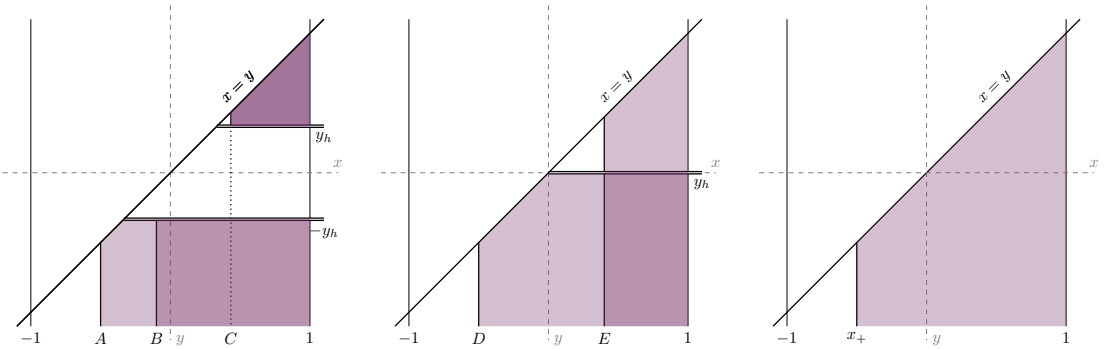

(a) $\mathrm{I}_{\mathrm{rapid}}$ (b) $\mathrm{I}_{\mathrm{saturated}}$ (c) $\mathrm{I}_{\mathrm{slow}}$

Figure 6.1: Coordinate ranges for single-tensioned-wall solutions constructed from metrics of Class I (with t timelike). Three qualitatively distinct solutions are shown in figure 6.1a, three in 6.1b, and one in 6.1c.

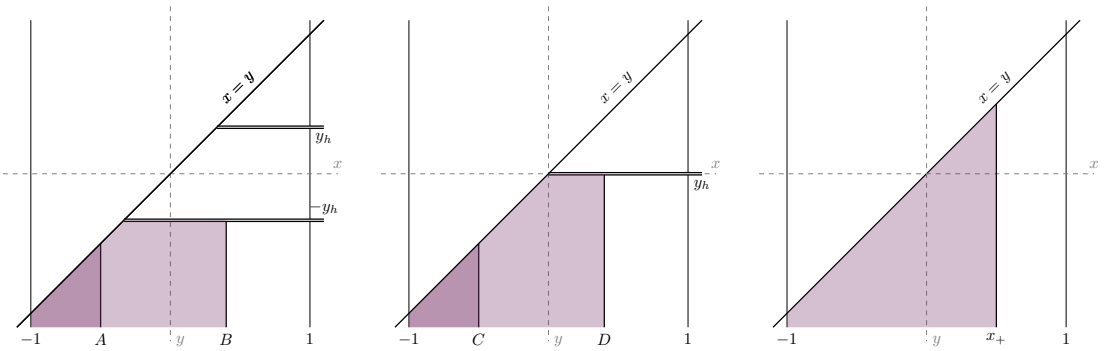

(a) $\mathrm{I}_{\mathrm{rapid}}$ (b) $\mathrm{I}_{\mathrm{saturated}}$ (c) $\mathrm{I}_{\mathrm{slow}}$

Figure 6.2: Coordinate ranges for single-strut solutions constructed from metrics of Class I (with t timelike). Two qualitatively distinct solutions are shown in figure 6.2a, two in 6.2b, and one in 6.2c.

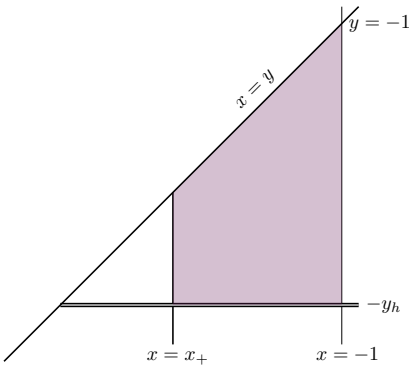

(a) $\mathrm{II}_{\mathrm{left}}$

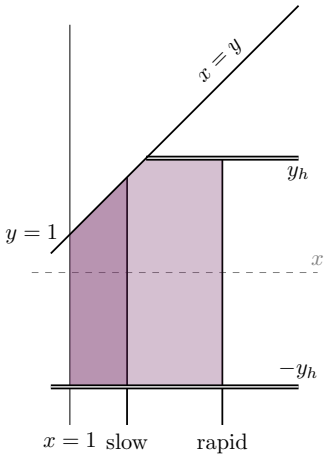

(b) $\mathrm{II}_{\mathrm{right}}$

Figure 6.3: Coordinate ranges for single-defect solutions constructed from metrics of Class II. Figure 6.3a shows a tensioned-wall solution, while 6.3b shows two qualitatively distinct strut solutions.

the x coordinate, fixing the range of ϕ to be $(-\pi, \pi)$. The metric is now

$$\begin{aligned} ds^2 &= \frac{1}{\left[1 + Ar\cos\left(\phi/K\right)\right]^2}\left[f(r)\frac{dt^2}{\alpha^2} - \frac{dr^2}{f(r)} - r^2\frac{d\phi^2}{K^2}\right], \\ f(r) &= 1 + (1 - A^2\ell^2)\frac{r^2}{\ell^2}\,. \end{aligned} \tag{6.3.1}$$

With foresight, we have left explicit the possibility of rescaling t by some dimensionless parameter α. This coordinate system covers both of the conjoined (x, y) patches when $y < 0$ for positive r values and both glued (x, y) patches when $y > 0$ for negative r values.

The conical deficit, if present, lies at $r = 0$. Moving out from the conical defect along a fixed angle ϕ and in the direction of increasing r, one meets first the conformal boundary if $|\phi|$ is large enough, an acceleration horizon at $r_h = (A\sqrt{1 - A^{-2}\ell^{-2}})^{-1}$ if both $|\phi|$ is smaller and $A^2\ell^2 \geq 1$, or a breakdown of the coordinate system with r diverging if $|\phi| < \pi/2$ and $A^2\ell^2 < 1$.

The conical deficit, which one may be inclined to refer to as the "particle mass" [202], is

$$m_c = \frac{1}{4}\left(1 - \frac{1}{K}\right), \tag{6.3.2}$$

while the tension in the domain wall is

$$\mu = \frac{A}{4\pi}\sin\left(\frac{\pi}{K}\right). \tag{6.3.3}$$

We have that $K \geq 1$. When $K = 1$, both the conical deficit (6.3.2) and domain wall

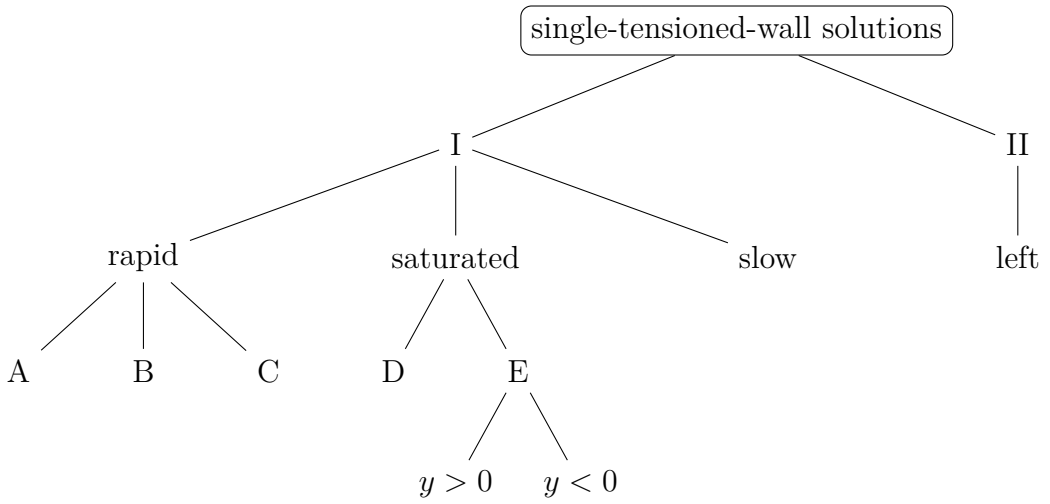

Figure 6.4: Classification of distinct single-tensioned-wall solutions with t timelike. Each leaf node represents a qualitatively-distinct solution.

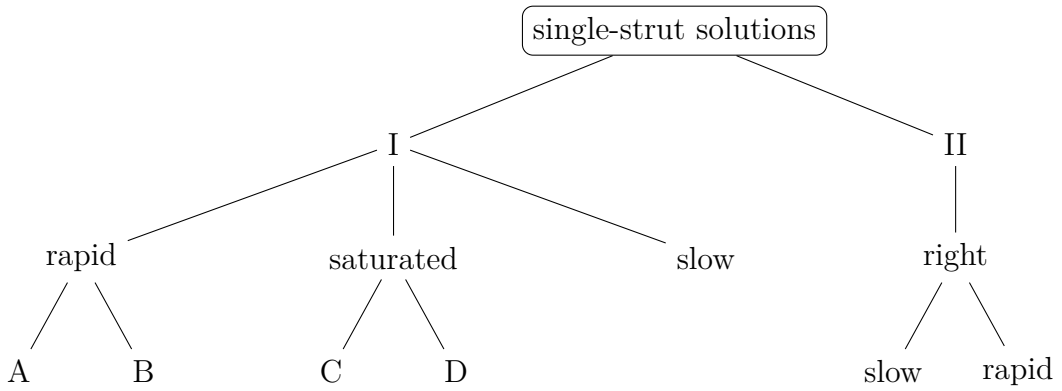

Figure 6.5: Classification of distinct single-strut solutions with t timelike. Each leaf node represents a qualitatively-distinct solution.

tension (6.3.2) vanish, and the geometry becomes global AdS_3 written in an accelerated frame. We have monotonically increasing particle mass as K increases. As $K \to \infty$, the particle mass asymptotes $1/4$, and the domain wall tension asymptotes zero. The domain wall tension lies within the range $(0, A/4\pi)$; see figure 6.7. As $A \to 0$, the mass of the particle is unaffected and the tension of the domain wall goes to zero. Note that, in the rapid or saturated phases, it is the magnitude of the particle mass relative to the other scales in the system which determines the horizon structure. For light particles $m_c \sim 0$ ($x_+ \sim -1$, $K \sim 1$), the acceleration horizon is non-compact and the domain wall reaches the boundary. For heavy particles, the acceleration horizon compactifies and one attains the de Sitter-like state.

To identify that the conical defect is accelerating, consider the four-acceleration along the worldline traced by the origin. The origin $r = 0$ of the coordinates (6.3.1)

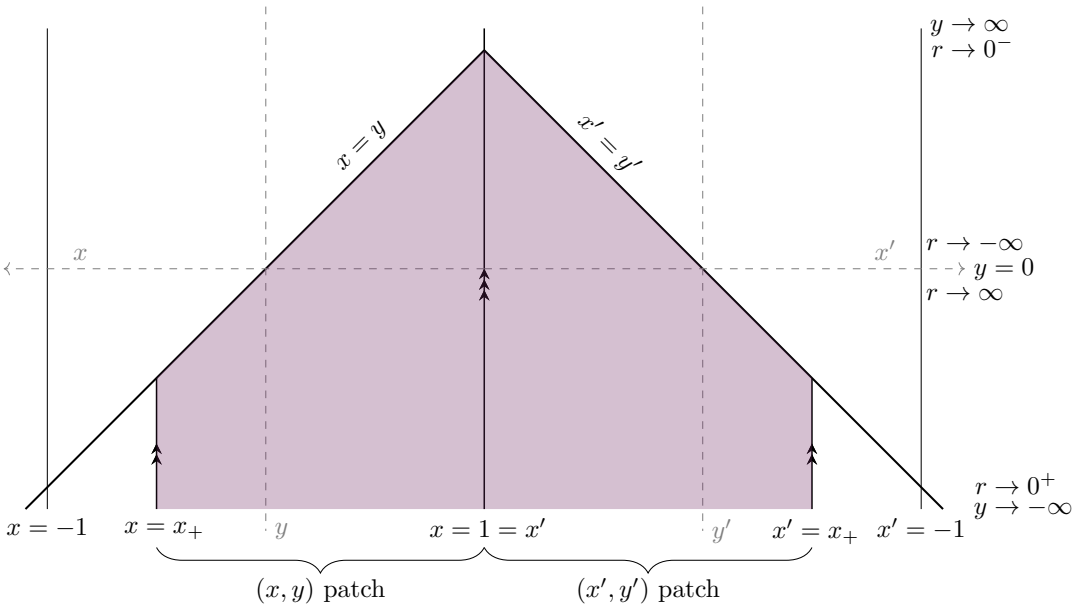

Figure 6.6: The two patches of type I spacetime used to construct a slowly accelerating conical defect pulled by a domain wall under tension.

has normalised four-velocity

$$\mathbf{u} = \frac{\alpha\Omega}{\sqrt{f}}\bigg|_{r\to 0} \partial_t \,. \tag{6.3.4}$$

The associated four-acceleration is then given by a covariant derivative,

$$\mathbf{a} = \nabla_{\mathbf{u}}\mathbf{u} \,, \tag{6.3.5}$$

which has magnitude

$$|\mathbf{a}| = \sqrt{-\left(\nabla_{\mathbf{u}}\mathbf{u}\right)^2} = A \,. \tag{6.3.6}$$

We see that the acceleration parameter gives the locally experienced acceleration of the particle.

One can also identify the particle's acceleration by considering the temperature of the horizon in the rapid phase. In this phase, demanding regularity of the Euclidean section indicates a horizon temperature of

$$T = \frac{A}{2\pi\alpha}\sqrt{1 - \frac{1}{A^2\ell^2}} \,. \tag{6.3.7}$$

For accelerations which are large compared to the AdS scale, $A \gg \ell^{-1}$, the particle is close to the acceleration horizon and provides effects which dominate the effect of the background curvature. In this regime, the geometry is approximately flat, and one should expect $\alpha \sim 1$. The horizon is then seen to be Rindler, with temperature

$T = (2\pi)^{-1}A$.

We now wish to identify the correct mass associated with this solution. This is typically tricky in the presence of acceleration horizons, though we refer the reader to chapter 5 for some recent progress. To sidestep the issue, focus on the slowly accelerating phase, $A^2\ell^2 < 1$, which possesses no horizons. In order to identify the correct mass, one must normalise the generator of time translations ∂_t to that of an observer located at the boundary [82]. That is, we wish to choose α in (6.3.1) such that t is the same time coordinate as when the geometry is written in global gauge

$$ds^2 = \left(1 + \frac{R^2}{\ell^2}\right) dt^2_{\text{Global}} - \frac{dR^2}{\left(1 + \frac{R^2}{\ell^2}\right)} - R^2 d\vartheta^2 \,. \tag{6.3.8}$$

Note that the function f has the same form as the comparable function in the C-metric in four dimensions, in the limit of vanishing mass parameter [189]. Hence, the transformation between local and global coordinates is already known to be

$$\left(1 + \frac{R^2}{\ell^2}\right) = \frac{f(r)}{\alpha^2 \Omega(r,\phi)^2} \,, \qquad R\sin\vartheta = \frac{r\sin\left(\phi/K\right)}{\Omega(r,\phi)} \,. \tag{6.3.9}$$

This holds only if the temporal rescaling is

$$\alpha = \sqrt{1 - A^2\ell^2} \,. \tag{6.3.10}$$

This mapping to global gauge allows for an intuitive picture of the spacetime to be constructed. By compactifying onto the Poincaré disk, we attain figure 6.8 for the slowly accelerating conical deficit, which is plotted at some fixed time t. The details of the compactification are given in appendix C. One must use two (x, y) patches to cover both the eastern and western hemicircles, as in figure 6.6. Note that, since t aligns with the global time coordinate, one may stack an infinite number of identical diagrams to visualise the complete space. We find a conical deficit "pulled" closer

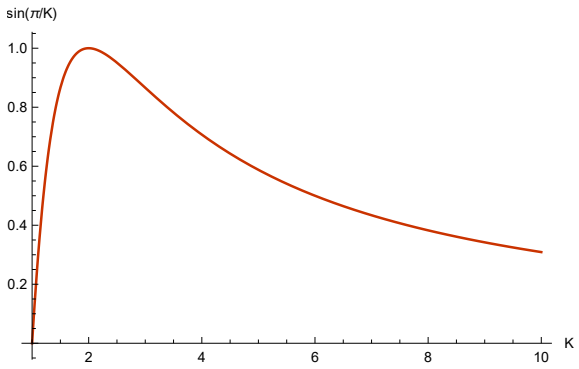

Figure 6.7: Plot of $4\pi A^{-1}\mu$, showing the effect of K on the wall tension.

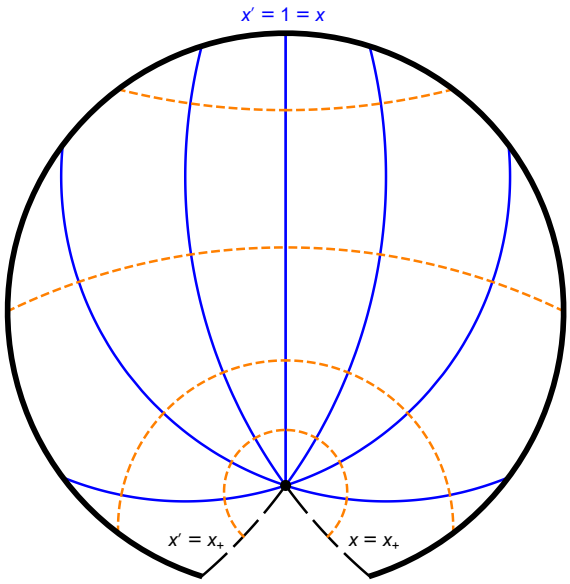

Figure 6.8: The slowly accelerating conical deficit with $A = 0.9\ell$, pulled by a domain wall, mapped onto the Poincaré disk. The deficit is shown as a black point and accelerates southwards. A "wedge" is removed from the global space, with its edges $x = x_+$ and $x' = x_+$ (long-dashed black) identified to attain a domain wall under tension. Several lines of constant x are shown in blue, with lines of constant y in dashed orange.

to the boundary than the origin of global coordinates by the removal of a distorted wedge.

In fact, although defining a mass in the rapidly accelerating case is difficult, we can already determine the appropriate Killing vector one should use once a reliable definition becomes available. Consider the portion of AdS_3 described by the metric

$$ds^2 = \left(-1 + \frac{R^2}{\ell^2}\right) dt^2_{\text{Rindler}} - \frac{dR^2}{\left(-1 + \frac{R^2}{\ell^2}\right)} - R^2 d\vartheta^2 \,, \tag{6.3.11}$$

with $r > -1$ and $\vartheta \in \mathbb{R}$. This geometry possesses a non-compact bifurcate Killing horizon at $r = -1$, generated by ∂_t, and we will refer to it as either the *planar BTZ geometry* or *Rindler wedge*. Close to the conformal boundary at large r, t is the usual timelike coordinate of the Poincaré patch. This time coordinate provides the zero-mass state for AdS_3 [93]. As such, the appropriate normalisation of t for the rapidly accelerating particle is given by choosing α such that the time coordinate of the solution (6.3.1) matches that of the Rindler wedge (6.3.11). This choice of Killing vector closely mirrors the choice made in chapter 5, where—for four-dimensional accelerating black holes without cosmological constant—the generator of the Rindler horizon was shown to provide a mass satisfying a first law. The transformation

between the rapid Class I and planar BTZ geometries is given by

$$\left(-1+\frac{R^2}{\ell^2}\right)=\frac{f(r)}{\alpha^2\Omega(r,\phi)^2}\,,\qquad R\sinh\vartheta=\frac{r\sin\left(\phi/K\right)}{\Omega(r,\phi)}\,, \tag{6.3.12}$$

where we must take

$$\alpha=\sqrt{A^2\ell^2-1}\,. \tag{6.3.13}$$

Much like the slowly accelerating case, the transformation between local coordinates and the Rindler wedge may be used to understand the rapidly accelerating conical deficit as a subset of AdS_3. For light conical deficits ($m_c \sim 0$), this space is the planar BTZ geometry with a wedge removed. This is shown in figure 6.9. We must plot two (x, y) patches in order to cover the Rindler wedge. Details of the mapping onto the global space given in appendix C. A key feature is that the Rindler time coordinate and the global time do not align. In figure 6.9, global time runs vertically, aligned with the axis of the cylinder. The conical defect on the other hand is seen to accelerate in from the conformal boundary at early times t, then move back out towards the boundary as $t \to \infty$. Both of these events happen in finite global time, resulting in the particle experiencing an acceleration horizon. It is already known that the planar BTZ geometry describes an acceleration horizon for test particles [195]; our solution describes a particular physical object undergoing acceleration, with the force of acceleration provided by a physical domain wall.

For heavy conical deficits (m_c large enough that $x_+ > -y_h$), the "wedge" removed is so large that includes all of the conformal boundary. This is shown in figure 6.10. In this phase, the bifurcation surface is compactifies to become a circle and the horizon structure is similar to that of de Sitter space.

6.3.1 The holographic mass

In this subsection, we identify the holographic mass of the slowly accelerating conical deficit.

Following the prescription of Brown and York [51], a quasi-local gravitational energy can be obtained by varying the action with respect to the boundary metric, provided the variational problem is well-posed. To correctly formulate the variational problem for an asymptotically AdS spacetime, one can add counterterms to regulate the UV divergences arising near the boundary [93, 203].

Following the recipe, one expands the metric in the Fefferman-Graham frame

$$ds^2=-\frac{\ell^2}{z^2}dz^2+\frac{\ell^2}{z^2}\left(g_{(0)}+z^2g_{(2)}+z^4g_{(4)}\right)\,. \tag{6.3.14}$$

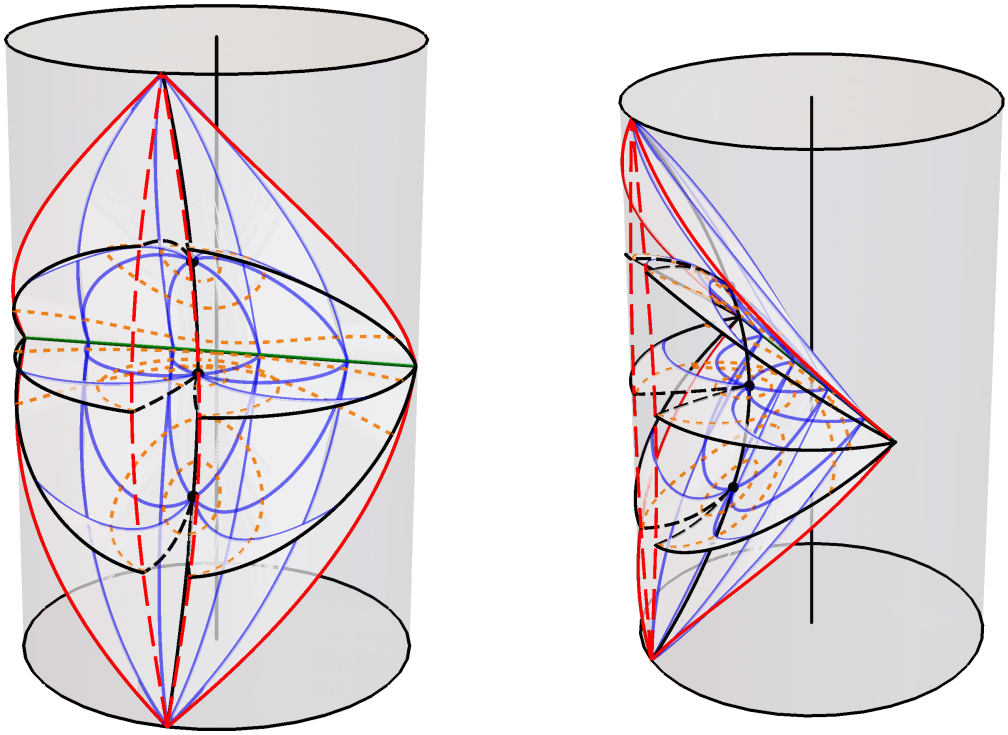

Figure 6.9: The Class $\mathrm{I}_{\mathrm{rapid,A}}$ solution embedded within global AdS_3. The deficit's worldline is shown in solid black. Several surfaces of constant t are plotted. The event horizons are demonstrated by the surfaces at early and late t. The bifurcation surface is shown as a green line. A "wedge" is removed, with its edges $x = x_+$ and $x' = x_+$ identified. These edges are shown in long-dashed black within each time-slice, and in dashed red at the boundary. The boundary of the classically accessible subset of the global boundary is shown in red. Lines of constant x are shown in blue, with lines of constant y in dashed orange. To guide the eye, the axis of the cylinder is also shown in black.

Here, $g_{(0)}$, $g_{(2)}$, and $g_{(4)}$ are covariant two-tensors. Note that this expression is exact; in $2+1$ dimensions the series terminates at order z^2 [93, 153, 204]. The holographic stress tensor $\langle T \rangle$ is completely determined by $g_{(0)}$ and $g_{(2)}$:

$$\langle T \rangle = -\frac{\ell}{8\pi}\left(g_{(2)} - g_{(0)}\,\mathrm{Tr}[g_{(0)}^{-1}g_{(2)}]\right) . \tag{6.3.15}$$

We now transform the metric (6.2.7) to Fefferman-Graham gauge near the boundary, as in [149], using the transformation

$$y = \xi + \sum_{m=1}^{\infty} F_m(\xi)\left(\frac{z}{\ell}\right)^m , \qquad x = \xi + \sum_{m=1}^{\infty} G_m(\xi)\left(\frac{z}{\ell}\right)^m . \tag{6.3.16}$$

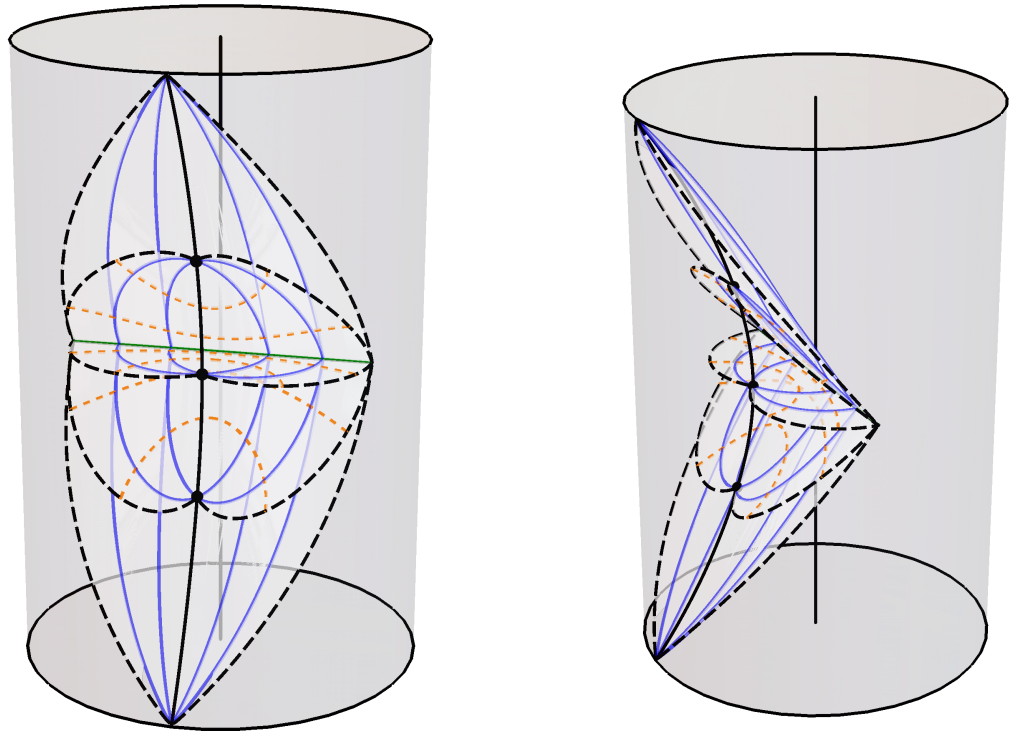

Figure 6.10: The Class $\mathrm{I}_{\mathrm{rapid,B}}$ solution embedded within global AdS_3. The deficit's worldline is shown in solid black. Several surfaces of constant t are plotted. The event horizons are demonstrated by the surfaces at early and late t. The bifurcation surface is shown as a green line. The surfaces $x = x_+$ and $x' = x_+$ identified. Lines of constant t within these surfaces are shown in long-dashed black. None of the conformal boundary is included in the solution. Lines of constant x are shown in blue, with lines of constant y in dashed orange. To guide the eye, the axis of the cylinder is also shown in black.

It is then straightforward to solve for the unknown functions order by order. For example, to determine G_1 we perform the above transformation, expand the resulting metric to order z^{-2}, and enforce the lack of a cross term $g_{z\xi} = 0$. We then expand to order z^{-1}, then z^{-2}, and so on, sequentially fixing the F_m's and G_m's to acquire Fefferman-Graham form. In this process, F_1 remains unfixed, appearing as a conformal factor in the boundary metric $g_{(0)}$. Also, the metric expansion explicitly terminates at $\mathcal{O}(z^2)$: once one gauge fixes $g_{zz} = \ell^2 z^{-2}$ and $g_{z\xi} = 0$ at order $m = 7$, the other metric components at the same order vanish identically. This property persists at orders $m > 7$; one is always able to add terms to the coordinate expansions (6.3.16) such that the $g_{(n)}$ with $i \geq 5$ are identically zero to arbitrary order.

For notational convenience, we define a dimensionless quantity $\Upsilon(\xi) \equiv 1 - A^2\ell^2(1-\xi^2)$.

A strategic redefinition of conformal factor

$$F_1(\xi) = \frac{\Upsilon^{3/2}}{A\ell\omega(\xi)} \tag{6.3.17}$$

in terms of a new (non-zero) function ω simplifies the boundary metric found by the process described above:

$$g_{(0)} = \frac{\omega(\xi)^2}{A^2}\left[d\tau^2 - A^2\ell^2\frac{d\xi^2}{1-\xi^2}\right]. \tag{6.3.18}$$

Note that $g_{(0)}$ has the correct dimensions of length squared. The leading correction is also diagonal:

$$g_{(2)} = \frac{1}{2A^2\ell^2}\left[1 - A^2\ell^2 + (1-\xi^2)\Upsilon^2\left(\frac{\omega'(\xi)}{\omega(\xi)}\right)^2\right]d\tau^2 + \left[\frac{1-A^2\ell^2}{2(1-\xi^2)\Upsilon^2}\right.$$
$$\left. + \left(1 - 3A^2\ell^2(1-\xi^2)\right)\frac{\xi}{(1-\xi^2)\Upsilon}\left(\frac{\omega'(\xi)}{\omega(\xi)}\right)^2 + \frac{3}{2}\left(\frac{\omega'(\xi)}{\omega(\xi)}\right)^2 - \frac{\omega''(\xi)}{\omega(\xi)}\right]d\xi^2\,. \tag{6.3.19}$$

Note that $g_{(2)}$ is dimensionless, as expected. We will not write down $g_{(4)}$ as it will not be needed. Raising and lowering indices with $g_{(0)}$, the non-zero components of the stress tensor are

$$16\pi\omega(\xi)^2\ell\langle T^\tau_\tau\rangle = -\left(1 - A^2\ell^2\right) - 2\xi\left(1 - 3A^2\ell^2\left(1-\xi^2\right)\right)\Upsilon\left(\frac{\omega'(\xi)}{\omega(\xi)}\right)$$
$$+ \left(1-\xi^2\right)\Upsilon^2\left[2\frac{\omega''(\xi)}{\omega(\xi)} - 3\left(\frac{\omega'(\xi)}{\omega(\xi)}\right)^2\right] \tag{6.3.20}$$

and

$$16\pi\omega(\xi)^2\ell\langle T^\xi_\xi\rangle = \left(1 - A^2\ell^2\right) + \left(1-\xi^2\right)\Upsilon^2\left(\frac{\omega'(\xi)}{\omega(\xi)}\right)^2. \tag{6.3.21}$$

As expected for a two-dimensional boundary theory [153, 205], tracing this stress reproduces the usual Weyl anomaly

$$\langle \mathrm{Tr}[g_{(0)}^{-1}T]\rangle = \frac{c_{\mathrm{Virasoro}}}{24\pi}R(g_{(0)})\,, \tag{6.3.22}$$

where $R(g_{(0)})$ is the Ricci scalar of the boundary metric $g_{(0)}$:

$$R(g_{(0)}) = -\frac{2\Upsilon}{\ell^2\omega(\xi)^2}\left(\xi\left(1 - 3A^2\ell^2(1-\xi^2)\right)\frac{\omega'(\xi)}{\omega(\xi)}\right.$$
$$\left. + (1-\xi^2)\Upsilon\left[\left(\frac{\omega'(\xi)}{\omega(\xi)}\right)^2 - \frac{\omega''(\xi)}{\omega(\xi)}\right]\right). \tag{6.3.23}$$

The central charge is calculated to be $c_{\mathrm{Virasoro}} = 3\ell/2$, suggesting the existence of

a locally Virasoro asymptotic symmetry group. The stress tensor is covariantly conserved; $\nabla_\mu T^\mu{}_\nu = 0$.

We are now in a position to write down the mass. Being careful to include the contributions from both (x, y) patches, accounting for their orientations, the mass—calculated with respect to ∂_t—is

$$M = 2A \int_{x_+}^{1} \sqrt{-\det g_{(0)}}\, \langle T^\tau_\tau \rangle \, d\xi \,, \tag{6.3.24}$$

where the integrand is

$$\sqrt{-\det g_{(0)}}\, \langle T^\tau_\tau \rangle = -\frac{1}{8\pi A \alpha \sqrt{1-\xi^2}} \left\{ \frac{1 - A^2\ell^2}{2\Upsilon} + \xi \left(1 - 3A^2\ell^2(1-\xi^2)\right) \left(\frac{\omega'(\xi)}{\omega(\xi)}\right) \right. \\ \left. + (1-\xi^2)\Upsilon \left[\frac{3}{2} \left(\frac{\omega'(\xi)}{\omega(\xi)}\right)^2 - \frac{\omega''(\xi)}{\omega(\xi)} \right] \right\}. \tag{6.3.25}$$

The dependence upon the conformal representative arises as a result of the usual transformation properties of the stress tensor for a two-dimensional CFT. The stress tensor in two dimensions is not a primary operator (it is only quasi-primary). Such an operator transforms under conformal mappings with additional terms involving a Schwarzian derivative [206]. Since in dimensions greater than two all quasi-primary fields are primary, such terms do not appear in the boundary stress tensor for the four-dimensional C-metric. In order to obtain the correct holographic information in two dimensions, we need to choose a particular conformal representative of the boundary metric. For three-dimensional gravity, we should choose the Brown-Henneaux condition [205, 207, 208], setting the boundary metric to be a cylinder. In fact, this is necessary for a well defined variational problem [92]. This choice corresponds to selecting the ground state for the boundary CFT. We thus fix the conformal factor to be $\omega = 1$. The integral then takes the form

$$M = -\frac{1}{8\pi\alpha}\sqrt{1 - A^2\ell^2} \int_{x_+}^{1} \frac{d\xi}{\Upsilon\sqrt{1-\xi^2}} \,, \tag{6.3.26}$$

which is readily integrated, yielding

$$M = -\frac{1}{8\pi\alpha}\sqrt{1 - A^2\ell^2} \left(\frac{\pi}{2} - \arctan\left[\frac{x_+}{\sqrt{1 - A^2\ell^2}\sqrt{1 - x_+^2}} \right] \right) . \tag{6.3.27}$$

To make this expression more intuitive, let's use the parameter K instead and substitute the value of α from (6.3.10). The mass is then written

$$M = -\frac{1}{8\pi} \left(\frac{\pi}{2} - \arctan\left[\frac{\cot\left(\frac{\pi}{K}\right)}{\sqrt{1 - A^2\ell^2}} \right] \right) . \tag{6.3.28}$$

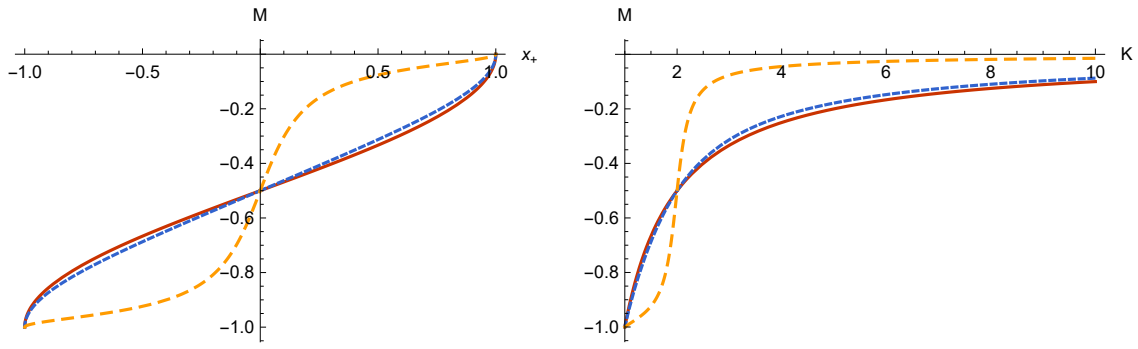

Figure 6.11: The holographic mass of the conical deficit pulled by a domain wall under tension with various acceleration parameters: $A = 0$ (solid red), $A = 0.5\ell$ (dotted blue), $A = 0.99\ell$ (dashed orange).

The mass is plotted for various acceleration parameters in figure 6.11. In comparison to the magnitude of the conical deficit, the value of the acceleration parameter A is seen to make little difference until it becomes comparable to ℓ.

As a check, one can take the limit of vanishing acceleration parameter A. We recover exactly the Casimir energy of pure (global) AdS_3 with a conical deficit [93, 153, 209]

$$M_{AdS_3} = -\frac{1}{8K}\,. \tag{6.3.29}$$

6.4 Class I: A particle pushed by a strut

One can also construct a conical deficit accelerated by a strut. In fact, the asymptotically flat counterpart of this construction (which can be achieved by taking the $\ell \to \infty$ limit) has been studied by Anber [200].

Start with the metric (6.2.7) with the Class I metric functions and coordinate ranges given in table 6.2. Choose some value $x_+ \in (-1, 1)$ and define a patch with $x \in [-1, x_+)$. Glue two copies of this patch, mirroring along both $x = -1$ and $x = x_+$. The identifications are shown in figure 6.12. The $x = -1$ axis of the newly formed spacetime is regular along $x = -1$, with the $x = x_+$ axis marking the position of a domain wall of negative tension $\mu = -A(4\pi)^{-1}\sqrt{Q(x_+)}$. This solution shares many features in common with the solution of section 6.3 so we will discuss it in less detail.

The solution can be written more intuitively in dimensionful coordinates $r = -(Ay)^{-1}$ and $t = \alpha A^{-1}\tau$. We also introduce an angular coordinate $x = -\cos(\phi/K)$ with the parameter $K = \pi/\arccos(-x_+)$ encoding the range of angular coordinate. The

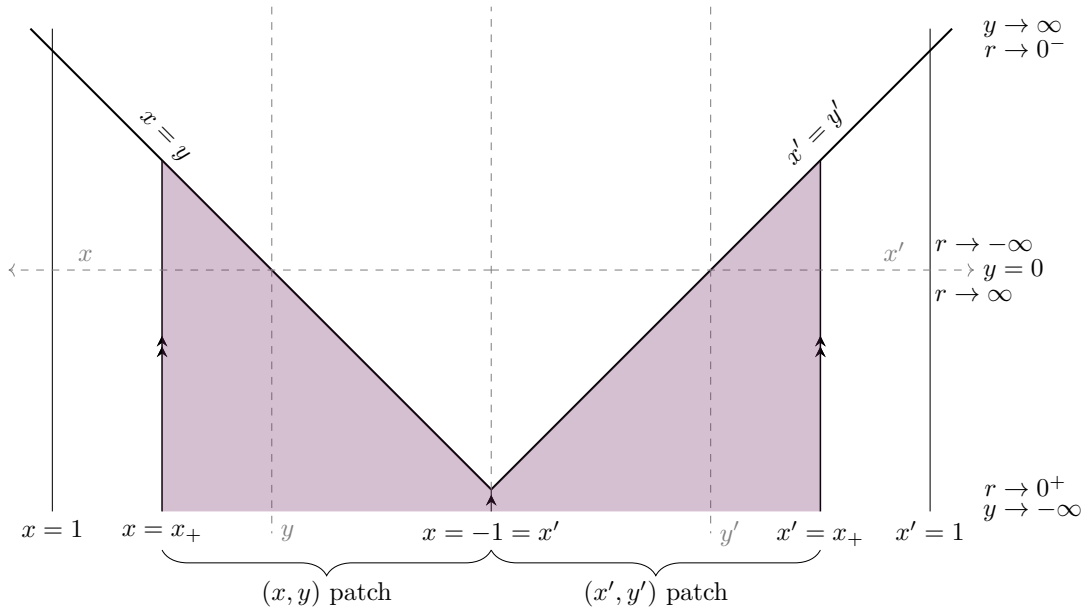

Figure 6.12: The two patches of type I spacetime used to construct a conical defect accelerated by a pushing strut.

metric then takes the form

$$\begin{aligned} ds^2 &= \frac{1}{[1 - Ar\cos(\phi/K)]^2}\left[f(r)\frac{dt^2}{\alpha^2} - \frac{dr^2}{f(r)} - r^2\frac{d\phi^2}{K^2}\right], \\ f(r) &= 1 + (1 - A^2\ell^2)\frac{r^2}{\ell^2}. \end{aligned} \tag{6.4.1}$$

We anticipate a rescaling of time by α. By similar arguments to those of section 6.3, we find that one should take $\alpha = \sqrt{|1 - A^2\ell^2|}$. The local acceleration of the particle is again $|\mathbf{a}| = A$, by the same reasoning. The particle mass and wall tension are, respectively,

$$m_c = \frac{1}{4}\left(1 - \frac{1}{K}\right) \tag{6.4.2}$$

and

$$\mu = -\frac{A}{4\pi}\sin\left(\frac{\pi}{K}\right). \tag{6.4.3}$$

By mapping the solution to a portion of global space, we attain figure 6.13 for the slowly accelerating deficit. The details of the mapping are given in appendix C. The interpretation of this figure is similar to that for the particle accelerated by a domain wall under tension, (cf. figure 6.8 and the discussion given in section 6.3).

In the rapid and saturated phases, much like with the particle accelerated by a tensioned-wall, changing the magnitude of conical deficit can induce a phase transition. For light conical deficits ($m_c \sim 0$), the gluing surface $x = x_+$ connects the conical defict's worldline to a horizon. In this case, one removes a "wedge" which in-

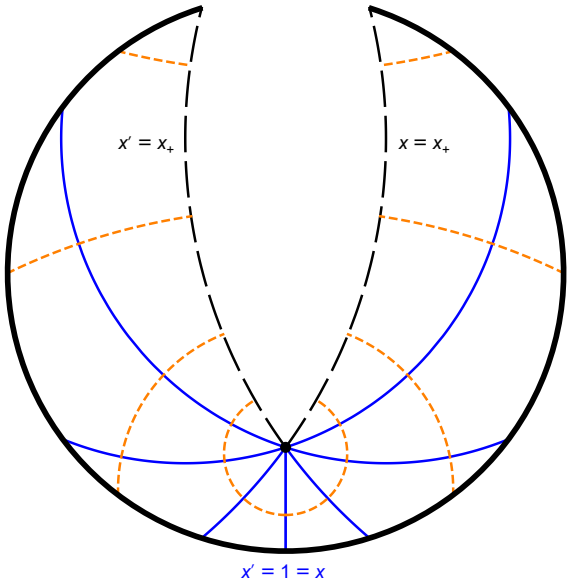

Figure 6.13: The slowly accelerating conical deficit with $A = 0.9\ell$, pushed by a strut, mapped onto the Poincaré disk. The deficit is shown as a black point and accellerates southwards. A "wedge" is removed from the global space, with its edges $x = x_+$ and $x' = x_+$ (long-dashed black) identified to attain a domain wall under compression. Several lines of constant x are shown in blue, with lines of constant y in dashed orange.

cludes part of the acceleration horizon from the planar BTZ geometry. This situation arises for the $\mathrm{I}_{\mathrm{rapid,B}}$ and $\mathrm{I}_{\mathrm{saturated,D}}$ single-strut solutions. The $\mathrm{I}_{\mathrm{rapid,B}}$ single-strut solution is shown in figure 6.9. On the other hand, for heavier conical deficits (m_c large enough that $x_+ < y_h$), the identified surfaces connect the deficit's worldline to the conformal boundary. The portion of space then removed from the Rindler geometry is then so large that it includes the entireity of the horizon. This situation arises for the $\mathrm{I}_{\mathrm{rapid,A}}$ and $\mathrm{I}_{\mathrm{saturated,C}}$ single-strut solutions. The $\mathrm{I}_{\mathrm{rapid,A}}$ single-strut solution is shown in figure 6.10.

6.4.1 The holographic mass

Considering again the slowly accelerating phase, the holographic calculation proceeds identically to that of section 6.3. In particular, the expressions for the Fefferman-Graham expansion (6.3.17), (6.3.18), (6.3.19); the stress tensor (6.3.20), (6.3.21); and the Ricci scalar of the boundary metric (6.3.23) all hold.

The limits for the mass integration must be updated,

$$M = 2A \int_{-1}^{x_+} \sqrt{-g_{(0)}} \langle T_\tau^\tau \rangle d\xi \,, \tag{6.4.4}$$

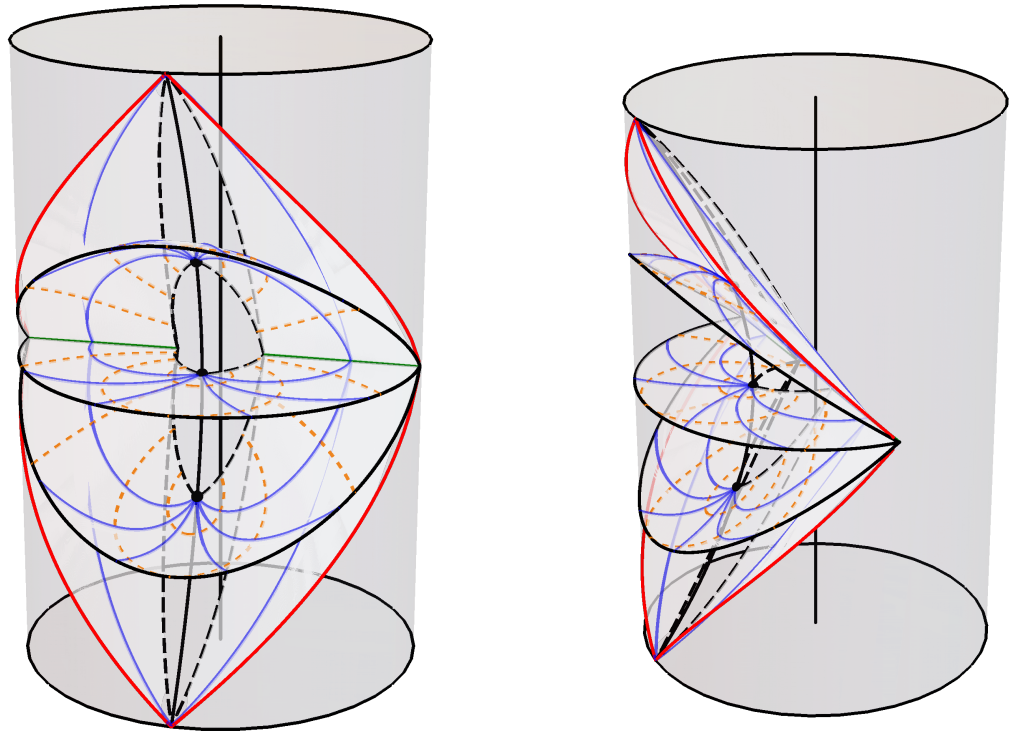

Figure 6.14: The rapidly accelerating light conical deficit with $A > \ell^{-1}$, pushed by a strut, embedded within global AdS_3. The deficit's worldline is shown in solid black. Several surfaces of constant t are plotted. The event horizon is demonstrated by the surfaces at early and late t. The bifurcation surface is shown as a green line. A "wedge" is removed, with its faces $x = x_+$ and $x' = x_+$ identified. These faces are indicated by long-dashed black curves within each time-slice, and in dashed red at the boundary. The boundary of the classically accessible subset of the global boundary is shown in solid red. Lines of constant x are shown in blue, with lines of constant y in dashed orange. To guide the eye, the axis of the cylinder is also shown in black.

however evaluation gives the same result (6.3.28). Thus, it appears that although one might naïvely associate a negative mass with the negative tension domain wall [200], this is erroneous. The mass again reduces to that of global AdS_3 with a conical deficit in the limit of vanishing A.

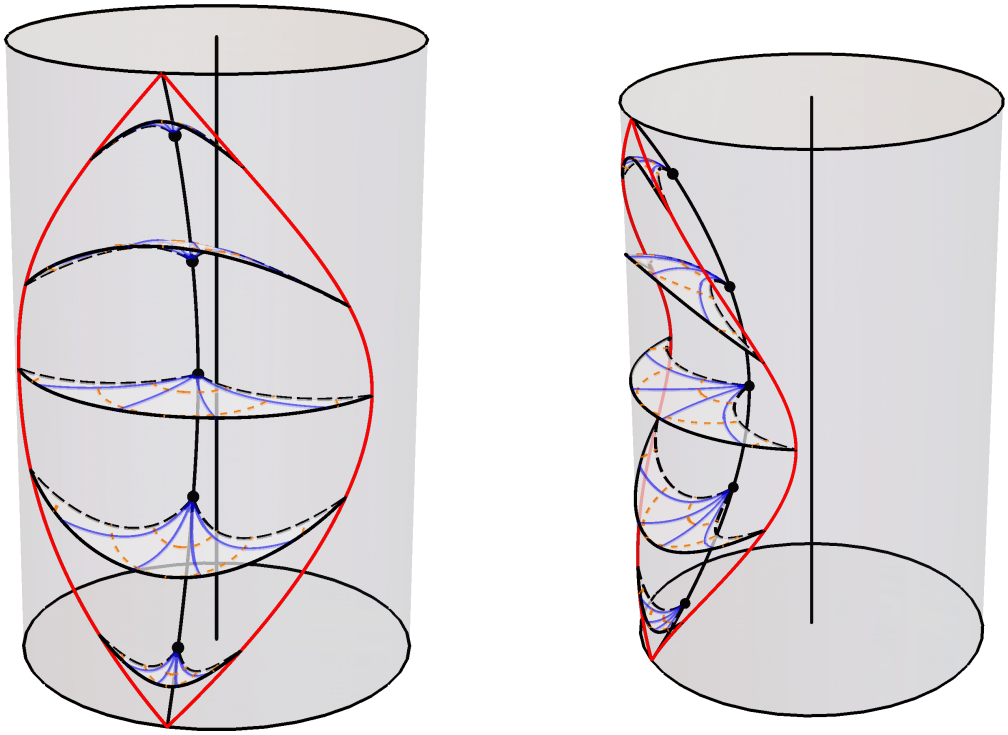

Figure 6.15: The rapidly accelerating heavy conical deficit with $A > \ell^{-1}$, pushed by a strut, embedded within global AdS_3. The deficit's worldline is shown in solid black. Several surfaces of constant t are plotted. The surfaces $x = x_+$ and $x' = x_+$ are identified. Edges of $x = x_+$ are shown in long-dashed black within each time-slice. x_+ is taken positive enough that the entireity of the boundary is removed from the space before identification. The boundary of the classically accessible subset of the global boundary is shown in red. Lines of constant x are shown in blue, with lines of constant y in dashed orange. To guide the eye, the axis of the cylinder is also shown in black.

6.5 Class $\mathrm{I_C}$: A black hole pulled by a domain-wall

It is also possible to construct from the Class I geometry a black hole with a topologically circular bifurcation surface, together with a single domain wall of positive tension extending from its horizon out to the conformal boundary. We may do so in either the rapid or saturated phase, from which we get the $\mathrm{I}_{\mathrm{rapid,C}}$ or $\mathrm{I}_{\mathrm{saturated,E},y>0}$ single-tensioned-wall solutions respectively.

Consider a Class I geometry in the rapid (or saturated) phase, so that $A^2\ell^2 \geq 1$. Choosing to consider positive values of y, there is a Killing horizon in the space at

$y_h = \sqrt{1 - A^{-2}\ell^{-2}}$. One can constuct a single-tensioned-wall solution by choosing some value $x_+ \in (y_h, 1)$; cutting the space along $x = x_+$; and gluing two copies of the chart, mirroring along both $x = x_+$ and $x = 1$. Diagrammatically, we are joining two copies of the most heavily shaded region in figure 6.1a, wherin the relevant value of x_+ is denoted by C. There is no tension along the gluing surface $x = 1$. Along $x = x_+$, there is a domain wall with positive tension

$$\mu = \frac{A}{4\pi}\sqrt{1 - x_+^2}\,. \tag{6.5.1}$$

This positive tension domain wall extends out in the direction of increasing y from the compact horizon to the conformal boundary at $y = x$.

We can form another coordinate system

$$\tau = \frac{At}{\alpha}\,, \qquad y = \frac{1}{A\rho}\,, \qquad x = \cos\left(\phi/K\right)\,, \tag{6.5.2}$$

where $K = \pi/\arccos(x_+)$. Since for these solutions $x_+ \in (y_h, 1)$ and $y_h \geq 0$, we have that $K > \pi/\arccos(y_h) > 2$. K can only approach its minimal value of 2 as the solution becomes close to saturated. The metric takes the form

$$\begin{aligned} ds^2 &= \frac{1}{\left[A\rho\cos\left(\frac{\phi}{K}\right) - 1\right]^2}\left(f(\rho)\frac{dt^2}{\alpha^2} - \frac{d\rho^2}{f(\rho)} - \rho^2\frac{d\phi^2}{K^2}\right)\,, \\ f(\rho) &= 1 - (A^2\ell^2 - 1)\rho^2/\ell^2\,. \end{aligned} \tag{6.5.3}$$

The range of ϕ is $(-\pi, \pi)$, covering both (x, y) patches. The horizon lies at $\rho_h = (Ay_h)^{-1}$, with the conformal boundary $\rho_{\text{conf.}} = (A\cos(\phi/K))^{-1}$ satisfying $0 < \rho_{\text{conf.}} < \rho < \rho_h$. With this parameterisation, the domain wall lies on the line $\phi = \pm\pi$ and has tension

$$\mu = \frac{A}{4\pi}\sin\left(\frac{\pi}{K}\right)\,. \tag{6.5.4}$$

The tension is bounded above by

$$\mu_{\max} = \frac{A}{4\pi}\,, \tag{6.5.5}$$

which is only approachable for saturated or (nearly saturated) solutions with values of K very close to 2. It is monotonically decreasing with K and bounded below by zero.

An alternative parameterisation of the solution is available via the substitutions

$$m = \frac{1}{K}\,, \qquad \mathcal{A} = \frac{A}{m}\,; \qquad \tilde{t} = \frac{t}{m}\,, \qquad r = m\rho\,. \tag{6.5.6}$$

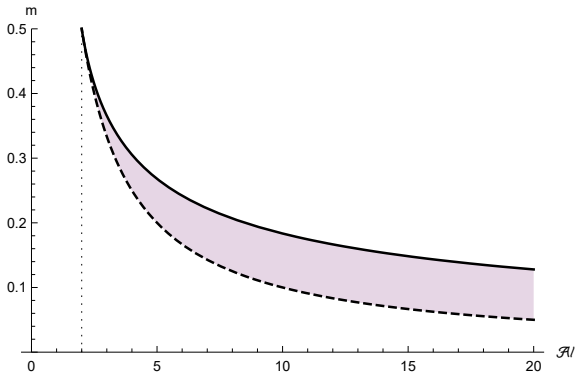

Figure 6.16: The parameter space of the $\mathrm{I}_{\mathrm{rapid,C}}$ solution (shaded purple).

The metric becomes

$$\begin{aligned} ds^2 &= \frac{1}{\Omega(r,\phi)^2}\left(F(r)\frac{d\tilde{t}^2}{\alpha^2} - \frac{dr^2}{F(r)} - r^2 d\phi^2\right), \\ F(r) &= -m^2(\mathcal{A}^2 r^2 - 1) + \frac{r^2}{\ell^2}, \\ \Omega(r,\phi) &= \mathcal{A} r\cos(m\phi) - 1\,. \end{aligned} \tag{6.5.7}$$

The bounds on K translate into bounds on m:

$$0 < m < \frac{1}{\pi}\arccos(y_h) < \frac{1}{2}\,. \tag{6.5.8}$$

Since m is bounded above by one half, no geometries of this type are possible with $\mathcal{A}\ell < 2$. In fact, after the reparameterisation, y_h now depends on m. This makes the second inequality in (6.5.8) slightly tricky; it is more easily expressed as a bound on $\mathcal{A}\ell$:

$$\frac{1}{m} \leq \mathcal{A}\ell < \frac{1}{m\sin(m\pi)}\,. \tag{6.5.9}$$

This effective upper bound on m combines with the lower bound provided by the rapid acceleration condition to form an allowed range of m values for a given $\mathcal{A}\ell$, shown in figure 6.16.

The conformal boundary lies at $r_{\text{conf.}} = (\mathcal{A}\cos(m\phi))^{-1} \geq \mathcal{A}^{-1}$. The minimal value of $\mathcal{A}^{-1}$ is achieved only at a single point: the point on the boundary for which $\phi = 0$. For a rapid ($m\mathcal{A}\ell > 1$) solution, the horizon lies at

$$r_h = \frac{m\ell}{\sqrt{m^2\mathcal{A}^2\ell^2 - 1}} \tag{6.5.10}$$

and satisfies $r_h > \mathcal{A}^{-1}$. As the solution becomes saturated ($m\mathcal{A}\ell = 1$), the horizon moves out to infinity and these coordindates become less useful.

One might be concerned that r is decreasing as one nears the conformal boundary.

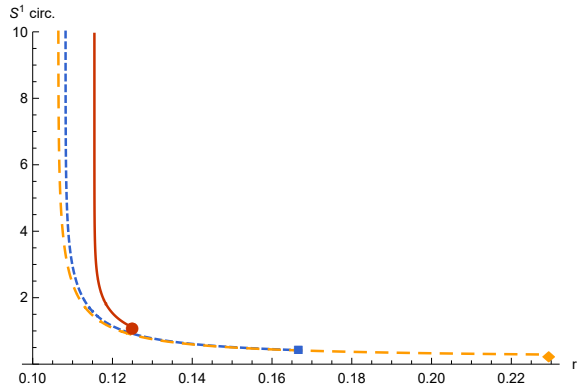

Figure 6.17: The "circumference" of loops of constant r. ℓ is set to unity with $\mathcal{A} = 10$. Three values of m (6^{-1}, 8^{-1}, and 9^{-1}) are shown (in solid red, dotted blue, and dashed orange respectively). The value at the horizon radius $r = r_h$ is marked by a shape.

The length of a closed ring of constant r is

$$\int_{-\pi}^{\pi} \frac{r}{\mathcal{A}r\cos(m\phi) - 1} d\phi = \frac{r}{m\sqrt{\mathcal{A}^2 r^2 - 1}} \operatorname{arctanh}\left[\sqrt{\frac{\mathcal{A}r+1}{\mathcal{A}r-1}} \tan\left(\frac{m\pi}{2}\right)\right] . \quad (6.5.11)$$

This function is monotonically decreasing with r, as shown in figure 6.17. A ring close to the horizon is smaller than a ring close to the boundary; the system is behaving in an intuitive fashion, despite the unintuitive metric.

To better understand the solution, we can map it to a subset of global AdS_3 and plot it by compactifying the spatial section. This process is described in appendix C, with the result being figure 6.18. One finds a result qualitatively similar to the BTZ black hole, (cf. figure C.1), but with non-zero stress present in the identification surface. This is the key to understanding the $I_{\text{rapid,C}}$ and $I_{\text{saturated,E},y>0}$ solutions. The static BTZ black hole is constructed by taking the AdS_3 Rindler wedge (6.3.11) and identifying complete orbits of the Killing vector generating rotations, (see appendix C.2 for a short review). The Class I_C black hole is constructed similarly, though one is identifying instead surfaces of constant x.

6.5.1 Physical properties

A short discussion of the time coordinate we have written down for the solution is warranted. The coordinate t of (6.5.3) is in fact the Rindler time of the gauge (6.3.11). The explicit mapping of the Class I_C geometry to the planar BTZ geometry (6.3.11) is given by

$$\left(-1 + \frac{R^2}{\ell^2}\right) = \frac{F(r)}{m^2\alpha^2\Omega(r,\phi)^2} , \qquad R\sinh\vartheta = \frac{r\sin(m\phi)}{m\Omega(r,\phi)} , \quad (6.5.12)$$

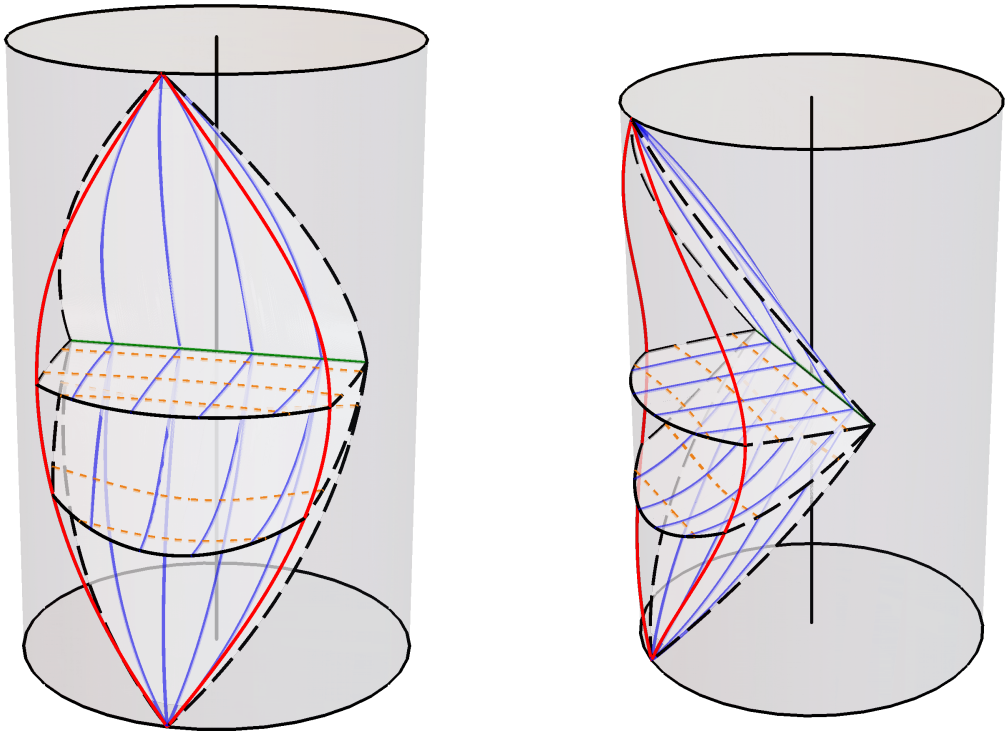

Figure 6.18: The Class $\mathrm{I}_{\mathrm{rapid,C}}$ solution, as a portion of global AdS_3. Several surfaces of constant t are shown. The horizon is shown by the surfaces at early and late times, with the bifuration surface shown in green. The lines $x = x_+$ and $x' = x_+$ within each time-slice (shown in long-dashed black) are identified, which imbues the birfurcation surface with the topology of a circle. Lines of constant x are shown in blue, with lines of constant y shown in dashed orange. The classically accessible subset of the global boundary is delimited in red. To guide the eye, the locus of the cylinder is shown in solid black.

where the time coordinates are related by

$$\tilde{t} = \frac{t_{\mathrm{Rindler}}}{m}\,. \tag{6.5.13}$$

The above transformation necessitates

$$\alpha = \sqrt{m^2\mathcal{A}^2\ell^2 - 1}\,. \tag{6.5.14}$$

There are then two obvious candidates, ∂_t and $\partial_{\tilde{t}}$, for the Killing vector from which to compute physical quantities such as the mass and temperature. It is not clear which, if either, of these is the correct choice, as the solution is not smoothly connected to any familiar ones. In this subsection we compute quantities with respect to the Rindler time Killing vector ∂_t.

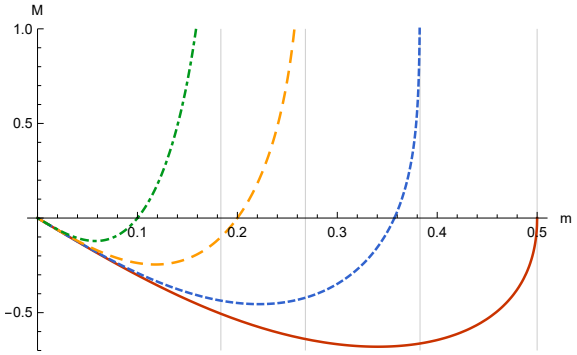

Figure 6.19: A plot of $8\pi\alpha M$ at various values of $\mathcal{A}\ell$: $\mathcal{A}\ell = 2.0$ (solid red), $\mathcal{A}\ell = 2.8$ (dotted blue), $\mathcal{A}\ell = 5.0$ (dashed orange), $\mathcal{A}\ell = 10$ (dot-dashed green). The grey vertical lines denote the asymptotes where the divergences $\mathcal{A}\ell = (m\sin(m\pi))^{-1}$ are met. Negative values of M are forbidden by the lower bound $m \geq (\mathcal{A}\ell)^{-1}$.

Since the geometry possesses one isolated, compact horizon, the calculation of holographic mass goes through similarly to those for the accelerating particle solutions constructed in sections 6.3 and 6.4. The limits of integration need updating for the $\mathrm{I}_{\mathrm{rapid,C}}$ solution:

$$M = 2m\mathcal{A}\int_{x_+}^{1}\sqrt{-\det g_{(0)}}\,\langle T^{\tau}_{\tau}\rangle\,d\xi\,, \tag{6.5.15}$$

where recall that now $x_+ > 0$ and $m\mathcal{A}\ell \geq 1$. The integral may be evaluated to obtain

$$M = \frac{1}{8\pi\alpha}\sqrt{m^2\mathcal{A}^2\ell^2 - 1}\,\mathrm{arcoth}\left[\frac{\cot(m\pi)}{\sqrt{m^2\mathcal{A}^2\ell^2-1}}\right]. \tag{6.5.16}$$

As we approach saturation, $m\mathcal{A}\ell \to 1$ from above, the mass vanishes. The mass, with the normalisation (6.5.14), is plotted against m in figure 6.19. Though it might appear that negative values of M are possible for small m, in fact, negative masses are forbidden by the condition that the solution is rapid or saturated; the roots of M occur exactly at the saturation point $m = (\mathcal{A}\ell)^{-1}$. The mass spectrum of the solutions is non-negative, although there is a narrow range of allowed m for each $\mathcal{A}\ell$. Within the allowed parameter space, the holographic mass is monotonically increasing with m, and can become unboundedly large.

Calculating the minimal value of (6.5.11), the horizon is seen to have entropy

$$S = \ell\,\mathrm{arctanh}\left[m\mathcal{A}\ell\,(1+y_h)\tan\left(\frac{m\pi}{2}\right)\right]. \tag{6.5.17}$$

The entropy is monotonically increasing in m, with the massless solution attaining the minimal entropy

$$S_{M=0} = \ell\,\mathrm{arctanh}\left[\tan\left(\frac{\pi}{2\mathcal{A}\ell}\right)\right]. \tag{6.5.18}$$

The entropy is plotted against m, for various values of $\mathcal{A}\ell$, in figure 6.20. In the

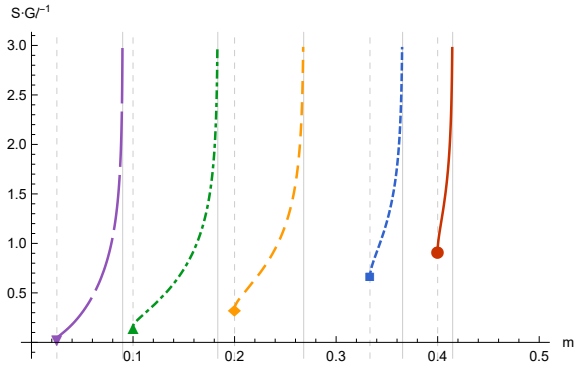

Figure 6.20: The entropy $\ell^{-1}S$ of the $\mathrm{I}_{\mathrm{rapid,C}}$ solution at various values of $\mathcal{A}\ell$: $\mathcal{A}\ell = 2.5$ (solid red), $\mathcal{A}\ell = 3.0$ (dotted blue), $\mathcal{A}\ell = 5.0$ (dashed orange), $\mathcal{A}\ell = 10$ (dot-dashed green), $\mathcal{A}\ell = 40$ (long-dashed purple). A solid grey vertical line denotes an asymptote where the divergence $\mathcal{A}\ell = (m\sin(m\pi))^{-1}$ is met. A dashed grey line dentotes the value of m for a massless solution; the entropy at this point is marked with a shape.

figure, the entropy of the massless solution is marked by a shape. The entropy is monotonically increasing with the mass and diverges as m approaches its supremum.

By regularity of the Euclidean section, the horizon temperature is

$$T = \frac{|f'(r_h)|}{4\pi\alpha} = \frac{1}{2\pi\ell\alpha}\sqrt{m^2\mathcal{A}^2\ell^2 - 1}\,. \tag{6.5.19}$$

It is interesting to note that either of the possible normalisations ∂_t and $\partial_{\bar{t}}$ yield a temperature independent of the acceleration parameter $\mathcal{A}$. At the saturation point $m\mathcal{A}\ell = 1$, where the solution is massless, the system approaches absolute zero.

6.6 Class $\mathrm{II}_{\mathrm{right}}$: A BTZ black hole pushed by a strut

Starting from a patch of Class II spacetime (6.2.7) with $x > 1$, as presented in table 6.2, one may construct a one parameter extension of the static BTZ solution describing a black hole with a strut defect emerging from its horizon. The existence of such a black hole was proposed in [40], although several features, including the possibilty of a "rapid" phase possessing a non-compact acceleration horizon, went unacknowledged. We seek to clarify the discussion and highlight these additional features here.

Choose some value $x_+ > 1$ and define a patch with $x \in [1, x_+)$. Glue two copies of

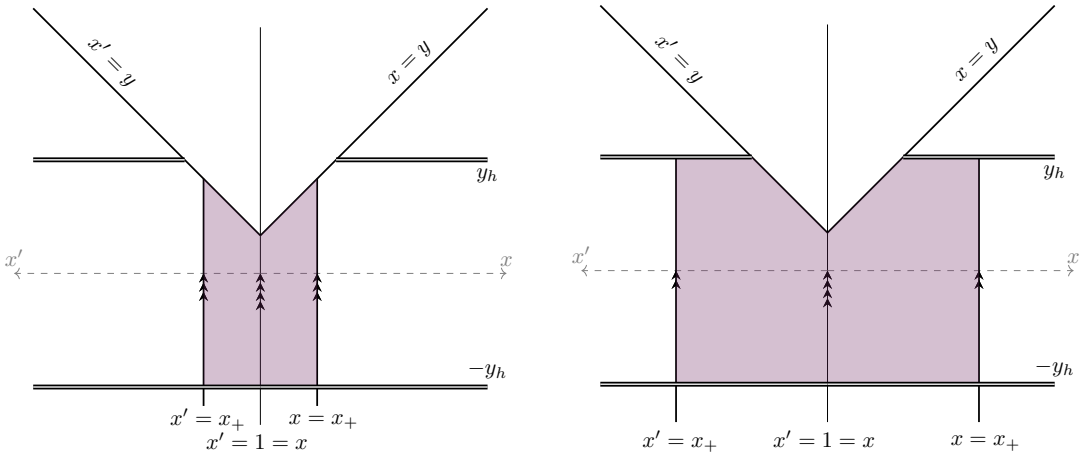

(a) $\mathrm{II}_{\mathrm{right,slow}}$ (b) $\mathrm{II}_{\mathrm{right,rapid}}$

Figure 6.21: The two patches of type II spacetime—with $x > 1$—and the identifications used to construct a black hole accelerated by a pushing strut. Separate diagrams are given for the case when $x_+ < y_h$ where there is no acceleration horizon, and the rapid phase $x_+ > y_h$.

this patch, mirroring along both $x = 1$ and $x = x_+$. The identifications are shown in figure 6.21. The $x = 1$ axis of the newly formed spacetime is regular, while $x = x_+$ marks the position of a domain wall of negative tension $\mu = -A(4\pi)^{-1}\sqrt{Q(x_+)}$.

The resulting spacetime describes the exterior of a black hole with horizon located at $-y_h = -\sqrt{1 + A^{-2}\ell^{-2}}$. If x_+ is larger than y_h, there is also a "droplet" horizon [199] present at $y = y_h$ for $x > y_h$. This rapid phase is a novel feature which went unacknowledged in [40]. The existence of such a phase strengthens the analogy with the four-dimensional accelerating black hole.

To cast the metric in more intuative coordinates, take $x = \cosh(\psi/K)$ where $K = \pi/\operatorname{arcosh}(x_+)$. Defining dimensionful coordinates $\rho = -(Ay)^{-1}$ and $t = \alpha A^{-1}\tau$, the metric becomes

$$\begin{aligned} ds^2 &= \frac{1}{\left(1 + A\rho\cosh\left(\frac{\psi}{K}\right)\right)^2}\left(f(\rho)\frac{dt^2}{\alpha^2} - \frac{d\rho^2}{f(\rho)} - \rho^2\frac{d\psi^2}{K^2}\right), \\ f(r) &= -1 + (1 + A^2\ell^2)\rho^2/\ell^2\,, \end{aligned} \tag{6.6.1}$$

where again we leave room for the possibility that t should be scaled by some dimensionless quantity α. The parameter K has been chosen such that the range of ψ is $(-\pi, \pi)$. We require both $K > 0$ and $\pi/K < \operatorname{arcosh}(y_h)$. This patch does not cover the entire region between the black hole horizon and the boundary (and the acceleration horizon). The region immediately exterior to the black hole has $r > 0$. Proceeding from the black hole along a line of constant ψ in the direction

of increasing r, one encounters a coordinate singularity as $r \to \infty$, which is a geometrically uninteresting locus. One must take a second patch with $r < 0$ to cover the region bounded by the conformal boundary (for small ψ) and possibly also the acceleration horizon (for large ψ). The conformal boundary is then approached as $r \to -\left[A \cosh\left(\psi/K\right)\right]^{-1}$. There is a regular semi-axis at $\psi = 0$, while along $\psi = \pm\pi$ there lies a domain wall of (negative) tension

$$\mu = -\frac{A}{4\pi} \sinh\left(\frac{\pi}{K}\right) . \tag{6.6.2}$$

These Class $\mathrm{II}_{\mathrm{right}}$ solutions form a one parameter extension of the well-known family of static BTZ black holes. To highlight the relationship, take the metric (6.6.1) and make the parameter redefinitions $K = m^{-1}$ and $A = m\mathcal{A}$. Also, make the coordinate rescalings $r = m\rho$ and $\tilde{t} = m^{-1}t$. The metric becomes

$$\begin{aligned} ds^2 &= \frac{1}{\Omega(r,\psi)^2}\left[F(r)\frac{d\tilde{t}^2}{\alpha^2} - \frac{dr^2}{F(r)} - r^2 d\psi^2\right] , \\ F(r) &= -m^2(1 - \mathcal{A}^2 r^2) + \frac{r^2}{\ell^2} , \\ \Omega(r,\psi) &= 1 + \mathcal{A} r \cosh(m\psi) . \end{aligned} \tag{6.6.3}$$

We require that both $m > 0$ and the slow acceleration condition—which is now $m \sinh\left(m\pi\right) < \left(\mathcal{A}\ell\right)^{-1}$— hold. A chart with $r > 0$ covers the region immediately exterior to the black hole horizon, which lies at $r = m\ell(1 + m^2\mathcal{A}^2\ell^2)^{-1/2}$. A second chart with $r < 0$ covers the region bordered by the conformal boundary, which lies at $r \to -\left[\mathcal{A} \cosh(m\psi)\right]^{-1}$.

To understand the solution, we can again perform a mapping to global AdS_3, the details of which are given in appendix C. A solution in the slow phase $x_+ < y_h$ is shown in figure 6.22, while one in the rapid phase $x_+ > y_h$ is shown in figure 6.23. In the slow phase, there is a single bifurcate Killing horizon generated by ∂_t. Upon making the appropriate identification, the bifurcation surface of this horizon aquires the topology of a circle. All of the lines of constant x (and t) connect the bifurcation surface of this horizon to the conformal boundary (consider the blue lines in figure 6.22). This construction mirrors that of the usual, static BTZ black hole (cf. figure C.1). Of course, when constructing the Class $\mathrm{II}_{\mathrm{right,slow}}$ black hole, surfaces of constant x are glued. This effects a domain wall under compression. In the usual BTZ construction the surfaces to identify are specifically chosen—by quotienting (the universal covering space of) AdS_3 by the group of integers—to maintain regularity. In the rapid phase, ∂_t generates two disjoint bifurcate horizons. There exist lines of constant $x > y_h$ (and t) which connect the black hole bifurcation surface to a second, disjoint bifurcation surface with topology $\mathbb{R}$. While the slow phase is qualitatively

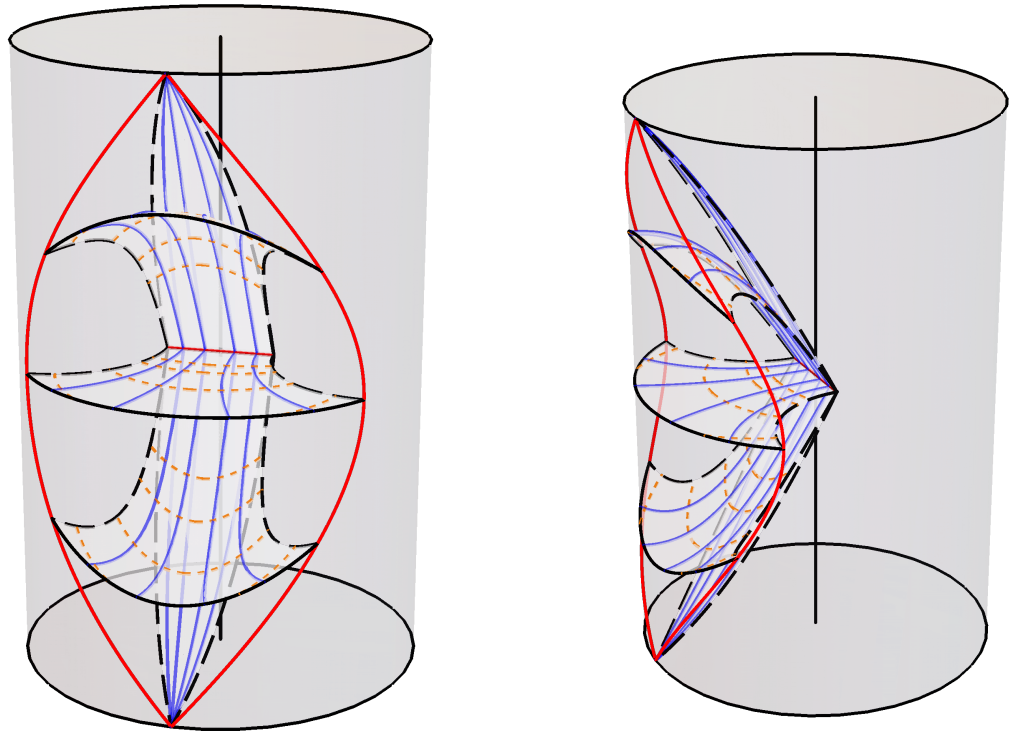

Figure 6.22: The Class $\text{II}_{\text{right,rapid}}$ black hole. Several surfaces of constant t are shown. The lines $x = x_+ < y_h$ are shown in dashed black, and are identified with their partner within the same time slice, wrapping the bifurcation surface (shown as a horizontal red line) into a circle. The early and late time-slices demonstrate the event horizon. Lines of constant y are shown in dashed orange. Lines of constant x are shown in blue. The classically accessible region of the boundary is delimited in red.

similar to the traditional, static BTZ solution—albeit with induced tension in the identified surface—the rapid phase hitherto absent from the literature is qualitively distinct.

6.6.1 The holographic mass

Proceeding as for the accelerating deficits, we calculate the holographic mass from the metric (6.2.7) with the Class II metric functions given in table 6.2. Once again, it is difficult to define the mass of a gravitational solution in the presence of a non-compact horizon. Sidestepping this issue, we focus on the case where the parameter A is small enough that

$$\pi/K < \operatorname{arcosh}\left(\sqrt{1 + A^{-2}\ell^{-2}}\right) . \tag{6.6.4}$$

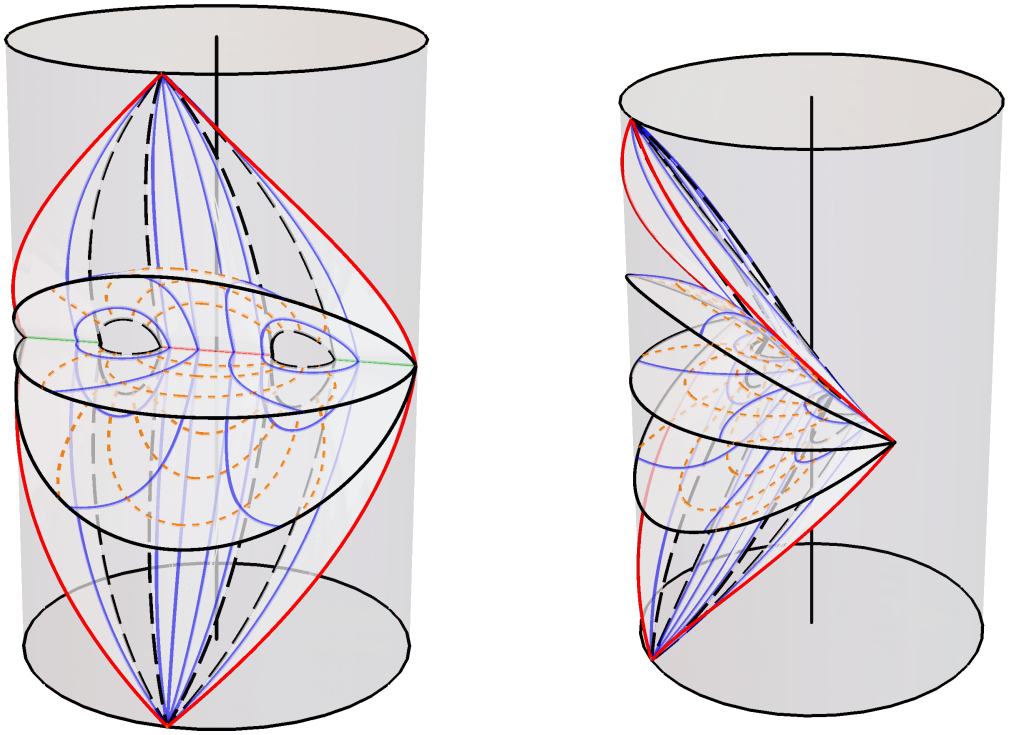

Figure 6.23: The Class $\mathrm{II}_{\mathrm{right,rapid}}$ black hole. Several surfaces of constant t are shown. The lines $x = x_+ < y_h$ are shown in dashed black, and are identified with their partner within the same time slice. The early and late time-slices show the event horizons. The black hole event horizon has a compact bifurcation surface with topology S^1, shown in red, while the green line denotes the "acceleration horizon" or droplet's bifurcation line with topology $\mathbb{R}$. Lines of constant y are shown in dashed orange. Lines of constant x are shown in blue. The classically accessible region of the boundary is delimited in red.

Before proceeding with the calculation, a comment is warranted on the choice of Killing vector from which to calculate the conserved charge. To identify α, one might try to again posit that ∂_t is the appropriate Killing vector with which to calculate the mass when it coincides with the time coordinate of the Rindler wedge. In fact, a slight modification of this procedure is required: one should scale the time coordinate by a factor of m in order to reproduce the zero-mass of AdS_3 as the black hole horizon size is taken to zero [194]. The mapping between the Class II geometry and the Rindler geometry is

$$\left(-1+\frac{R^2}{\ell^2}\right) = \frac{F(r)}{m^2\alpha^2\Omega(r,\psi)^2}\,, \qquad R\sinh\vartheta = \frac{r\sinh(m\psi)}{m\Omega(r,\psi)}\,, \tag{6.6.5}$$

where we must also scale the time coordinate

$$\tilde{t} = \frac{t_{\text{Rindler}}}{m} \tag{6.6.6}$$

and set

$$\alpha = \sqrt{1 + m^2 \mathcal{A}^2 \ell^2}\,. \tag{6.6.7}$$

Note that, as m is taken to zero, the metric (6.6.3) becomes

$$ds^2 = \frac{1}{(1+\mathcal{A}r)^2}\left(\frac{r^2}{\ell^2}d\tilde{t}^2 - \frac{\ell^2}{r^2}dr^2 - r^2 d\psi^2\right)\,. \tag{6.6.8}$$

The transformation

$$R = \frac{r}{1+\mathcal{A}r} \tag{6.6.9}$$

reveals the parameter $\mathcal{A}$ to then be a gauge artifact; the geometry is simply Poincaré AdS_3:

$$ds^2 = -\frac{\ell^2}{R^2}dR^2 + \frac{R^2}{\ell^2}\left(d\tilde{t}^2 - \ell^2 d\psi^2\right)\,. \tag{6.6.10}$$

This conclusion is solidified by noticing that the stress

$$\mu = -\frac{m\mathcal{A}}{4\pi}\sinh\left(m\pi\right) \tag{6.6.11}$$

inducing the domain wall also vanishes in this limit. Poincaré AdS_3 sets the zero-point energy of three-dimensional gravity holographically [93]. As such, it is natural that the mass of the Class II solutions should be calculated with respect to $\tilde{t}$, using equation (6.6.6). Though rather ad hoc, this prescription to calculate the mass with respect to $\tilde{t} = m^{-1}t_{\text{Rindler}}$ is the one usually followed for the BTZ black hole. Indeed it has led to a number of interesting results including providing a first law [86]. We proceed to calculate the conserved mass with respect to $\partial_{\tilde{t}}$, and leave a detailed justification for future work.

We expand the Class II metric given in table 6.2 using (6.3.16), and seek Fefferman-Graham form order by order. Again, a sensible redefinition of conformal factor

$$F_1(\xi) = \frac{\Upsilon^{3/2}}{A\ell\omega(\xi)}\,, \tag{6.6.12}$$

where now

$$\Upsilon = 1 - A^2\ell^2(\xi^2 - 1)\,, \tag{6.6.13}$$

simplifies proceedings. The boundary metric is then

$$g_{(0)} = \frac{\omega(\xi)^2}{A^2}\left[\frac{dt^2}{\alpha^2} - \frac{A^2\ell^2}{(\xi^2-1)\,\Upsilon^2}d\xi^2\right]\,. \tag{6.6.14}$$

The leading correction in the Fefferman-Graham expansion is

$$g_{(2)} = -\frac{1}{2A^2\ell^2\alpha^2}\left[1 + A^2\ell^2 - \left(\xi^2-1\right)\Upsilon^2\left(\frac{\omega'(\xi)}{\omega(\xi)}\right)^2\right]dt^2 + \left(\frac{1}{(\xi^2-1)\,\Upsilon}\left[\frac{1}{2\Upsilon}\left(1+A^2\ell^2\right) + \xi\left(1-3A^2\ell^2(\xi^2-1)\right)\frac{\omega'(\xi)}{\omega(\xi)}\right] + \frac{3}{2}\left(\frac{\omega'(\xi)}{\omega(\xi)}\right)^2 - \frac{\omega''(\xi)}{\omega(\xi)}\right)d\xi^2\,. \quad (6.6.15)$$

The non-zero components of the stress tensor are

$$8\pi\omega(\xi)^2\ell\langle T^\tau_\tau\rangle = \frac{1}{2}\left(1+A^2\ell^2\right) + \xi\left(1-3A^2\ell^2(\xi^2-1)\right)\Upsilon\frac{\omega'(\xi)}{\omega(\xi)} + (\xi-1)\,\Upsilon^2\left[\frac{\omega''(\xi)}{\omega(\xi)} - \frac{3}{2}\left(\frac{\omega'(\xi)}{\omega(\xi)}\right)^2\right] \quad (6.6.16)$$

and

$$16\pi\omega(\xi)^2\ell\langle T^\xi_\xi\rangle = -\left(1+A^2\ell^2\right) + (\xi-1)\,\Upsilon^2\left(\frac{\omega'(\xi)}{\omega(\xi)}\right)^2\,. \quad (6.6.17)$$

The Ricci scalar of the boundary metric is

$$R(g_{(0)}) = \frac{2\Upsilon}{\ell^2\omega(\xi)^2}\Big(\xi\left(1-3A^2\ell^2(\xi^2-1)\right)\frac{\omega'(\xi)}{\omega(\xi)} + \left(\xi^2-1\right)\Upsilon\left[\frac{\omega''(\xi)}{\omega(\xi)} - \left(\frac{\omega'(\xi)}{\omega(\xi)}\right)^2\right]\Big)\,, \quad (6.6.18)$$

which satisfies the conformal anomaly relation (6.3.22) with central charge $c_{\text{Virasoro}} = 3\ell/2$.

Accounting for the two patches needed to cover the full region exterior to the horizon, the mass associated with $\partial_{\tilde{t}}$ is given by

$$M = 2mA\int_1^{x_+}\sqrt{-g_{(0)}}\langle T^\tau_\tau\rangle d\xi\,, \quad (6.6.19)$$

which when evaluated gives

$$M = \frac{m}{8\pi\alpha}\sqrt{1+m^2\mathcal{A}^2\ell^2}\,\text{arctanh}\left[\sqrt{1+m^2\mathcal{A}^2\ell^2}\tanh\left(m\pi\right)\right]\,. \quad (6.6.20)$$

This is plotted at various values of $\mathcal{A}$ in figure 6.24, both as a function of m and of x_+. In the limit of vaishing $\mathcal{A}$—where the geometry reduces to that of the static BTZ black hole—the formula for mass reproduces the expected $M = m^2/8$.

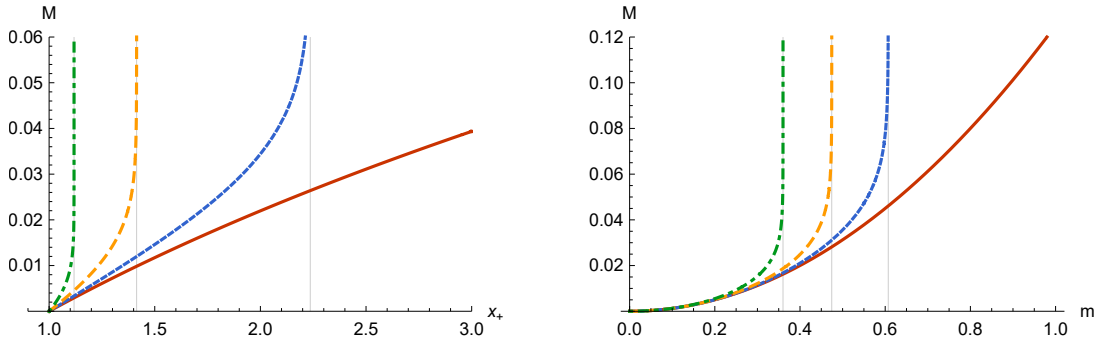

Figure 6.24: The holographic mass M of the BTZ black-hole pushed by a strut at various values of the acceleration parameter: $\mathcal{A} = 0$ (solid red), $\mathcal{A} = 0.5\ell^{-1}$ (dotted blue), $\mathcal{A} = \ell^{-1}$ (dashed orange), $\mathcal{A} = 2\ell^{-1}$ (dot-dashed green).

6.7 Class II_{left}: A BTZ black hole pulled by a domain-wall

It is also possible to construct another one parameter extension to the family of static BTZ black holes, where the defect emerging from the horizon has a positive energy density. As such, this solution is arguably more physical than the solution of section 6.6.

Starting from a patch of Class II spacetime (6.2.7) with $x < -1$, as presented in table 6.2, choose some value $x_+ \in (-y_h, -1)$, where $y_h = \sqrt{1 + A^{-2}\ell^{-2}}$, and define a patch with $x \in (x_+, -1]$. Glue two copies of this patch, mirroring along both $x = x_+$ and $x = -1$. The identifications are shown in figure 6.25. The $x = -1$ axis of the newly formed spacetime is regular. Along $x = x_+$, one finds a domain wall of positive tension $\mu = A(4\pi)^{-1}\sqrt{Q(x_+)}$. In contrast to the soluton with a strut, here there is always one—and only one—compact horizon present at $y = -y_h$, regardless of the values of A and x_+. As $|x_+| \to y_h$, instead of the system forming a non-compact horizon. the black hole horizon merges with the conformal boundary,

To cast the metric in more familiar coordinates, take $x = -\cosh(\psi/K)$, where $K = \pi/\operatorname{arcosh}(-x_+)$. Defining dimensionful coordinates $\rho = -(Ay)^{-1}$ and $t = \alpha A^{-1}\tau$, the metric becomes

$$\begin{aligned} ds^2 &= \frac{1}{[1 - A\rho\cosh(\psi/K)]^2}\left[f(\rho)\frac{dt^2}{\alpha^2} - \frac{d\rho^2}{f(\rho)} - \rho^2\frac{d\psi^2}{K^2}\right], \\ f(\rho) &= -1 + (1 + A^2\ell^2)\rho^2/\ell^2\,. \end{aligned} \tag{6.7.1}$$

Yet again, we anticipate a rescaling of t by α. The range of ψ is $(-\pi, \pi)$. This (ρ, ψ) patch covers both (x, y) coordinate patches; it covers the entire region region

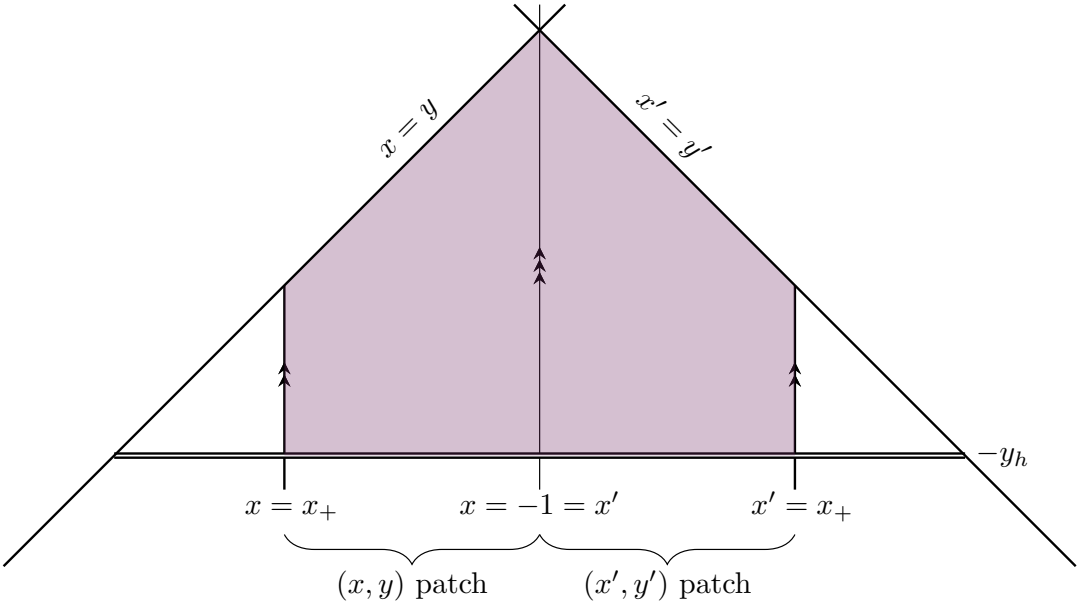

Figure 6.25: The two patches of type II spacetime used to construct a black hole with a domain wall under tension.

between the black hole horizon and the conformal boundary (the region shaded purple in figure 6.25). The coordinate ρ is everywhere positive in this domain. As long as the acceleration parameter A is sufficiently small, it is possible to set the magnitude of x_+ as large as one wishes. We thus have two conditions on K for this solution: $K > 0$ and $\pi/K < \operatorname{arcosh}(y_h)$.

The semiaxis $\psi = 0$ is regular, while the domain wall, which now lies along $\psi = \pm\pi$, has tension

$$\mu = \frac{A}{4\pi} \sinh\left(\frac{\pi}{K}\right) . \tag{6.7.2}$$

Much like the solutions with a strut considered in section 6.6, the solutions we have constructed in this section comprise a one parameter extension to the family of static BTZ black holes. One may demonstrate this in a similar way. Take the metric (6.7.1) and again make the parameter redefinitions $K = m^{-1}$ and $A = m\mathcal{A}$. Also, make the coordinate rescalings $r = m\rho$ and $\tilde{t} = m^{-1}t$. The metric becomes

$$\begin{aligned} ds^2 &= \frac{1}{\Omega(r,\psi)^2}\left[F(r)\frac{d\tilde{t}^2}{\alpha^2} - \frac{dr^2}{F(r)} - r^2 d\psi^2\right] , \\ F(r) &= -m^2(1 - \mathcal{A}^2 r^2) + \frac{r^2}{\ell^2} , \\ \Omega(r,\psi) &= 1 - \mathcal{A} r \cosh(m\psi) . \end{aligned} \tag{6.7.3}$$

We now have the conditions $0 \leq m \sinh(m\pi) < (\mathcal{A}\ell)^{-1}$. Note that, much as for the solution with a strut, the point $m = 0$ in parameter space was inaccessible using the

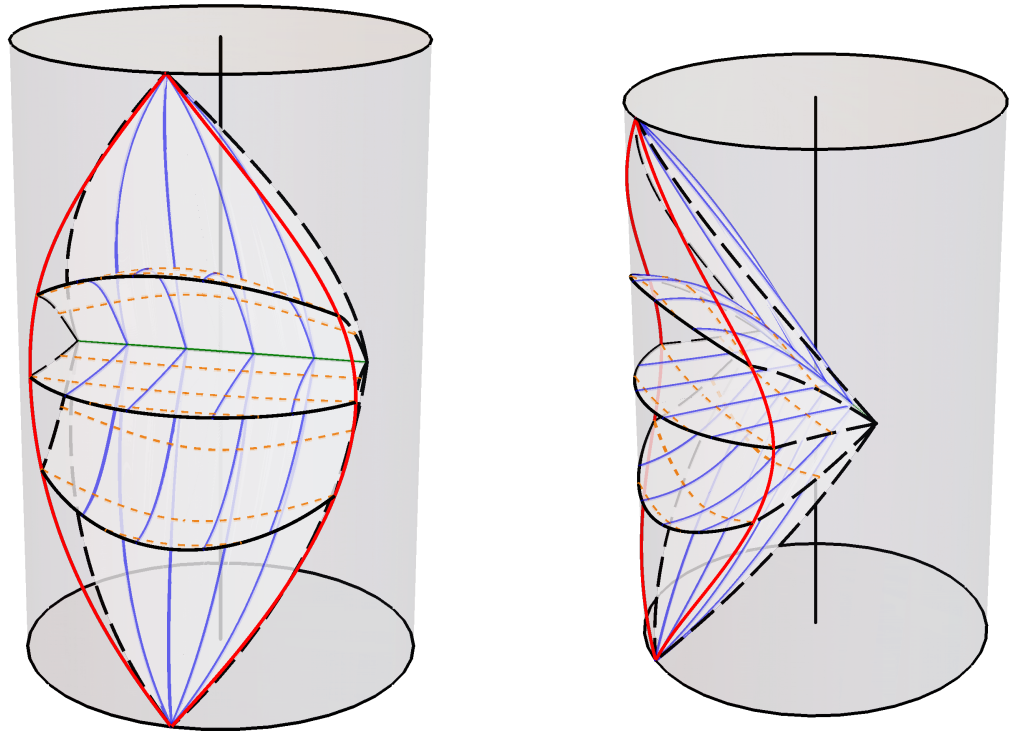

Figure 6.26: The Class $\mathrm{II}_{\mathrm{left}}$ black hole. Several surfaces of constant t are shown; those of large positive and negative t outline the event horizon. The surface $x = x_+$ – shown in dashed black – is identified with its partner within each time-slice. The bifurcation surface of the Killing horizon is shown in green and has topology S^1. Lines of constant x and y are shown in solid blue and dashed orange respectively. The classically accessible region of the conformal boundary is delimited in red.

parameterisation (6.7.1). The black hole horizon lies at $r = m\ell(1 + m^2\mathcal{A}^2\ell^2)^{-1/2}$. The tension in the domain wall is an increasing function of m:

$$\mu = \frac{m\mathcal{A}}{4\pi} \sinh(m\pi) \,. \tag{6.7.4}$$

It is interesting to note that the bounds on m translate into bounds on the induced defect stress:

$$0 \leq \mu < \frac{1}{4\pi\ell} \,. \tag{6.7.5}$$

To understand the geometry, we map onto a subset of global AdS_3 and plot the geometry by compactifying the spatial section. This process is described in appendix C, with the result being figure 6.26. One finds a spacetime qualitatively similar to the BTZ black hole, (cf. figure C.1), but with non-zero tensile force present in the identification surface. The bifurcate Killing horizon generated by ∂_t has a compact bifurcation surface, with the topology of a circle.

6.7.1 The holographic mass

As the geometry never forms an acceleration horizon, one is free to calculate the holographic mass over the entire range of K (equivalently m). We again make the decision to calculate the conserved charge with respect to $\partial_{\tilde{t}}$, where $\tilde{t} = m^{-1} t_{\text{Rindler}}$. This is justified similarly to the argument given in subsection 6.6.1. The transformations as written in (6.6.5) hold in the present case (though of course one must use the appropriate Ω), leading to the same value of α (6.6.7). The procedure to construct the holographic stress tensor is then identical to the one performed in section 6.6; we will not repeat the details. In particular, the expressions for the Fefferman-Graham expansion (6.6.12), (6.6.14), (6.6.15); the stress tensor (6.6.16), (6.6.17); and the Ricci scalar of the boundary metric (6.6.18) are all identical.

The limits for the mass integration must be updated for the present case,

$$M = 2A \int_{x_+}^{-1} \sqrt{-g_{(0)}} \langle T_\tau^\tau \rangle d\xi \,, \tag{6.7.6}$$

but the evaluated value is identical to the mass of the black hole with a strut:

$$M = \frac{m}{8\pi\alpha} \sqrt{1 + m^2 \mathcal{A}^2 \ell^2} \operatorname{arctanh} \left[\sqrt{1 + m^2 \mathcal{A}^2 \ell^2} \tanh (m\pi) \right] . \tag{6.7.7}$$

The mass is plotted at various values of $\mathcal{A}$ in figure 6.27, both as a function of m and of x_+. As $\mathcal{A} \to 0$, M approaches the mass of a standard BTZ black hole [93] $M_{\text{BTZ}} = m^2/8$ appropriately. As $m \to 0$, the expression (6.7.7) for M vanishes. In this limit, simple coordinate transformation

$$R = \frac{r}{1 - \mathcal{A} r} \tag{6.7.8}$$

applied to the line element (6.7.3) recovers (6.6.10), the Poincaré patch of AdS_3 with a periodically identified spatial coordinate. In consonance with (6.7.7), this geometry has vanishing mass [93].

6.8 Class III

As stated in section 6.2, if $A^2\ell^2 \geq 1$ then P is everywhere non-positive. We thus restrict to the case where $A^2\ell^2 < 1$. There are then two disconected, non-compact horizons in the spacetime at $y = \pm y_h$, where $y_h \equiv \sqrt{A^{-2}\ell^{-2} - 1}$. Solutions of Class III have no roots for $Q(x)$ and so the acceptable range of x is $x > y > -y_h$. The (x, y) parameter space is shown in figure 6.28. Since there are no roots of Q at which to form a regular semi-axis, it is not possible to form a single-tensioned-wall solution

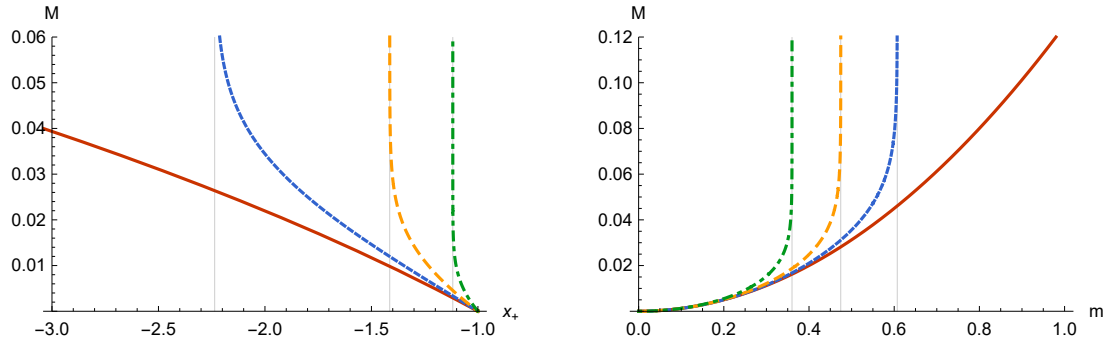

Figure 6.27: The holographic mass M of the BTZ black-hole pulled by a tensioned-wall at various acceleration parameters: $\mathcal{A} = 0$ (solid red), $\mathcal{A} = 0.5\ell^{-1}$ (dotted blue), $\mathcal{A} = \ell^{-1}$ (dashed orange), $\mathcal{A} = 2\ell^{-1}$ (dot-dashed green).

with the interpretation of x as an angular coordinate. While it is possible to form a black hole solution with two tensioned-walls, we do not do so here.

Although it is not possible to make a single-tensioned-wall solution with a periodic x coordinate, One could—if one desired—cut the patch denoted in figure 6.29 along some line $x = x_+$ which connects the $y = -y_h$ horizon to either the conformal boundary (for $x_+ < y_h$) or the $y = -y_h$ horizon (for $x_+ > y_h$). Identifying two copies for the remaining space along the cut still gives a solution, although x is not periodic. Four such solutions are possible, depending on a choice of signs for $x_+ - y_h$ and $x - x_+$. This solution is a stark departure from the ones we have considered in previous sections. In particular, the resulting space is some subset of *two* copies of the anti-de Sitter covering space, $AdS_3 \times AdS_3$; the solution is no-longer guaranteed

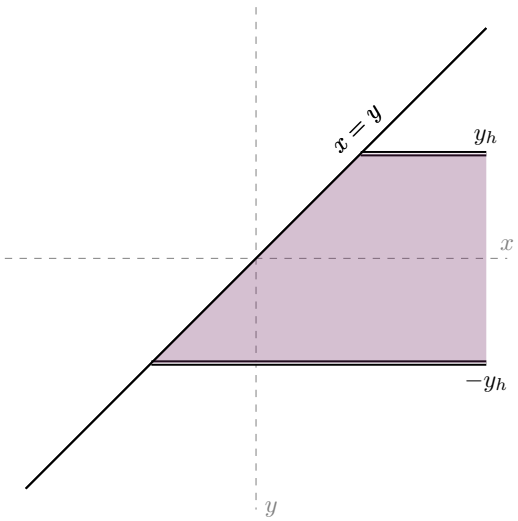

Figure 6.28: Coordinate ranges for the Class III solution.

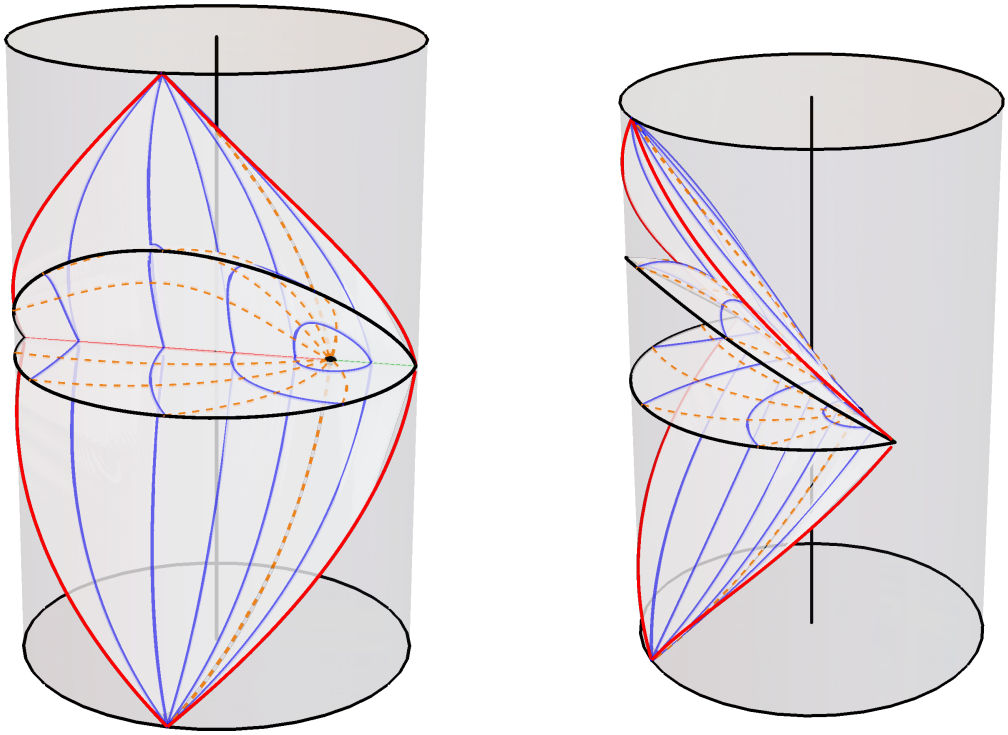

Figure 6.29: The Class III solution. Several surfaces of constant τ are shown, with those at very early and very late times outlining the two disjoint bifurcate Killing horizons. The red bifurcation surface is $y = -y_h$, while the green bifurcation surface is $y = +y_h$. The black dot denotes the point $x \to \infty$. Lines of constant finite x are shown in solid blue, with lines of constant y shown in dashed orange.

to be embeddable within a single copy of AdS_3. This is a "braneworld solution", with the brane at $x = x_+$ dividing the two copies of global space. We will not comment on the detailed properties of these solutions here, but it is worth acknowledging as a curiosity.

6.9 Conclusions

In this chapter, we have constructed within three-dimensional general relativity a broad family of solutions resembling the four-dimensional C-metric, showing that the set of possible geometries is much richer than acknowledged in [40]. We found solutions describing both conical defects and black holes, and computed the mass of each holographically for phases without non-compact horizons. It is interesting to note that even with the presence of domain walls, a qualitative property of the theory's spectrum is unchanged: the theory is "gapped", with conical defect solutions

and black holes occupying the negative and positive-mass sectors, respectively.

In sections 6.3 and 6.4, we found a set of solutions wherein a conical defect is accelerated by a domain wall. We demonstrated the existence of both rapidly and slowly accelerating phases, showing that there is a region of parameter space for which the formation of a non-compact acceleration horizon may be circumvented. Much of the behaviour of such a conical defect is reminiscent of a very small four-dimensional accelerated black hole described by the C-metric (with negative cosmological constant). Both the three and four-dimensional solutions possess slowly and rapidly accelerating phases. In their slowly accelerating phases, both solutions describe a (nearly) point-like object held a fixed distance from the origin of pure anti-de Sitter space by a topological defect under compression/tension. This defect guides the object along a worldline with a constant four-acceleration. The rapidly accelerating phases of the four-dimensional C-metric and three-dimensional conical defect solutions also share similarities. In particular—at least for small black holes in four dimensions—both geometries are approxiately Rindler [189, 190].

On the other hand, the three-dimensional conical defects possess novel-phases which are not shared by their four-dimensional cousins. Consider for example the Class $\mathrm{I}_{\mathrm{rapid,A}}$ single-tensioned-wall solution, describing a rapidly accelerating particle pulled by a domain wall under tension. While for light conical defects the structure is similar to a small, accelerating black hole in four dimensions, as particle mass increases a phase transition occurs and one attains the Class $\mathrm{I}_{\mathrm{rapid,B}}$ single-tensioned-wall solution. This latter solution is compact and entirely distinct from any of the four-dimensional phases. After compactification the only access to the conformal boundary is at the two points in the far future and past of the Rindler worldline; one may say that the dimensionality of the (previously two-dimensional) boundary theory drops to that of an instantaneous point. A similar compactification occurs for the Class $\mathrm{I}_{\mathrm{rapid,A}}$ and $\mathrm{I}_{\mathrm{rapid,B}}$ single-strut solutions, although in this case the accessible region of conformal boundary is still two-dimensional. The interpretation of such novel compact phases is not clear.

It should also be acknowledged that the topological nature of three-dimensional gravity creates further distinctions from the four-dimensional theory. Consider again the Class $\mathrm{I}_{\mathrm{rapid,A}}$ single-tensioned-wall solution. As we said, this is similar to a four-dimensional accelerating black hole with vanishingly small mass parameter. As discussed in section 3, analytic extension necessitates the existence of a "mirror black hole" on the other side of the acceleration horizon [190]. However, for this three-dimensional solution the domain wall was inserted topologically, by choosing some value of x at which to cut and identify. As such, there is no requirement that one identifies similarly in the "mirror" region when performing an analytic extension;

one may simply find oneself in a region of pure AdS_3 spacetime after crossing the event horizon.

We also constructed black holes with domain wall appendages in sections 6.6 and 6.7. In particular, the Class II_{left} and Class II_{right} single-defect solutions each form a one-parameter extension of the standard family of static BTZ black holes. We showed how these solutions may be constructed from identifications of the Rindler wedge of AdS_3, as the BTZ black hole was by Banados et al. [195]. It is the choice to identify across a surface of constant tension which induces the domain wall; the particular choice of identification surface giving zero tension produces the static BTZ solution. Apart from the presence of a string-like domain wall, the Class II_{left} solution is qualitatively similar to the usual BTZ black hole without a defect. It does not form a second horizon for any value of the acceleration parameter. However, this is not true of the Class II_{right} single-strut solution. Here, both "rapid" and "slow" phases exist. The rapid phase attained for large acceleration parameter is qualitatively distinct from the usual BTZ black hole, possessing a non-compact horizon reminiscent of the acceleration horizon which can be present in the four-dimensional AdS C-metric geometry. In some sense the solution is a hybrid between the BTZ black hole and the four-dimensional AdS C-metric.

However, one should be careful not to carry this analogy too far. While the conical deficit solutions of sections 6.3 and 6.4 may uncontroversially be called accelerating objects, it is not so clear that the same may be said of the Class II black holes. This statement was made by Astorino of the Class $II_{right,slow}$ solution [40]. It is the author's view that this was overzealous: there is no meaningful sense in which these solutions are "accelerating BTZ black holes". As mentioned above, one may argue that the four-dimensional AdS C-metric describes an accelerating black hole by shrinking its (compact) horizon size to zero and calculating the four-acceleration of the resulting object [210]. In taking this limit, one retains a cosmic string under tension which provides the acceleration for the small black hole. However, for either of the Class II black holes, shrinking the horizon size to nothing would require taking the limit $m \to 0$. Note that from equations (6.6.11) and (6.7.4) we see that in either case this necessitates removing the domain wall; the residual geometry is simply Poincaré AdS_3. Physically, there is then no object with which to "accelerate" anything. Mathematically, one can understand the issue from the topological nature of three-dimensional gravity. While the four-dimensional solution is a "true" black hole, the three-dimensional black hole is constructed by imposing identifications on the acceleration horizon of a fictitious observer [195]. There is then no meaningful sense hitherto established in which one may talk of the acceleration of this extended object. For the Class II_{right} black hole in its rapid phase, the temperature of the

non-compact "acceleration" horizon also suggests that the black hole is inertial. By regularity of the Euclidean section, the temperature—with the correct normalisation of Killing vector (6.6.7)—is found to be $T = m(2\pi\ell)^{-1}$, which is independent of $\mathcal{A}$. If the parameter $\mathcal{A}$ did in some way parametrise an acceleration of the black hole, the Unruh effect would be violated.

An obvious next step in understanding the three-dimensional C-metric is to establish a consistent thermodynamic description of the system. Given the four-dimensional results described and explored in chapters 3, 4, and 5, one should expect that the tension of the domain wall should take the role of a thermodynamic charge. This may also provide interesting perspectives from which to understand the role of the defect in the boundary theory, since two-dimensional conformal field theories are radically different from higher-dimensional ones. Realising these topological solutions as truncations of supergravity solutions is also an open problem.

Chapter 7

Summary

In this thesis, we have taken several approaches to understand the impact of acceleration on black holes.

After motivating the study of black holes as thermodynamic systems in chapter 2, we discussed the features of the C-metric in chapter 3 and reviewed some recent successes [149] in utilising holographic technology to define consistent thermodynamic quantities for it. These quantities satisfy a first law of thermodynamics, with each defect's tension playing the role of a thermodynamic charge.

In chapter 4, by managing to rewrite the thermodynamic potentials as rational functions of the thermodynamic charges, we saw how the tensions in the antipodal strings may the naturally be grouped into one quantity which tracks an overall average deficit through the spacetime and another which tracks the acceleration. A Christodoulou-Ruffini formula for the asymptotically locally anti-de Sitter C-metric was shown, providing evidence for the mass formula found in the literature [150]. This formula also indicated a peculiar "exothermic" nature of acceleration: as the black hole is accelerated, the enthalpy of the solution drops. This exothermicity was used to explain the recently observed "snapping swallowtail" phenomenon exhibited by accelerating black holes [167].

We also utilised the accelerating black hole to provide support for extended thermodynamics in general. By scattering particles from a rotating, accelerating black hole, we performed a thought experiment supporting the interpretation of black hole mass as a true thermodynamic enthalpy. Our conclusion mirrors the resolutions to apparent incongruities in similar thought experiments [70, 80] involving the absorption of charged particles by near-extremal Reissner-Nordström black holes.

We then advanced to arrays of asymptotically-locally flat black holes in chapter 5, attempting to utilise their source-rod structure to define their mass. This led to a first law mirroring the holographic system: the string tensions act as thermodynamic

charges with conjugate thermodynamic lengths. We demonstrated that the array behaves as a coupled system, with the defects transferring energy between the individual black holes. In the particular case of the C-metric, Our thermodynamic quantities satisfied a Christodoulou-Ruffini formula showing that accelerating the black hole is, again, an exothermic process. The finite length strings' thermodynamic lengths were confirmed to be the worldvolumes of the defects. However, the nature of the semi-infinite strings' thermodynamic lengths remains a mystery. Presumably some sort of renormalisation of their (divergent) worldvolume is required. This would be an interesting direction for future work, especially within a holographic framework where renormalisation procedures are typically well-defined.

Finally, in chapter 6, building on the work of Astorino [40], we worked in three spacetime dimensions and examined geometries with a C-metric-like ansatz for their metrics. The two most interesting solutions we formulated were a conical deficit accelerated by a line-like defect of codimension one, and a black hole resembling the static BTZ solution with a domain wall appendage emanating from its horizon. Both solutions are much like the four-dimensional C-metric, though in different ways. The accelerating particle pulled by a domain wall under tension behaves like a small four-dimensional black hole. The solution exhibits both a slowly accelerating phase, in which the particle is held a fixed proper distance from the boundary of global anti-de Sitter space, and a rapid phase for which the particle follows a Rindler worldline. For these phases the particle may reasonably be called "an accelerating object"; it is hoped that the solution may be used to shed light on the nature of accelerating bulk objects from a holographic perspective. The black hole solutions we discussed resemble the BTZ black hole. We showed how one can construct them in a similar way, via identifications of the Rindler wedge. The solution of section 6.6 in particular resembles the anti-de Sitter C-metric, possessing a "rapid" phase for which a non-compact horizon forms. However, we questioned the legitimacy of the claim that it is an accelerating object. Although it may not be accelerating, given the relative simplicity topological gravity, we hope that the solution will provide new perspectives on the C-metric. Understanding the common features of black holes with topological defect appendages[1]in both two and three dimensions may assist with the quest to find C-metrics in higher-dimensional gravity [212–215].

A number of open questions still remain. In particular, although the role of string tension within the laws of black hole mechanics is understood, it is not clear what microscopic thermodynamic property they quantify. This question mirrors the historical development of horizon area and surface gravity, which were initially thought to merely be analogous to true thermodynamic entropy and temperature. Similarly,

[1]See [211] for a non-C-metric example.

both the string tension and thermodynamic length are geometric quantities, given by the magnitude of conical defect and string worldvolume. It would be interesting to understand if these have thermodynamic interpretations.

An obvious open question is if the three-dimensional solutions of chapter 6 admit similar thermodynamic laws to the four-dimensional C-metric, with the domain wall tension acting as a charge. One would expect so. Confirmation may help to shed light on the thermodynamic nature of the defect quantities, since computation of microscopic quantities is often easier for two-dimensional boundary theories [216, 217]. In such holographic setups, it would also be interesting to understand the role of the defects in the boundary theory. As our cosmic strings (or domain walls) extend to the boundary, in some sense the conformal symmetry in the ultraviolet is broken. The point at which it meets the boundary corresponds to a non-renormalisable modification of the ultraviolet theory, known as a "conformal defect" [218]. For the four-dimensional accelerating black hole described in section 3.3, the $SO(3,2)$ conformal symmetry of the boundary theory is broken to that of a one-dimensional conformal theory cross rotation, $SO(2,1) \times U(1)$. The group $SO(2,1)$ gives the symmetries a conformal quantum mechanics extending along the vortex worldline; one may say that there is a conformal quantum mechanics living on the boundary defect [192]. In a similar way, the three-dimensional black hole solutions—for example that of section 6.7—should have their $SL(2,\mathbb{R})_{\mathrm{L}} \times SL(2,\mathbb{R})_{\mathrm{R}}$ conformal symmetries broken to a conformal quantum mechanics. These ideas suggest an approach towards identifying the microscopic quantities macroscopically quantified by string (or domain wall) tension and thermodynamic length.

Appendix A

A proposed violation of the second law in extended thermodynamics

In this appendix, we review the argument due to Gwak [70] that, within the extended thermodynamics framework, the second law is violated during the absorbsion of a particle by a near-extremal, electrically charged black hole. We present the subsequent resolution due to Hu, Ong, and Page, who argued that no violation of the second law occurs if the enthalpy of spacetime is considered the true measure of black hole energy. The argument of this appendix should be compared with the one given in section 4.4.

Consider the static, charged, spherically symmetric black hole with negative cosmological constant in four dimensions

$$\begin{aligned} ds^2 &= f(r)dt^2 - \frac{dr^2}{f(r)} - r^2 d\Omega^2 \,, \\ f(r) &= 1 - \frac{2m}{r} + \frac{e^2}{r^2} + \frac{r^2}{\ell^2} \,, \end{aligned} \tag{A.0.1}$$

The thermodynamic parameters of the solution are

$$\begin{aligned} M &= m \,, & S &= \pi r_+^2 \,, & T &= \frac{f'(r_+)}{4\pi} \,, \\ Q &= e \,, & \Phi &= \frac{e}{r_+} \,, & P &= \frac{3}{8\pi\ell^2} \,, & V &= \frac{4\pi r_+^3}{3} \,, \end{aligned} \tag{A.0.2}$$

which satisfy

$$\delta M = T\delta S + V\delta P + \Phi\delta Q \,. \tag{A.0.3}$$

The energy of a particle of charged particle of charge $e_{\rm p}$, dropped radially with momentum $|p^r|$ across the horizon, is

$$E_{\rm p} = \Phi e_{\rm p} + |p^r| \,. \tag{A.0.4}$$

First, let us assume that the particle both transfers its charge to, and contributes its energy to the internal energy of, the black hole:

$$E_{\rm p} = \delta U\,, \qquad\qquad e_{\rm p} = \delta Q\,. \tag{A.0.5}$$

Employing the first law, we find

$$\begin{aligned} \Phi\delta e_{\rm p} + |p^r| &= \delta\left(M - VP\right) \\ &= T\delta S - P\delta V + \Phi\delta Q\,. \end{aligned} \tag{A.0.6}$$

That is,

$$|p^r| = T\delta S - P\delta V\,. \tag{A.0.7}$$

For near extremal black holes, T is close to zero, which implies that $P\delta V < 0$. In terms of the variation of metric quantities, this statement is equivalent to $\delta r_+ < 0$. On the other hand, the second law of thermodynamics—or Hawking area law—$\delta S > 0$, implies the exact opposite: $\delta r_+ > 0$.

Assume instead that the particle transfers its energy to the total enthalpy of the spacetime:

$$E_{\rm p} = \delta M\,, \qquad\qquad e_{\rm p} = \delta Q\,, \tag{A.0.8}$$

In this case,

$$\begin{aligned} \Phi\delta e_{\rm p} + |p^r| &= \delta M \\ &= T\delta S + V\delta P + \Phi\delta Q\,. \end{aligned} \tag{A.0.9}$$

That is,

$$|p^r| = T\delta S + V\delta P\,. \tag{A.0.10}$$

If the process occurs isobarically, we have $|p^r| = T\delta S > 0$. In this case we have resolved the issue, as the second law holds. If the process occurs at variable pressure, then $\delta S \geq 0$ if and only if $|p^r| \geq V\delta P = -r_+^3\ell^{-3}\delta\ell$. If somehow $|p^r| < -r_+^3\ell^{-3}\delta\ell$, then an additional contribution to δM would be needed, though we do not consider this possibility[1].

[1]In holography, one works with a large number of degrees of freedom N in the boundary conformal field theory. In order to change N, one could imagine embedding the field theory within a larger boundary theory containing some dynamical fields which determine an effective N for the conformal part. As these dynamical fields evolve, the effective N varies. In this process, energy is transferred between these fields and the conformal sector and so the bulk energy changes. In order to determine how changes in N affect the black hole entropy, one would need to know the specifics of the complete theory. The salient point is that there is no solid argument here that the second law is violated; the classical bulk geometry may not be sensitive to all of the degrees of freedom in the complete quantum field theory.

Appendix B

Coordinate systems for the C-metric

In this appendix, we collect the transformation formulae between the standard C-metric (expressed in Hong-Teo form [129]) and the Weyl form of section 5.2. Similar transformations have been performed in the literature for the rotating C-metric [117, 219, 220]. The C-metric in Weyl form is

$$ds^2 = \frac{X_1X_3}{\ell_\gamma X_2}dt^2 - \frac{\ell_\gamma E_{12}E_{23}}{4R_1R_2R_3E_{13}}\left(\frac{V_3+1}{2}\right)^2[dr^2+dz^2] - r^2\frac{\ell_\gamma X_2}{X_1X_3}\frac{d\phi^2}{K^2}\,, \qquad \text{(B.0.1)}$$

where $\ell_\gamma = z_3 - z_0 = z_3 - (z_1+z_2)/2$ is the z-distance to the centre of the black hole rod.

Now let $m = (z_2 - z_1)/2$ and $A = \ell_\gamma^{-1}$. Define

$$\begin{aligned} r &= \frac{\bar{r}\sin\theta\sqrt{f(\bar{r})g(\theta)}}{(1+A\bar{r}\cos\theta)^2}\,, \\ z - z_0 &= \frac{\bar{r}\,(A\bar{r}+\cos\theta)\left(1-\frac{m}{\bar{r}}+mA\cos\theta\right)}{(1+A\bar{r}\cos\theta)^2}\,, \end{aligned} \qquad \text{(B.0.2)}$$

where

$$f(R) = (1-A^2\bar{r}^2)\left(1-\frac{2m}{\bar{r}}\right)\,, \qquad g(\theta) = (1+2mA\cos\theta)\,. \qquad \text{(B.0.3)}$$

Then the Weyl metric (B.0.1) transforms to the C-metric in Hong-Teo coords [129], rather than the standard Kinnersley-Walker coordinates discussed in [182]:

$$ds^2 = \frac{1}{(1+A\bar{r}\cos\theta)^2}\left[\bar{f}(\bar{r})dt^2 - \frac{d\bar{r}^2}{\bar{f}(\bar{r})} - \bar{r}^2\left(\frac{d\theta^2}{\bar{g}(\theta)} - \bar{g}(\theta)\sin^2\theta d\phi^2\right)\right]\,. \qquad \text{(B.0.4)}$$

Here we see the interpretation of ℓ_γ as the acceleration length scale; for small m,

$A = \ell_\gamma^{-1}$ corresponds to the magnitude of the four-acceleration of the black hole [189].

Appendix C

Embedding coordinates for the three-dimensional C-metric

In this appendix, we collate mappings from the geometries constructed in chapter 6 to subsets of global AdS_3. These mappings were used to create the 3D embedding diagrams 6.8, 6.9, 6.10, 6.13, 6.14, 6.15, 6.18, 6.22, 6.23. 6.26, and 6.29.

C.1 Global AdS_3

First, we define global AdS_3 by its embedding as a hyperboloid in $\mathbb{R}^{2,2}$. The embedding is

$$\begin{aligned} X_0 &= \ell\sqrt{1+\frac{R^2}{\ell^2}}\sin\left(\frac{T}{\ell}\right), \quad X_1 = R\sin\Theta\,, \\ X_3 &= \ell\sqrt{1+\frac{R^2}{\ell^2}}\cos\left(\frac{T}{\ell}\right), \quad X_2 = R\cos\Theta\,. \end{aligned} \tag{C.1.1}$$

The hyperboloid is

$$\sum_{i=0}^{3}\eta_{ii}X_i^2 = \ell^2\,, \tag{C.1.2}$$

with induced metric

$$\sum_{i=0}^{3}\eta_{ii}dX_i^2 = \left(1+\frac{R^2}{\ell^2}\right)dT^2 - \frac{dR^2}{\left(1+\frac{R^2}{\ell^2}\right)} - R^2d\Theta^2\,. \tag{C.1.3}$$

Note in the above two sums that η implements the signature $(+--+)$. The coordinates lie in the ranges $T\in\mathbb{R}$, $R\in(0,\infty)$, $\Theta\in(-\pi,\pi)$.

Conversely, the global coordinates are defined from the embedding coordinates by

$$\begin{aligned} T_G &= \arctan\left(\frac{X_0}{X_3}\right), \quad R_G = \sqrt{X_1^2+X_2^2}\,, \\ X_G &= X_1\,, \qquad\qquad Y_G = X_2\,. \end{aligned} \tag{C.1.4}$$

We may then compactify the spatial two-section to attain the Poincaré disk:

$$\hat{X} = \frac{X_G}{\ell + \sqrt{\ell^2 + X_G^2 + Y_G^2}}\,, \qquad \hat{Y} = \frac{Y_G}{\ell + \sqrt{\ell^2 + X_G^2 + Y_G^2}}\,. \tag{C.1.5}$$

The global space then appears as a cylinder in $(T_G, \hat{X}, \hat{Y})$ coordinates. This cylinder is defined by $|T_G| < \pi/2$, $\hat{X}^2 + \hat{Y}^2 < 1$.

Given some metric ds_3^2, by finding a set of embedding coordinates X_i such that

$$\sum_{i=0}^{3} \eta_{ii} X_i^2 = \ell^2\,, \tag{C.1.6}$$

and

$$\sum_{i=0}^{3} \eta_{ii} dX_i^2 = ds_3^2\,, \tag{C.1.7}$$

one may plot the geometry as a subset of the global cylinder by applying the transformations (C.1.4) and (C.1.5).

C.2 The Rindler wedge and the static BTZ black hole

For the non-rotating BTZ geometry,

$$ds_3^2 = \left(-m^2 + \frac{r^2}{\ell^2}\right) dt^2 - \frac{dr^2}{\left(-m^2 + \frac{r^2}{\ell^2}\right)} - r^2 d\phi^2\,, \tag{C.2.1}$$

the embedding is well known [195]:

$$\begin{aligned} X_0 &= \mathcal{B}(r) \sinh\left(\frac{r_h t}{\ell^2}\right)\,, \quad X_1 = \mathcal{A}(r) \sinh\left(\frac{r_h \phi}{\ell}\right)\,, \\ X_3 &= \mathcal{A}(r) \cosh\left(\frac{r_h \phi}{\ell}\right)\,, \quad X_2 = \mathcal{B}(r) \cosh\left(\frac{r_h t}{\ell^2}\right)\,, \end{aligned} \tag{C.2.2}$$

where

$$\mathcal{A}(r) = \ell \frac{r}{r_h}\,, \qquad \mathcal{B}(r) = \ell \sqrt{\left(\frac{r}{r_h}\right)^2 - 1}\,, \tag{C.2.3}$$

with

$$r_h = m\ell\,. \tag{C.2.4}$$

If ϕ is taken to be non-compact, then we have a portion of AdS_3 bounded by a bifurcate acceleration horizon and the conformal boundary [195]. This geometry is the *planar BTZ geometry* or *Rindler wedge*. In this case m is a gauge parameter which may be set to unity by a rescaling of both r and ϕ. Alternatively, one may

identify $\phi \to \phi + 2\pi$ to attain the static BTZ black hole [194]. We plot both geometries as subsets of global AdS_3 using the technique described above in figure C.1.

C.3 Class I solutions

The Class I geometry is given by

$$ds_3^2 = \frac{1}{\Omega^2}\left[P d\tau^2 - \frac{dy^2}{P} - \frac{dx^2}{Q}\right], \tag{C.3.1}$$

where

$$Q = 1 - x^2\,, \qquad \Omega = A(x-y)\,. \tag{C.3.2}$$

In the slowly accelerating phase, $A^2\ell^2 < 1$ and the lapse function is given by

$$P = y^2 + S^2\,, \qquad S = \sqrt{\frac{1}{A^2\ell^2} - 1}\,. \tag{C.3.3}$$

The embedding is then

$$\begin{aligned} X_0 &= \frac{\sqrt{P}}{S\Omega}\sin S\tau\,, \quad X_1 = \frac{\sqrt{Q}}{\Omega}\,, \\ X_3 &= \frac{\sqrt{P}}{S\Omega}\cos S\tau\,, \quad X_2 = \frac{A\ell}{\Omega}\left(Sx + \frac{y}{S}\right). \end{aligned} \tag{C.3.4}$$

In the rapid phase, $A^2\ell^2 > 1$, so the lapse function now has roots:

$$P = y^2 - y_h^2\,, \qquad y_h = \sqrt{1 - \frac{1}{A^2\ell^2}}\,. \tag{C.3.5}$$

We thus require the alternative embedding

$$\begin{aligned} X_0 &= \frac{\sqrt{P}}{y_h\Omega}\sinh y_h\tau\,, \qquad X_1 = \frac{\sqrt{Q}}{\Omega}\,, \\ X_3 &= \frac{A\ell}{\Omega}\left(y_h x - \frac{y}{y_h}\right), \quad X_2 = \frac{\sqrt{P}}{y_h\Omega}\cosh y_h\tau\,. \end{aligned} \tag{C.3.6}$$

C.4 Class II solutions

The Class II geometry is given by

$$ds_3^2 = \frac{1}{\Omega^2}\left[P d\tau^2 - \frac{dy^2}{P} - \frac{dx^2}{Q}\right], \tag{C.4.1}$$

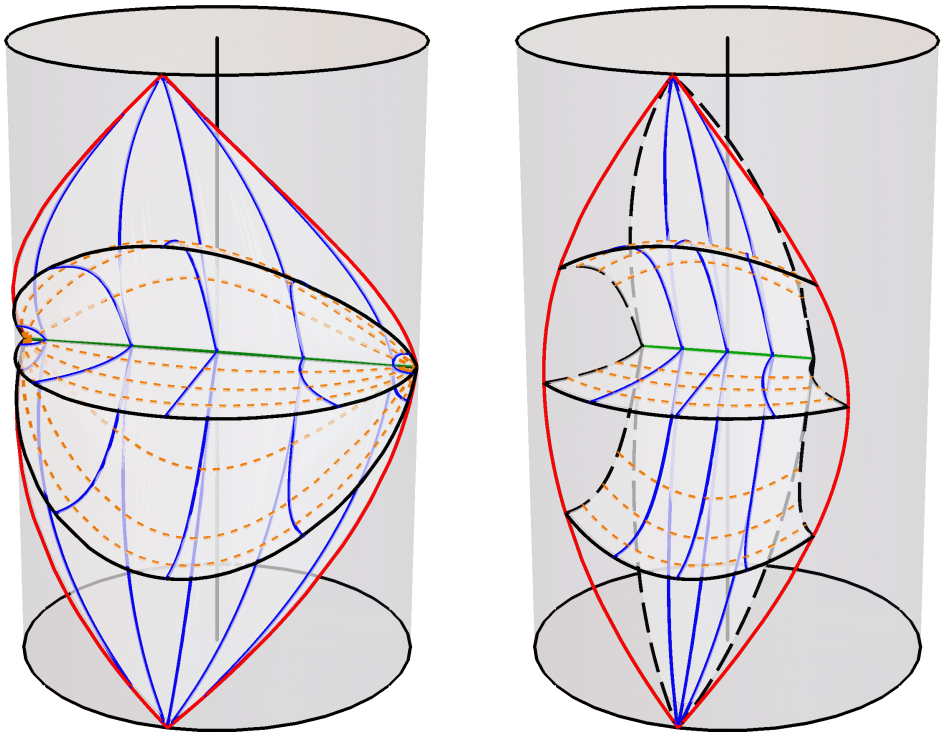

(a) Planar BTZ geometry (b) BTZ black hole

Figure C.1: The planar and compact (static) BTZ black holes. Lines of constant ϕ are shown in blue, with lines of constant r in dashed orange. Several surfaces of constant time t are shown. The classically accesible subset of the boundary is bounded in red. To guide the eye, the locus of the cylinder is shown in solid black. (a): $\phi \in \mathbb{R}$, giving the planar BTZ geometry or "Rindler wedge". The bifurcation surface (green) has topology $\mathbb{R}$. (b): ϕ identified with period 2π, giving the BTZ black hole. Lines of constant t and $\phi = \pm\pi$ are plotted in long-dashed black, pairs of which are identified across the same time-slice. The bifurcation surface (green) has topology S^1.

with metric functions

$$P = -y^2 + y_h^2\,, \qquad Q = x^2 - 1\,, \qquad \Omega = A(x-y)\,, \tag{C.4.2}$$

where

$$y_h = \sqrt{1 + \frac{1}{A^2\ell^2}}\,. \tag{C.4.3}$$

The embedding in the region where P is positive is then

$$\begin{aligned} X_0 &= \frac{\sqrt{P}}{y_h\Omega}\sinh y_h\tau\,, & X_1 &= \frac{\sqrt{Q}}{\Omega}\,, \\ X_3 &= \frac{A\ell}{\Omega}\left(y_h x - \frac{y}{y_h}\right)\,, & X_2 &= \frac{\sqrt{P}}{y_h\Omega}\cosh y_h\tau\,. \end{aligned} \tag{C.4.4}$$

C.5 Class III solutions

For the Class III solution of section 6.8, the line element is

$$ds_3^2 = \frac{1}{\Omega^2}\left[P d\tau^2 - \frac{dy^2}{P} - \frac{dx^2}{Q}\right]\,. \tag{C.5.1}$$

The metric functions are

$$P = -y^2 + y_h^2\,, \qquad Q = 1 + x^2\,, \qquad \Omega = A(x-y)\,, \tag{C.5.2}$$

where

$$y_h = \sqrt{\frac{1}{A^2\ell^2} - 1}\,. \tag{C.5.3}$$

The embedding for $|y| < y_h$ is then

$$\begin{aligned} X_0 &= \frac{\sqrt{P}}{y_h\Omega}\sinh y_h\tau\,, & X_1 &= \frac{A\ell}{\Omega}\left(y_h x + \frac{y}{y_h}\right)\,, \\ X_3 &= \frac{\sqrt{Q}}{\Omega}\,, & X_2 &= \frac{\sqrt{P}}{y_h\Omega}\cosh y_h\tau\,. \end{aligned} \tag{C.5.4}$$

Bibliography

[1]R. Gregory and A. Scoins, *Accelerating black hole chemistry*, Phys. Lett. B **796**, 191–195 (2019),
arXiv:1904.09660 [hep-th].

[2]W. Ahmed, H. Z. Chen, E. Gesteau, R. Gregory and A. Scoins, *Conical holographic heat engines*, Class. Quant. Grav. **36**, 214001 (2019),
arXiv:1906.10289 [hep-th].

[3]R. Gregory, Z. L. Lim and A. Scoins, *Thermodynamics of many black holes*, Front. in Phys. **9**, 187 (2021),
arXiv:2012.15561 [gr-qc].

[4]A. Einstein, *Zur Allgemeinen relativitätstheorie*, Sitzungsber. Preuss. Akad. Wiss. Berlin (Math. Phys.) **1915**, [Addendum: Sitzungsber.Preuss.Akad.Wiss.Berlin (Math.Phys.) 1915, 799–801 (1915)], 778–786 (1915).

[5]D. Hilbert, *Die Grundlagen der physik. 1.*, Gott. Nachr. **27**, edited by J.-P. Hsu and D. Fine, 395–407 (1915).

[6]B. Bertotti, L. Iess and P. Tortora, *A Test of general relativity using radio links with the Cassini spacecraft*, Nature **425**, 374–376 (2003).

[7]T. E. Collett et al., *A Precise extragalactic test of general relativity*, Science **360**, 1342 (2018),
arXiv:1806.08300 [astro-ph.CO].

[8]C. M. Will, *The Confrontation between general relativity and experiment*, Living Rev. Relativity **17**, 1433–8351 (2014).

[9]M. Parsa et al., *Investigating the relativistic motion of the stars near the supermassive black hole in the galactic center*, The Astrophysical Journal **845**, 22 (2017).

[10]A. Boehle et al., *An Improved distance and mass estimate for Sgr A* from a multistar orbit analysis*, The Astrophysical Journal **830**, 17 (2016).

[11]The GRAVITY Collaboration et al., *A Geometric distance measurement to the galactic center black hole with 0.3% uncertainty*, A&A **625**, L10 (2019).

[12]F. Peißker, A. Eckart and M. Parsa, *S62 on a 9.9 yr orbit around Sgr A**, The Astrophysical Journal **889**, 61 (2020).

[13]B. P. Abbott et al., *Observation of gravitational waves from a binary black hole merger*, Phys. Rev. Lett. **116**, 061102 (2016), arXiv:1602.03837 [gr-qc].

[14]K. Akiyama et al., *First M87 Event Horizon Telescope results. i. The shadow of the supermassive black hole*, Astrophys. J. Lett. **875**, L1 (2019), arXiv:1906.11238 [astro-ph.GA].

[15]K. Akiyama et al., *First M87 Event Horizon Telescope results. ii. Array and instrumentation*, Astrophys. J. Lett. **875**, L2 (2019), arXiv:1906.11239 [astro-ph.IM].

[16]K. Akiyama et al., *First M87 Event Horizon Telescope results. iii. Data processing and calibration*, Astrophys. J. Lett. **875**, L3 (2019), arXiv:1906.11240 [astro-ph.GA].

[17]K. Akiyama et al., *First M87 Event Horizon Telescope results. iv. Imaging the central supermassive black hole*, Astrophys. J. Lett. **875**, L4 (2019), arXiv:1906.11241 [astro-ph.GA].

[18]K. Akiyama et al., *First M87 Event Horizon Telescope results. vi. The shadow and mass of the central black hole*, Astrophys. J. Lett. **875**, L6 (2019), arXiv:1906.11243 [astro-ph.GA].

[19]R. P. Kerr, *Gravitational field of a spinning mass as an example of algebraically special metrics*, Phys. Rev. Lett. **11**, 237–238 (1963).

[20]S. Hod, *Late-time evolution of realistic rotating collapse and the no-hair theorem*, Phys. Rev. D **58**, 104022 (1998).

[21]K. Glampedakis and N. Andersson, *Late time dynamics of rapidly rotating black holes*, Phys. Rev. D **64**, 104021 (2001), arXiv:gr-qc/0103054.

[22]G. Rousseaux et al., *Horizon effects with surface waves on moving water*, New J. Phys. **12**, 095018 (2010), arXiv:1004.5546 [gr-qc].

[23]O. Lahav, A. Itah, A. Blumkin, C. Gordon and J. Steinhauer, *Realization of a sonic black hole analogue in a Bose-Einstein condensate*, Phys. Rev. Lett. **105**, 240401 (2010), arXiv:0906.1337 [cond-mat.quant-gas].

[24]F. Belgiorno et al., *Hawking radiation from ultrashort laser pulse filaments*, Phys. Rev. Lett. **105**, 203901 (2010), arXiv:1009.4634 [gr-qc].

[25]F. de Felice, *On the gravitational field acting as an optical medium*, Gen. Rel. Grav. **2**, 347 (1971).

[26]P. Chen and G. Mourou, *Accelerating plasma mirrors to investigate black hole information loss paradox*, Phys. Rev. Lett. **118**, 045001 (2017), arXiv:1512.04064 [gr-qc].

[27]J. Steinhauer, *Observation of quantum Hawking radiation and its entanglement in an analogue black hole*, Nature Phys. **12**, 959 (2016), arXiv:1510.00621 [gr-qc].

[28]V. I. Kolobov, K. Golubkov, Muñoz de Nova, J. Ramón and J. Steinhauer, *Observation of stationary spontaneous Hawking radiation and the time evolution of an analogue black hole*, Nature Physics **17**, 362–367 (2021).

[29]T. Torres et al., *Observation of superradiance in a vortex flow*, Nature Phys. **13**, 833–836 (2017), arXiv:1612.06180 [gr-qc].

[30]T. Torres et al., *Rotational superradiant scattering in a vortex flow*, Nature Physics **13**, 833–836 (2017).

[31]M. Cromb et al., *Amplification of waves from a rotating body*, Nature Phys. **16**, 1069–1073 (2020), arXiv:2005.03760 [physics.class-ph].

[32]M. Ishak, *Testing general relativity in cosmology*, Living Reviews in Relativity **22**, 1 (2018).

[33]S. Eckel, A. Kumar, T. Jacobson, I. B. Spielman and G. K. Campbell, *A Rapidly expanding Bose-Einstein condensate: An Expanding universe in the lab*, Phys. Rev. X **8**, 021021 (2018), arXiv:1710.05800 [cond-mat.quant-gas].

[34]P. T. Chrusciel, *"No hair" theorems: Folklore, conjectures, results*, Contemp. Math. **170**, 23–49 (1994), arXiv:gr-qc/9402032.

[35]P. T. Chruściel, J. L. Costa and M. Heusler, *Stationary black holes: Uniqueness and beyond*, Living Reviews in Relativity **15**, 7–80 (2012).

[36]J. M. Bardeen, B. Carter and S. W. Hawking, *The Four laws of black hole mechanics*, Commun. Math. Phys. **31**, 161–170 (1973).

[37]S. W. Hawking, *Black hole explosions?*, Nature **248**, 30–31 (1974).

[38]S. W. Hawking, *Particle creation by black holes*, Commun. Math. Phys. **43**, edited by G. W. Gibbons and S. W. Hawking, [Erratum: Commun. Math. Phys. **46**, 206 (1976)], 199–220 (1975).

[39]S. W. Hawking, *Black holes and thermodynamics*, Phys. Rev. D **13**, 191–197 (1976).

[40]M. Astorino, *Accelerating black hole in 2+1 dimensions and 3+1 black (st)ring*, JHEP **01**, 114 (2011),
arXiv:1101.2616 [gr-qc].

[41]B. Carter, *Axisymmetric black hole has only two degrees of freedom*, Phys. Rev. Lett. **26**, 331–333 (1971).

[42]B. Carter, *Black hole equilibrium states., in: Black Holes.* Edited by C. DeWitt and B. DeWitt (Gordon and Breach, New York, 1973), pp. 57–214.

[43]I. Racz and R. M. Wald, *Global extensions of space-times describing asymptotic final states of black holes*, Class. Quant. Grav. **13**, 539–553 (1996),
arXiv:gr-qc/9507055.

[44]S. Gao and R. M. Wald, *The "Physical process" version of the first law and the generalized second law for charged and rotating black holes*, Phys. Rev. D **64**, 084020 (2001),
arXiv:gr-qc/0106071.

[45]S. W. Hawking, *Gravitational radiation from colliding black holes*, Phys. Rev. Lett. **26**, 1344–1346 (1971).

[46]M. Lesourd, *A Remark on the energy conditions for hawking's area theorem*, Gen. Rel. Grav. **50**, 61 (2018),
arXiv:1711.06480 [gr-qc].

[47]W. Israel, *Third law of black-hole dynamics: A Formulation and proof*, Phys. Rev. Lett. **57**, 397 (1986).

[48]J. D. Bekenstein, *Black holes and entropy*, Phys. Rev. D **7**, 2333–2346 (1973).

[49]R. M. Wald, *On particle creation by black holes*, Commun. Math. Phys. **45**, 9–34 (1975).

[50]G. W. Gibbons and S. W. Hawking, *Action integrals and partition functions in quantum gravity*, Phys. Rev. D **15**, 2752–2756 (1977).

[51]J. D. Brown and J. W. York, *Quasilocal energy and conserved charges derived from the gravitational action*, Phys. Rev. D **47**, 1407–1419 (1993),
arXiv:gr-qc/9209012.

[52]J. M. Maldacena, *The Large N limit of superconformal field theories and supergravity*, Adv. Theor. Math. Phys. **2**, 231–252 (1998), arXiv:hep-th/9711200.

[53]E. Witten, *Anti-de Sitter space and holography*, Adv. Theor. Math. Phys. **2**, 253–291 (1998), arXiv:hep-th/9802150.

[54]S. S. Gubser, I. R. Klebanov and A. M. Polyakov, *Gauge theory correlators from noncritical string theory*, Phys. Lett. B **428**, 105–114 (1998), arXiv:hep-th/9802109.

[55]R. Emparan, C. V. Johnson and R. C. Myers, *Surface terms as counterterms in the AdS/CFT correspondence*, Phys. Rev. D **60**, 104001 (1999), arXiv:hep-th/9903238.

[56]C. Teitelboim, *The Cosmological constant as a thermodynamic black hole parameter*, Physics Letters B **158**, 293–297 (1985).

[57]J. D. Brown and C. Teitelboim, *Neutralization of the cosmological constant by membrane creation*, Nucl. Phys. B **297**, 787–836 (1988).

[58]M. J. Duff, B. E. W. Nilsson and C. N. Pope, *Kaluza-Klein supergravity*, Phys. Rept. **130**, 1–142 (1986).

[59]J. D. E. Creighton and R. B. Mann, *Quasilocal thermodynamics of dilaton gravity coupled to gauge fields*, Phys. Rev. D **52**, 4569–4587 (1995), arXiv:gr-qc/9505007.

[60]R. Gregory, D. Kastor and J. Traschen, *Black hole thermodynamics with dynamical Lambda*, JHEP **10**, 118 (2017), arXiv:1707.06586 [hep-th].

[61]R. Gregory, D. Kastor and J. Traschen, *Evolving black holes in inflation*, Class. Quant. Grav. **35**, 155008 (2018), arXiv:1804.03462 [hep-th].

[62]D. Kastor, S. Ray and J. Traschen, *Enthalpy and the mechanics of AdS black holes*, Class. Quant. Grav. **26**, 195011 (2009), arXiv:0904.2765 [hep-th].

[63]B. P. Dolan, D. Kastor, D. Kubiznak, R. B. Mann and J. Traschen, *Thermodynamic volumes and isoperimetric inequalities for de Sitter black holes*, Phys. Rev. D **87**, 104017 (2013), arXiv:1301.5926 [hep-th].

[64]N. Altamirano, D. Kubiznak, R. B. Mann and Z. Sherkatghanad, *Thermodynamics of rotating black holes and black rings: Phase transitions and thermodynamic volume*, Galaxies **2**, 89–159 (2014), arXiv:1401.2586 [hep-th].

[65]D. Kubiznak and R. B. Mann, *Black hole chemistry*, Can. J. Phys. **93**, edited by A. Dasgupta, 999–1002 (2015), arXiv:1404.2126 [gr-qc].

[66]D. Kubiznak, R. B. Mann and M. Teo, *Black hole chemistry: Thermodynamics with Lambda*, Class. Quant. Grav. **34**, 063001 (2017), arXiv:1608.06147 [hep-th].

[67]D. Kubiznak and R. B. Mann, *P-V criticality of charged AdS black holes*, JHEP **07**, 033 (2012), arXiv:1205.0559 [hep-th].

[68]A. Chamblin, R. Emparan, C. V. Johnson and R. C. Myers, *Charged AdS black holes and catastrophic holography*, Phys. Rev. D **60**, 064018 (1999), arXiv:hep-th/9902170.

[69]A. Rajagopal, D. Kubizňák and R. B. Mann, *Van der Waals black hole*, Phys. Lett. B **737**, 277–279 (2014), arXiv:1408.1105 [gr-qc].

[70]B. Gwak, *Thermodynamics with pressure and volume under charged particle absorption*, JHEP **11**, 129 (2017), arXiv:1709.08665 [gr-qc].

[71]B. Gwak, *Weak cosmic censorship with pressure and volume in charged anti-de Sitter black hole under charged scalar field*, JCAP **08**, 016 (2019), arXiv:1901.05589 [gr-qc].

[72]X.-X. Zeng, Y.-W. Han and D.-Y. Chen, *Thermodynamics and weak cosmic censorship conjecture of BTZ black holes in extended phase space*, Chin. Phys. C **43**, 105104 (2019), arXiv:1901.08915 [gr-qc].

[73]D. Chen, *Thermodynamics and weak cosmic censorship conjecture in extended phase spaces of anti-de Sitter black holes with particles' absorption*, Eur. Phys. J. C **79**, 353 (2019), arXiv:1902.06489 [hep-th].

[74]Y.-W. Han, X.-X. Zeng and Y. Hong, *Thermodynamics and weak cosmic censorship conjecture of the torus-like black hole*, Eur. Phys. J. C **79**, 252 (2019), arXiv:1901.10660 [hep-th].

[75]Y.-W. Han, M.-J. Lan and X.-X. Zeng, *Thermodynamics and weak cosmic censorship conjecture in (2+1)-dimensional regular black hole with nonlinear electrodynamics sources*, Eur. Phys. J. Plus **135**, 172 (2020), arXiv:1903.03764 [gr-qc].

[76]P. Wang, H. Wu and H. Yang, *Thermodynamics and weak cosmic censorship conjecture in nonlinear electrodynamics black holes via charged particle absorption*, (2019), arXiv:1904.12365 [gr-qc].

[77]W. Hong, B. Mu and J. Tao, *Thermodynamics and weak cosmic censorship conjecture in the charged rn-ads black hole surrounded by quintessence under the scalar field*, Nucl. Phys. B **949**, 114826 (2019), arXiv:1905.07747 [gr-qc].

[78]X.-X. Zeng, X.-Y. Hu and K.-J. He, *Weak cosmic censorship conjecture with pressure and volume in the Gauss-Bonnet AdS black hole*, Nucl. Phys. B **949**, 114823 (2019), arXiv:1905.07750 [hep-th].

[79]B. Gwak, *Weak cosmic censorship conjecture in Kerr-Newman-(anti-)de Sitter black hole with charged scalar field*, (2021), arXiv:2105.07226 [gr-qc].

[80]S.-Q. Hu, Y. C. Ong and D. N. Page, *No evidence for violation of the second law in extended black hole thermodynamics*, Phys. Rev. D **100**, 104022 (2019), arXiv:1906.05870 [gr-qc].

[81]L. Smarr, *Mass formula for Kerr black holes*, Phys. Rev. Lett. **30**, [Erratum: Phys. Rev. Lett. **30**, 521–521 (1973)], 71–73 (1973).

[82]M. M. Caldarelli, G. Cognola and D. Klemm, *Thermodynamics of Kerr-Newman-AdS black holes and conformal field theories*, Class. Quant. Grav. **17**, 399–420 (2000), arXiv:hep-th/9908022.

[83]Y. Sekiwa, *Thermodynamics of de Sitter black holes: Thermal cosmological constant*, Phys. Rev. D **73**, 084009 (2006), arXiv:hep-th/0602269.

[84]M. Urano, A. Tomimatsu and H. Saida, *Mechanical first law of black hole spacetimes with cosmological constant and its application to Schwarzschild-de Sitter spacetime*, Class. Quant. Grav. **26**, 105010 (2009), arXiv:0903.4230 [gr-qc].

[85]S. Wang, *Thermodynamics of Schwarzschild de Sitter spacetimes: Variable cosmological constant*, (2006),
arXiv:gr-qc/0606109.

[86]A. M. Frassino, R. B. Mann and J. R. Mureika, *Lower-dimensional black hole chemistry*, Phys. Rev. D **92**, 124069 (2015),
arXiv:1509.05481 [gr-qc].

[87]M. Cvetic, G. W. Gibbons, D. Kubiznak and C. N. Pope, *Black hole enthalpy and an entropy inequality for the thermodynamic volume*, Phys. Rev. D **84**, 024037 (2011),
arXiv:1012.2888 [hep-th].

[88]A. Komar, *Covariant conservation laws in general relativity*, Phys. Rev. **113**, 934–936 (1959).

[89]A. Komar, *Positive-definite energy density and global consequences for general relativity*, Phys. Rev. **129**, 1873–1876 (1963).

[90]S. L. Bazanski and P. Zyla, *A Gauss type law for gravity with a cosmological constant*, Gen. Rel. Grav. **22**, 379–387 (1990).

[91]D. Kastor, *Komar integrals in higher (and lower) derivative gravity*, Class. Quant. Grav. **25**, 175007 (2008),
arXiv:0804.1832 [hep-th].

[92]I. Papadimitriou and K. Skenderis, *Thermodynamics of asymptotically locally AdS spacetimes*, JHEP **08**, 004 (2005),
arXiv:hep-th/0505190.

[93]V. Balasubramanian and P. Kraus, *A Stress tensor for anti-de Sitter gravity*, Commun. Math. Phys. **208**, 413–428 (1999),
arXiv:hep-th/9902121.

[94]A. Ashtekar and S. Das, *Asymptotically anti-de Sitter space-times: Conserved quantities*, Class. Quant. Grav. **17**, L17–L30 (2000),
arXiv:hep-th/9911230.

[95]S. Das and R. B. Mann, *Conserved quantities in Kerr-anti-de Sitter space-times in various dimensions*, JHEP **08**, 033 (2000),
arXiv:hep-th/0008028.

[96]A. M. Awad and C. V. Johnson, *Holographic stress tensors for Kerr-AdS black holes*, Phys. Rev. D **61**, 084025 (2000),
arXiv:hep-th/9910040.

[97]M. K. Parikh, *The Volume of black holes*, Phys. Rev. D **73**, 124021 (2006),
arXiv:hep-th/0508108.

[98]D. Grumiller, *The Volume of 2D black holes*, J. Phys. Conf. Ser. **33**, edited by M. Cadoni, M. Cavaglia and J. E. Nelson, 361–366 (2006), arXiv:gr-qc/0509077.

[99]W. Ballik and K. Lake, *The Volume of stationary black holes and the meaning of the surface gravity*, (2010), arXiv:1005.1116 [gr-qc].

[100]W. Ballik and K. Lake, *Vector volume and black holes*, Phys. Rev. D **88**, 104038 (2013), arXiv:1310.1935 [gr-qc].

[101]M. Christodoulou and C. Rovelli, *How big is a black hole?*, Phys. Rev. D **91**, 064046 (2015), arXiv:1411.2854 [gr-qc].

[102]A. Gnecchi, K. Hristov, D. Klemm, C. Toldo and O. Vaughan, *Rotating black holes in 4D gauged supergravity*, JHEP **01**, 127 (2014), arXiv:1311.1795 [hep-th].

[103]R. A. Hennigar, D. Kubizňák and R. B. Mann, *Entropy inequality violations from ultraspinning black holes*, Phys. Rev. Lett. **115**, 031101 (2015), arXiv:1411.4309 [hep-th].

[104]M. Appels, L. Cuspinera, R. Gregory, P. Krtouš and D. Kubizňák, *Are "Superentropic" black holes superentropic?*, JHEP **02**, 195 (2020), arXiv:1911.12817 [hep-th].

[105]R. Gregory and M. Hindmarsh, *Smooth metrics for snapping strings*, Phys. Rev. D **52**, 5598–5605 (1995), arXiv:gr-qc/9506054.

[106]F. Dowker, J. P. Gauntlett, D. A. Kastor and J. H. Traschen, *Pair creation of dilaton black holes*, Phys. Rev. D **49**, 2909–2917 (1994), arXiv:hep-th/9309075.

[107]A. Vilenkin, *Cosmic strings and domain walls*, Phys. Rept. **121**, 263–315 (1985).

[108]H. B. Nielsen and P. Olesen, *Vortex line models for dual strings*, Nucl. Phys. B **61**, edited by J. C. Taylor, 45–61 (1973).

[109]D. Garfinkle, *General relativistic strings*, Phys. Rev. D **32**, 1323–1329 (1985).

[110]R. Gregory, *Gravitational stability of local strings*, Phys. Rev. Lett. **59**, 740 (1987).

[111]A. Achucarro, R. Gregory and K. Kuijken, *Abelian Higgs hair for black holes*, Phys. Rev. D **52**, 5729–5742 (1995), arXiv:gr-qc/9505039.

[112]R. Gregory, D. Kubiznak and D. Wills, *Rotating black hole hair*, JHEP **06**, 023 (2013),
arXiv:1303.0519 [gr-qc].

[113]R. Gregory, P. C. Gustainis, D. Kubizňák, R. B. Mann and D. Wills, *Vortex hair on AdS black holes*, JHEP **11**, 010 (2014),
arXiv:1405.6507 [hep-th].

[114]H. Weyl, *Zur Gravitationstheorie*, Annalen der Physik **359**, 117–145 (1917),
arXiv:https://onlinelibrary.wiley.com/doi/pdf/10.1002/andp.19173591804.

[115]J. F. Plebanski and M. Demianski, *Rotating, charged, and uniformly accelerating mass in general relativity*, Annals Phys. **98**, 98–127 (1976).

[116]R. Debever, *On type D expanding solutions of Einstein-Maxwell equations*, Bull.Soc.Math.Belg. **23**, 360–376 (1971).

[117]V. Pravda and A. Pravdova, *On the spinning C-metric*,
doi:10.1142/9789812776938_0008 (2002),
arXiv:gr-qc/0201025.

[118]W. B. Bonnor, *A New interpretation of the NUT metric in general relativity*, Mathematical Proceedings of the Cambridge Philosophical Society **66**, 145–151 (1969).

[119]J. G. Miller, *Global analysis of the Kerr-Taub-NUT metric*, Journal of Mathematical Physics **14**, 486–494 (1973),
arXiv:https://doi.org/10.1063/1.1666343.

[120]V. S. Manko and E. Ruiz, *Physical interpretation of NUT solution*, Class. Quant. Grav. **22**, 3555–3560 (2005),
arXiv:gr-qc/0505001.

[121]A. Ballon Bordo, F. Gray, R. A. Hennigar and D. Kubizňák, *The First law for rotating NUT's*, Phys. Lett. B **798**, 134972 (2019),
arXiv:1905.06350 [hep-th].

[122]A. B. Bordo, F. Gray, R. A. Hennigar and D. Kubizňák, *Misner gravitational charges and variable string strengths*, Class. Quant. Grav. **36**, 194001 (2019),
arXiv:1905.03785 [hep-th].

[123]J. Podolsky and A. Vratny, *Accelerating NUT black holes*, Phys. Rev. D **102**, 084024 (2020),
arXiv:2007.09169 [gr-qc].

[124]J. Podolsky and A. Vratny, *New improved form of black holes of type D*, (2021),
arXiv:2108.02239 [gr-qc].

[125]J. B. Griffiths and J. Podolsky, *A New look at the Plebanski-Demianski family of solutions*, Int. J. Mod. Phys. D **15**, 335–370 (2006), arXiv:gr-qc/0511091.

[126]J. Podolsky and J. B. Griffiths, *Uniformly accelerating black holes in a de Sitter universe*, Phys. Rev. D **63**, 024006 (2001), arXiv:gr-qc/0010109.

[127]J. Podolsky and J. B. Griffiths, *Accelerating Kerr-Newman black holes in (anti-)de Sitter space-time*, Phys. Rev. D **73**, 044018 (2006), arXiv:gr-qc/0601130.

[128]W. Kinnersley and M. Walker, *Uniformly accelerating charged mass in general relativity*, Phys. Rev. D **2**, 1359–1370 (1970).

[129]K. Hong and E. Teo, *A New form of the C-metric*, Class. Quant. Grav. **20**, 3269–3277 (2003), arXiv:gr-qc/0305089.

[130]K. Hong and E. Teo, *A New form of the rotating C-metric*, Class. Quant. Grav. **22**, 109–118 (2005), arXiv:gr-qc/0410002.

[131]S. W. Hawking, C. J. Hunter and M. Taylor, *Rotation and the AdS/CFT correspondence*, Phys. Rev. D **59**, 064005 (1999), arXiv:hep-th/9811056.

[132]R. P. Kerr, *Gravitational field of a spinning mass as an example of algebraically special metrics*, Phys. Rev. Lett. **11**, 237–238 (1963).

[133]B. Carter, *Hamilton-Jacobi and Schrodinger separable solutions of Einstein's equations*, Commun. Math. Phys. **10**, 280–310 (1968).

[134]G. W. Gibbons, H. Lu, D. N. Page and C. N. Pope, *The General Kerr-de Sitter metrics in all dimensions*, J. Geom. Phys. **53**, 49–73 (2005), arXiv:hep-th/0404008.

[135]J. Podolsky, *Accelerating black holes in anti-de Sitter universe*, Czech. J. Phys. **52**, 1–10 (2002), arXiv:gr-qc/0202033.

[136]M. Appels, 'Thermodynamics of accelerating black holes', PhD thesis (Durham U., Dept. of Math., 2018).

[137]J. Podolsky, M. Ortaggio and P. Krtous, *Radiation from accelerated black holes in an anti-de Sitter universe*, Phys. Rev. D **68**, 124004 (2003), arXiv:gr-qc/0307108.

[138]F. J. Ernst, *Removal of the nodal singularity of the C-metric*, Journal of Mathematical Physics **17**, 515–516 (1976), arXiv:https://aip.scitation.org/doi/pdf/10.1063/1.522935.

[139]F. J. Ernst, *Black holes in a magnetic universe*, J. Math. Phys. **17**, 54–56 (1976).

[140]K. D. Krori, S. Chaudhury and S. Dowerah, *Accelerating black hole in a magnetic field*, Journal of Mathematical Physics **25**, 607–611 (1984), arXiv:https://doi.org/10.1063/1.526162.

[141]M. Astorino, G. Compère, R. Oliveri and N. Vandevoorde, *Mass of Kerr-Newman black holes in an external magnetic field*, Phys. Rev. D **94**, 024019 (2016), arXiv:1602.08110 [gr-qc].

[142]M. Astorino, *Thermodynamics of regular accelerating black holes*, Phys. Rev. D **95**, 064007 (2017), arXiv:1612.04387 [gr-qc].

[143]M. Astorino and A. Viganò, *Charged and rotating multi-black holes in an external gravitational field*, (2021), arXiv:2105.02894 [gr-qc].

[144]M. Astorino and A. Viganò, *Many accelerating distorted black holes*, (2021), arXiv:2106.02058 [gr-qc].

[145]M. Aryal, L. H. Ford and A. Vilenkin, *Cosmic strings and black holes*, Phys. Rev. D **34**, 2263 (1986).

[146]M. Appels, R. Gregory and D. Kubiznak, *Thermodynamics of accelerating black holes*, Phys. Rev. Lett. **117**, 131303 (2016), arXiv:1604.08812 [hep-th].

[147]T. Jacobson and R. Parentani, *Horizon entropy*, Found. Phys. **33**, 323–348 (2003), arXiv:gr-qc/0302099.

[148]M. Appels, R. Gregory and D. Kubiznak, *Black hole thermodynamics with conical defects*, JHEP **05**, 116 (2017), arXiv:1702.00490 [hep-th].

[149]A. Anabalón, M. Appels, R. Gregory, D. Kubizňák, R. B. Mann and A. Ovgün, *Holographic thermodynamics of accelerating black holes*, Phys. Rev. D **98**, 104038 (2018), arXiv:1805.02687 [hep-th].

[150]A. Anabalón, F. Gray, R. Gregory, D. Kubizňák and R. B. Mann, *Thermodynamics of charged, rotating, and accelerating black holes*, JHEP **04**, 096 (2019),
arXiv:1811.04936 [hep-th].

[151]D. Cassani, J. P. Gauntlett, D. Martelli and J. Sparks, *Thermodynamics of accelerating and supersymmetric AdS_4 black holes*, (2021),
arXiv:2106.05571 [hep-th].

[152]P. Ferrero, J. P. Gauntlett, J. M. P. Ipiña, D. Martelli and J. Sparks, *Accelerating black holes and spinning spindles*, (2020),
arXiv:2012.08530 [hep-th].

[153]M. Henningson and K. Skenderis, *The Holographic Weyl anomaly*, JHEP **07**, 023 (1998),
arXiv:hep-th/9806087.

[154]S. W. Hawking and S. F. Ross, *Duality between electric and magnetic black holes*, Phys. Rev. D **52**, 5865–5876 (1995),
arXiv:hep-th/9504019.

[155]G. W. Gibbons, M. J. Perry and C. N. Pope, *The First law of thermodynamics for Kerr-anti-de Sitter black holes*, Class. Quant. Grav. **22**, 1503–1526 (2005),
arXiv:hep-th/0408217.

[156]V. A. Kostelecky and M. J. Perry, *Solitonic black holes in gauged N=2 supergravity*, Phys. Lett. B **371**, 191–198 (1996),
arXiv:hep-th/9512222.

[157]M. Henneaux and C. Teitelboim, *Asymptotically anti-de Sitter spaces*, Commun. Math. Phys. **98**, 391–424 (1985).

[158]B. P. Dolan, *The Cosmological constant and the black hole equation of state*, Class. Quant. Grav. **28**, 125020 (2011),
arXiv:1008.5023 [gr-qc].

[159]B. P. Dolan, *Pressure and volume in the first law of black hole thermodynamics*, Class. Quant. Grav. **28**, 235017 (2011),
arXiv:1106.6260 [gr-qc].

[160]D. Christodoulou and R. Ruffini, *Reversible transformations of a charged black hole*, Phys. Rev. D **4**, 3552–3555 (1971).

[161]R. Ruffini and J. A. Wheeler, *Introducing the black hole*, Phys. Today **24**, 30 (1971).

[162]P. T. Chrusciel, J. Lopes Costa and M. Heusler, *Stationary black holes: Uniqueness and beyond*, Living Rev. Rel. **15**, 7 (2012), arXiv:1205.6112 [gr-qc].

[163]R. Gregory, *Accelerating black holes*, J. Phys. Conf. Ser. **942**, edited by P. Nicolini, M. Kaminski, J. Mureika and M. Bleicher, 012002 (2017), arXiv:1712.04992 [hep-th].

[164]M. Astorino, *CFT duals for accelerating black holes*, Phys. Lett. B **760**, 393–405 (2016), arXiv:1605.06131 [hep-th].

[165]B. P. Dolan, *Where is the PdV in the first law of black hole thermodynamics?, in: Open Questions in Cosmology*, edited by G. J. Olmo (INTECH, 2012), arXiv:1209.1272 [gr-qc].

[166]S. W. Hawking and D. N. Page, *Thermodynamics of black holes in anti-de Sitter space*, Commun. Math. Phys. **87**, 577 (1983).

[167]N. Abbasvandi, W. Cong, D. Kubiznak and R. B. Mann, *Snapping swallowtails in accelerating black hole thermodynamics*, Class. Quant. Grav. **36**, 104001 (2019), arXiv:1812.00384 [gr-qc].

[168]N. Abbasvandi, W. Ahmed, W. Cong, D. Kubizňák and R. B. Mann, *Finely split phase transitions of rotating and accelerating black holes*, Phys. Rev. D **100**, 064027 (2019), arXiv:1906.03379 [gr-qc].

[169]J. D. Bekenstein, *Generalized second law of thermodynamics in black hole physics*, Phys. Rev. D **9**, 3292–3300 (1974).

[170]W. Israel and K. A. Khan, *Collinear particles and bondi dipoles in general relativity*, Il Nuovo Cimento **33**, 331–344 (1964).

[171]E. A. Martinez and J. W. York Jr., *Thermodynamics of black holes and cosmic strings*, Phys. Rev. D **42**, 3580–3583 (1990).

[172]M. S. Costa and M. J. Perry, *Interacting black holes*, Nucl. Phys. B **591**, 469–487 (2000), arXiv:hep-th/0008106.

[173]K. Dutta, S. Ray and J. Traschen, *Boost mass and the mechanics of accelerated black holes*, Class. Quant. Grav. **23**, 335–352 (2006), arXiv:hep-th/0508041.

[174]C. Herdeiro, B. Kleihaus, J. Kunz and E. Radu, *On the Bekenstein-Hawking area law for black objects with conical singularities*, Phys. Rev. D **81**, 064013 (2010), arXiv:0912.3386 [gr-qc].

[175]F. Bonjour, R. Emparan and R. Gregory, *Vortices and extreme black holes: The Question of flux expulsion*, Phys. Rev. D **59**, 084022 (1999), arXiv:gr-qc/9810061.

[176]J. H. Traschen and D. Fox, *Tension perturbations of black brane space-times*, Class. Quant. Grav. **21**, 289–306 (2004), arXiv:gr-qc/0103106.

[177]T. Harmark and N. A. Obers, *General definition of gravitational tension*, JHEP **05**, 043 (2004), arXiv:hep-th/0403103.

[178]D. Kastor and J. Traschen, *The Angular tension of black holes*, Phys. Rev. D **86**, 081501 (2012), arXiv:1207.5415 [hep-th].

[179]P. Krtouš and A. Zelnikov, *Thermodynamics of two black holes*, JHEP **02**, 164 (2020), arXiv:1909.13467 [gr-qc].

[180]C. J. Ramírez-Valdez, H. García-Compeán and V. S. Manko, *Thermodynamics of two aligned Kerr black holes*, Phys. Rev. D **102**, 024084 (2020), arXiv:2007.02918 [gr-qc].

[181]H. García-Compeán, V. S. Manko and C. J. Ramírez-Valdez, *Thermodynamics of two aligned Kerr-Newman black holes*, (2020), arXiv:2008.01213 [gr-qc].

[182]H. F. Dowker and S. N. Thambyahpillai, *Many accelerating black holes*, Class. Quant. Grav. **20**, 127–136 (2003), arXiv:gr-qc/0105044.

[183]I. Cabrera-Munguia, *Unequal binary configurations of interacting Kerr black holes*, Phys. Lett. B **786**, 466–471 (2018), arXiv:1806.05442 [gr-qc].

[184]V. S. Manko and E. Ruiz, *Metric for two arbitrary Kerr sources*, Phys. Lett. B **794**, 36–40 (2019), arXiv:1806.10408 [gr-qc].

[185]V. S. Manko, E. Ruiz and O. V. Manko, *Is equilibrium of aligned Kerr black holes possible?*, Phys. Rev. Lett. **85**, 5504–5506 (2000).

[186]R. Emparan and H. S. Reall, *Generalized Weyl solutions*, Phys. Rev. D **65**, 084025 (2002),
arXiv:hep-th/0110258.

[187]T. Dray, *On the asymptotic flatness of the C-metrics at spatial infinity*, Gen. Rel. Grav. **14**, 109–112 (1982).

[188]R. Arnowitt, S. Deser and C. W. Misner, *Dynamical structure and definition of energy in general relativity*, Phys. Rev. **116**, 1322–1330 (1959).

[189]J. B. Griffiths, P. Krtous and J. Podolsky, *Interpreting the C-metric*, Class. Quant. Grav. **23**, 6745–6766 (2006),
arXiv:gr-qc/0609056.

[190]O. J. C. Dias and J. P. S. Lemos, *Pair of accelerated black holes in anti-de Sitter background: AdS C-metric*, Phys. Rev. D **67**, 064001 (2003),
arXiv:hep-th/0210065.

[191]M. H. Dehghani, A. M. Ghezelbash and R. B. Mann, *Vortex holography*, Nucl. Phys. B **625**, 389–406 (2002),
arXiv:hep-th/0105134.

[192]Ó. J. C. Dias, G. T. Horowitz, N. Iqbal and J. E. Santos, *Vortices in holographic superfluids and superconductors as conformal defects*, JHEP **04**, 096 (2014),
arXiv:1311.3673 [hep-th].

[193]S. Deser and R. Jackiw, *Three-dimensional cosmological gravity: Dynamics of constant curvature*, Annals Phys. **153**, 405–416 (1984).

[194]M. Banados, C. Teitelboim and J. Zanelli, *The Black hole in three-dimensional space-time*, Phys. Rev. Lett. **69**, 1849–1851 (1992),
arXiv:hep-th/9204099.

[195]M. Banados, M. Henneaux, C. Teitelboim and J. Zanelli, *Geometry of the (2+1) black hole*, Phys. Rev. D **48**, [Erratum: Phys.Rev.D 88, 069902 (2013)], 1506–1525 (1993),
arXiv:gr-qc/9302012.

[196]E. Witten, *(2+1)-Dimensional gravity as an exactly soluble system*, Nucl. Phys. B **311**, 46 (1988).

[197]A. Maloney and E. Witten, *Quantum gravity partition functions in three dimensions*, JHEP **02**, 029 (2010),
arXiv:0712.0155 [hep-th].

[198]V. E. Hubeny, D. Marolf and M. Rangamani, *Black funnels and droplets from the AdS C-metrics*, Class. Quant. Grav. **27**, 025001 (2010),
arXiv:0909.0005 [hep-th].

[199]V. E. Hubeny, D. Marolf and M. Rangamani, *Hawking radiation in large N strongly-coupled field theories*, Class. Quant. Grav. **27**, 095015 (2010), arXiv:0908.2270 [hep-th].

[200]M. M. Anber, *AdS(4)/CFT(3) + gravity for accelerating conical singularities*, JHEP **11**, 026 (2008), arXiv:0809.2789 [hep-th].

[201]W. Xu, K. Meng and L. Zhao, *Accelerating BTZ spacetime*, Class. Quant. Grav. **29**, 155005 (2012), arXiv:1111.0730 [gr-qc].

[202]S. Deser, R. Jackiw and G. 't Hooft, *Three-dimensional Einstein gravity: Dynamics of flat space*, Annals Phys. **152**, 220 (1984).

[203]R. B. Mann, *Misner string entropy*, Phys. Rev. D **60**, 104047 (1999), arXiv:hep-th/9903229.

[204]S. de Haro, S. N. Solodukhin and K. Skenderis, *Holographic reconstruction of space-time and renormalization in the AdS/CFT correspondence*, Commun. Math. Phys. **217**, 595–622 (2001), arXiv:hep-th/0002230.

[205]J. Brown and M. Henneaux, *Central charges in the canonical realization of asymptotic symmetries: An Example from three-dimensional gravity*, Commun. Math. Phys. **104**, 207–226 (1986).

[206]R. Blumenhagen and E. Plauschinn, *Introduction to conformal field theory: With applications to string theory*, Vol. 779 (2009).

[207]M. Banados, *Three-dimensional quantum geometry and black holes*, AIP Conf. Proc. **484**, edited by H. Falomir, R. Gamboa Saravi and F. Schaposnik, 147–169 (1999), arXiv:hep-th/9901148.

[208]M. Banados, *Notes on black holes and three-dimensional gravity*, AIP Conf. Proc. **490**, edited by J. D'Olivo, M. Mondragon and G. Lopez Castro, 198–216 (1999), arXiv:hep-th/9903244.

[209]S. Carlip, *Lectures on (2+1)-dimensional gravity*, J. Korean Phys. Soc. **28**, S447–S467 (1995), arXiv:gr-qc/9503024.

[210]P. Krtous, *Accelerated black holes in an anti-de Sitter universe*, Phys. Rev. D **72**, 124019 (2005), arXiv:gr-qc/0510101.

[211]F. Faedo, S. Klemm and A. Viganò, *Supersymmetric black holes with spiky horizons*, (2021),
arXiv:2105.02902 [hep-th].

[212]D. Kubiznak and P. Krtous, *On conformal Killing-Yano tensors for Plebański-Demiański family of solutions*, Phys. Rev. D **76**, 084036 (2007),
arXiv:0707.0409 [gr-qc].

[213]H. Lu, J. Mei and C. N. Pope, *New black holes in five dimensions*, Nucl. Phys. B **806**, 436–455 (2009),
arXiv:0804.1152 [hep-th].

[214]H. Lu, J. Mei and C. N. Pope, *New charged black holes in five dimensions*, Class. Quant. Grav. **27**, 075013 (2010),
arXiv:0806.2204 [hep-th].

[215]H. Lü and J. F. Vázquez-Poritz, *C-metrics in gauged STU supergravity and beyond*, JHEP **12**, 057 (2014),
arXiv:1408.6531 [hep-th].

[216]J. L. Cardy, *Operator content of two-dimensional conformally invariant theories*, Nucl. Phys. B **270**, 186–204 (1986).

[217]A. Strominger, *Black hole entropy from near horizon microstates*, JHEP **02**, 009 (1998),
arXiv:hep-th/9712251.

[218]J. L. Cardy, *Boundary conformal field theory*, (2004),
arXiv:hep-th/0411189.

[219]J. Bicak and V. Pravda, *Spinning C-metric: Radiative space-time with accelerating, rotating black holes*, Phys. Rev. D **60**, 044004 (1999),
arXiv:gr-qc/9902075.

[220]P. S. Letelier and S. R. Oliveira, *On uniformly accelerated black holes*, Phys. Rev. D **64**, 064005 (2001),
arXiv:gr-qc/9809089.